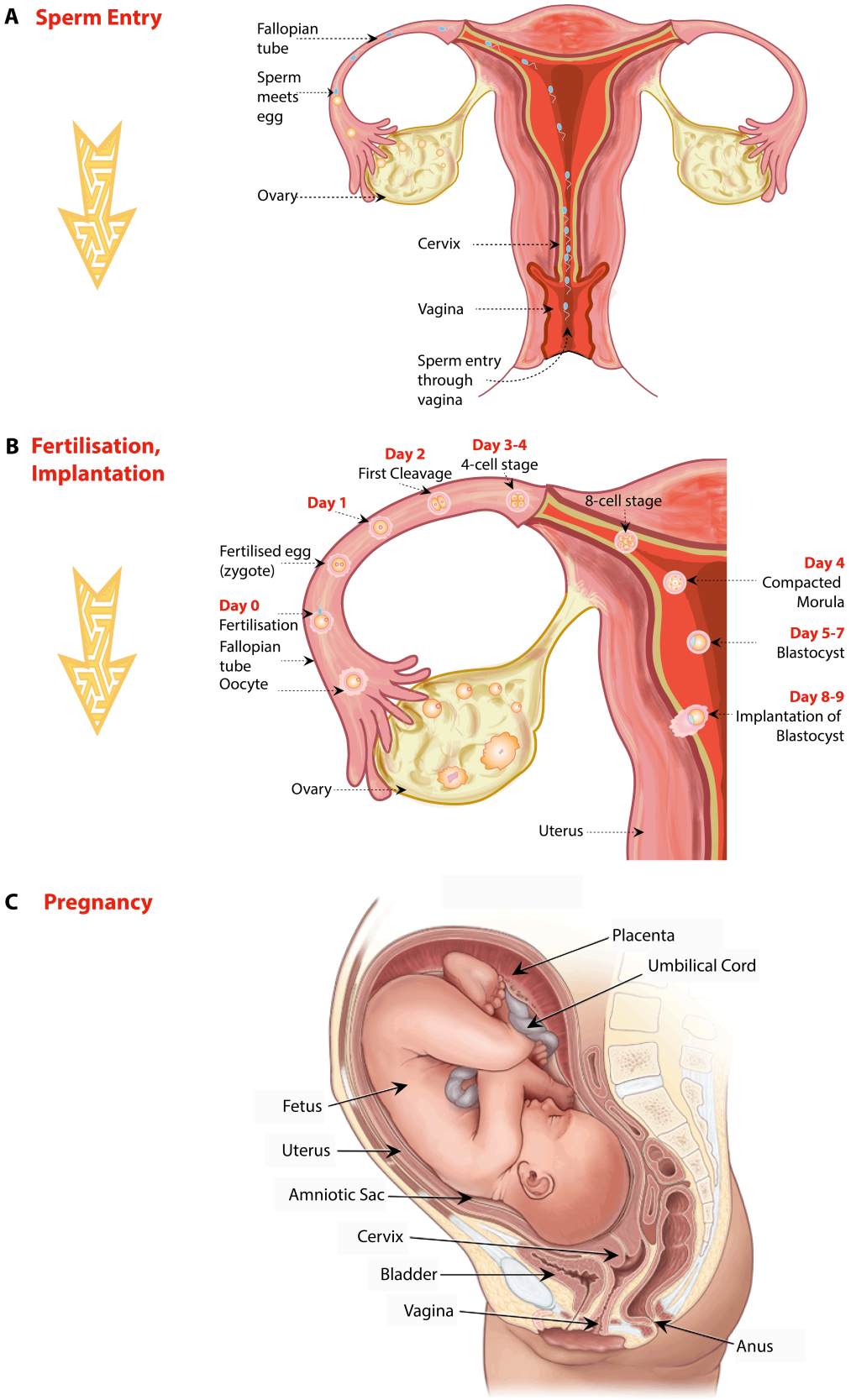


Figure 1.1: Early stages of development in the female reproductive tract. (A) The journey of the sperm through the uterus; (B) Fertilisation, stages of early embryonic development and implantation; and (C) Fetus *in utero*. Diagrams A and B are drawn by the author. Diagram C has been modified from birthinjuryjustice.org.

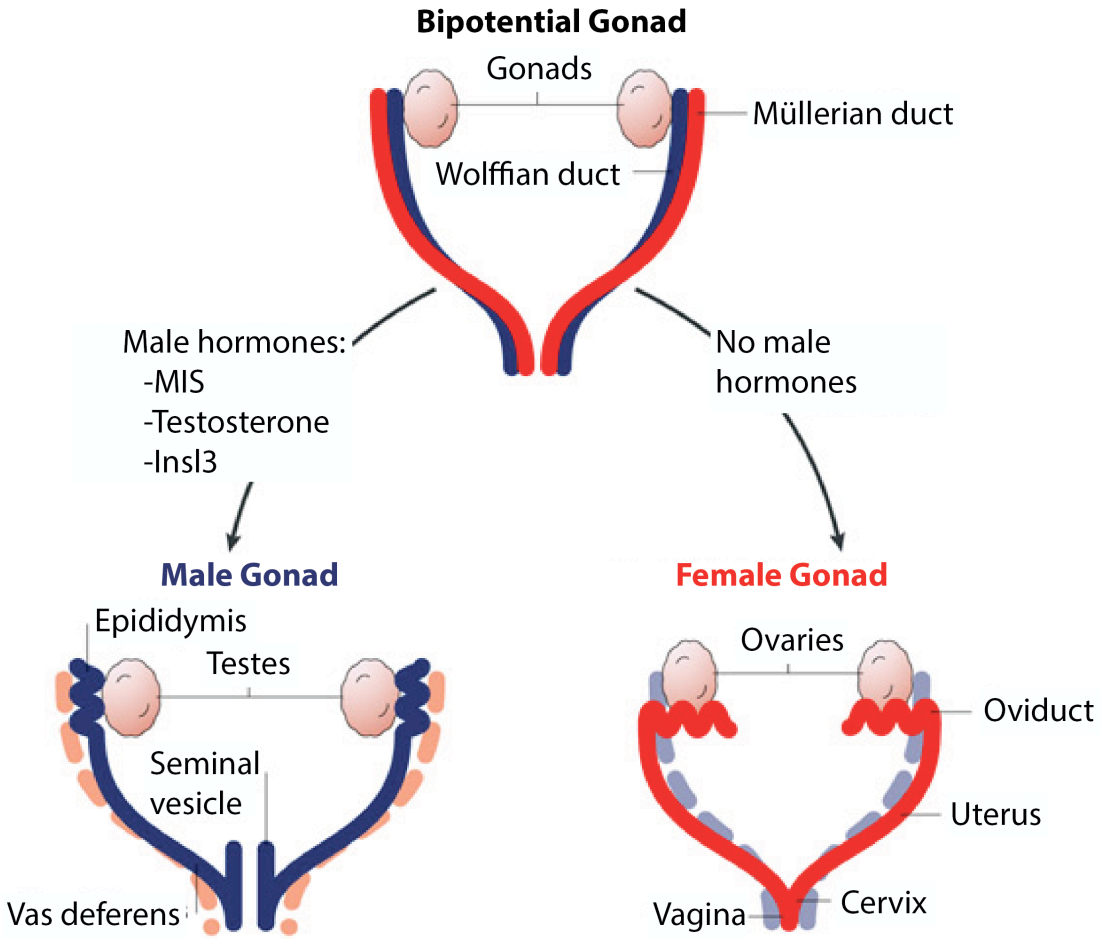


Figure 1.2: The origin of the male and female reproductive systems. The Müllerian duct is formed during early fetal development. In males, Müllerian-inhibiting substance (MIS) leads to the regression of these ducts, while in the absence of this hormone in females the ducts give rise to the oviduct and the uterus. Diagram adapted from Kobayashi and Behringer (2003).

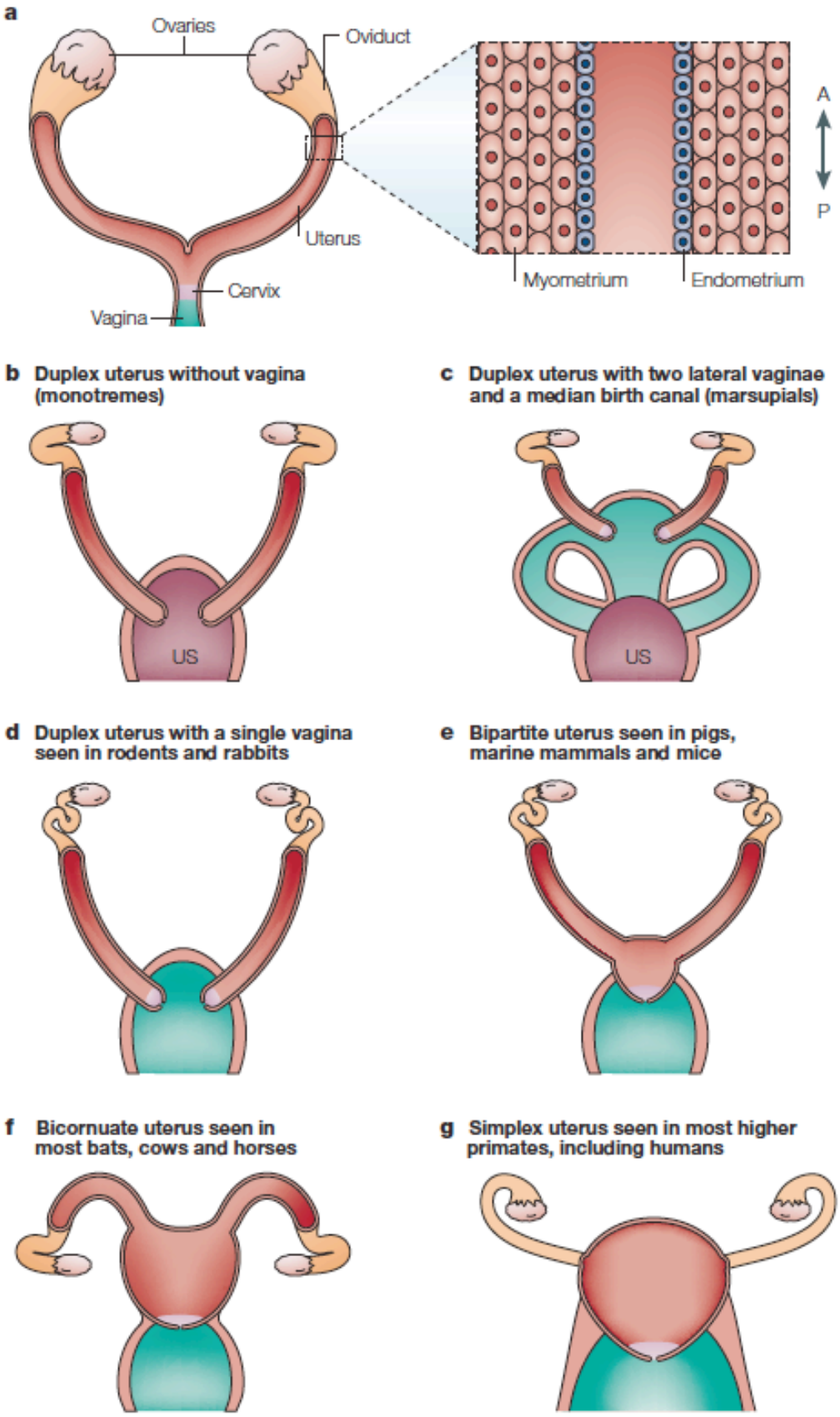


Figure 1.3: Types of uteri amongst different mammalian species. Basic anatomical features of the female reproductive tract (a) and amongst different mammalian species (b-g). Diagram adapted from Kobayashi and Behringer (2003). US-urogential sinus

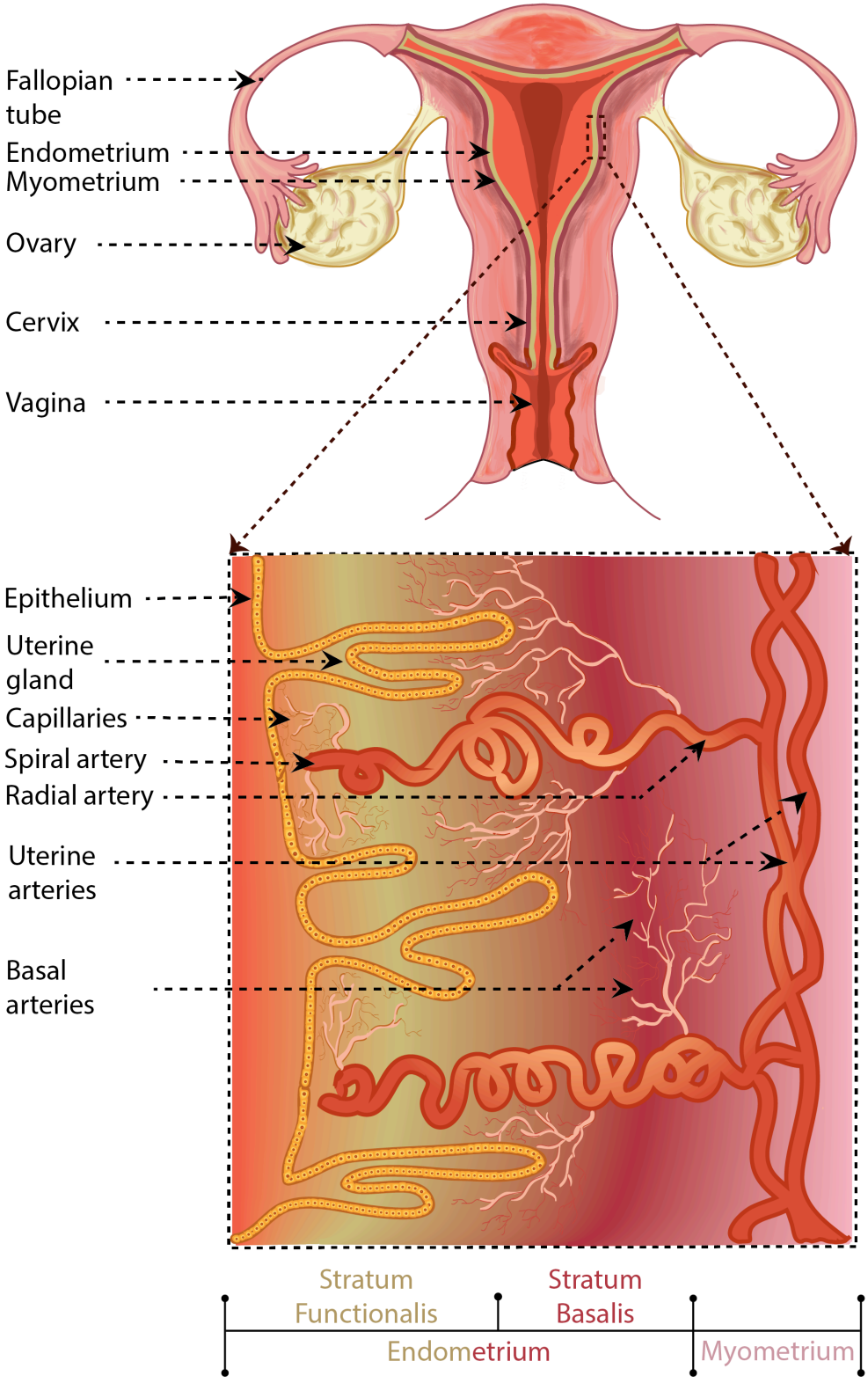


Figure 1.4: Uterine vasculature. Arcuate arteries form the radial arteries, which in turn branch into basal and spiral arteries. While basal arteries supply the basal layer, spiral arteries supply the functional layer of the endometrium. Diagram drawn by the author.

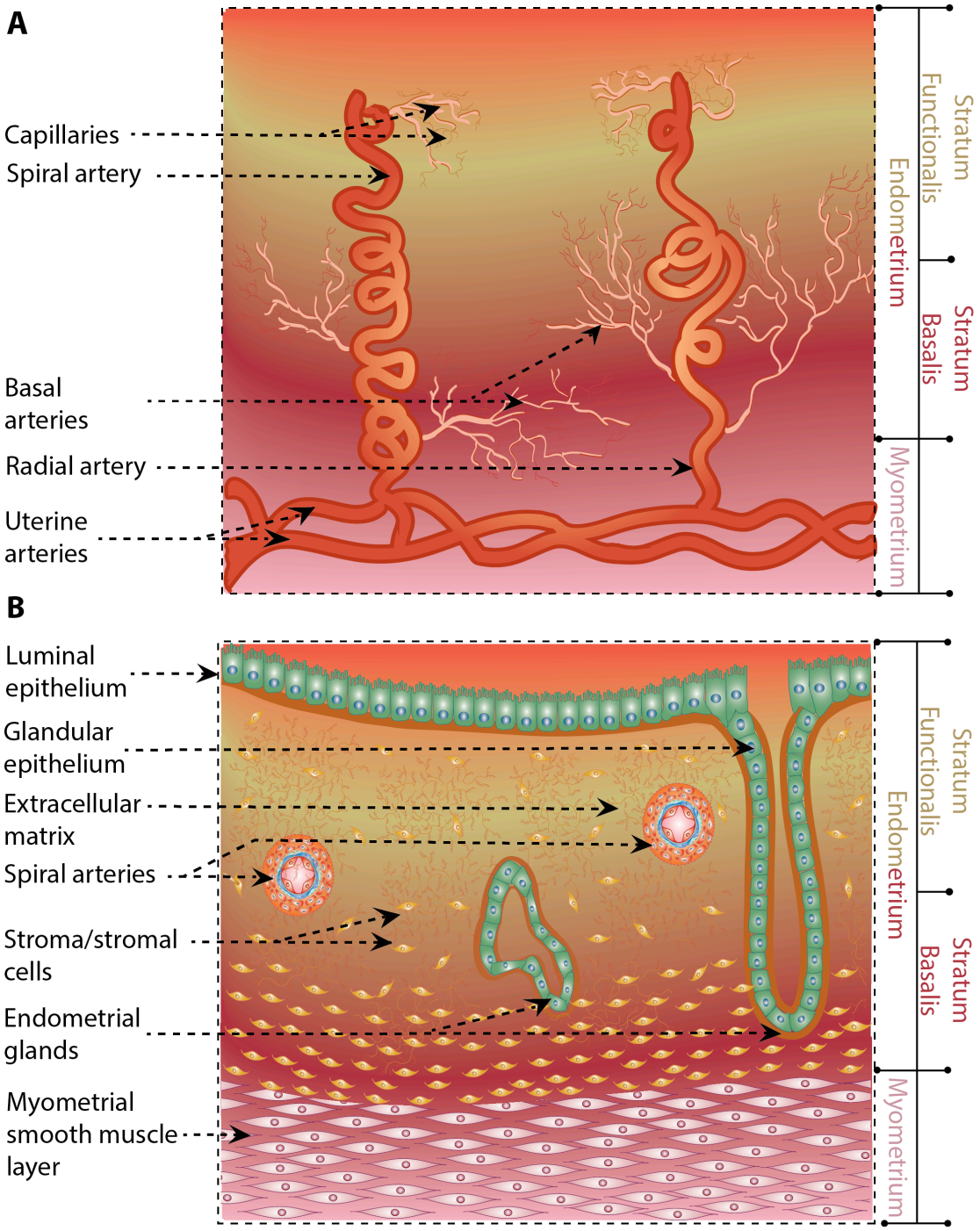


Figure 1.5: Structure of the endometrium. (**A**) The blood supply to the endometrium through the spiral arteries and capillary bed. (**B**) The cellular components of the stratum functionalis and stratum basalis of the endometrium.

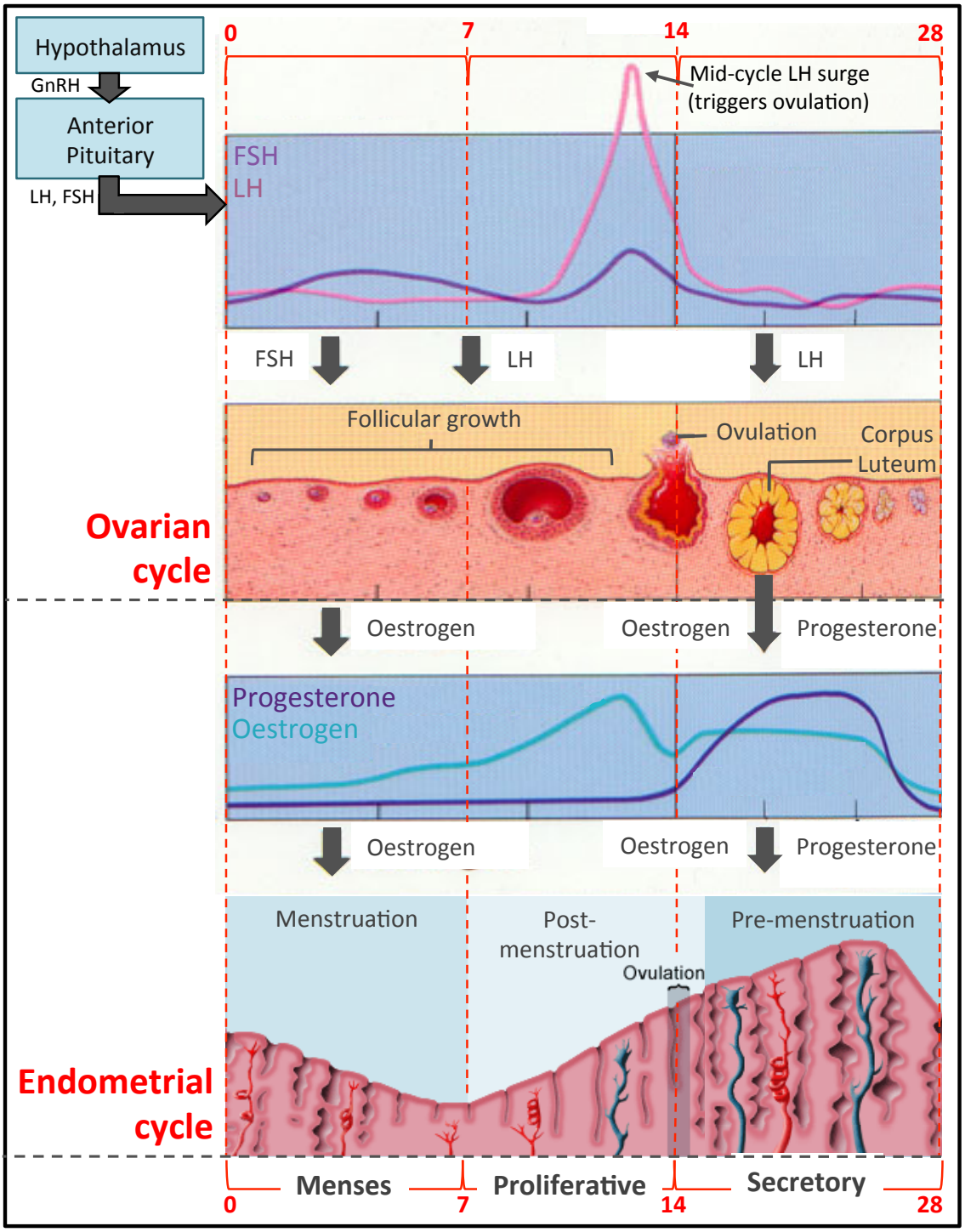


Figure 1.6: Hormonal control of the menstrual cycle with relation to ovulation and the changes in the endometrium. Diagram compiled and modified by the author from lpch.org; SBayram. GnRH-gonadotropin releasing hormone; LH-luteinising hormone; FSH-follicle stimulating hormone.

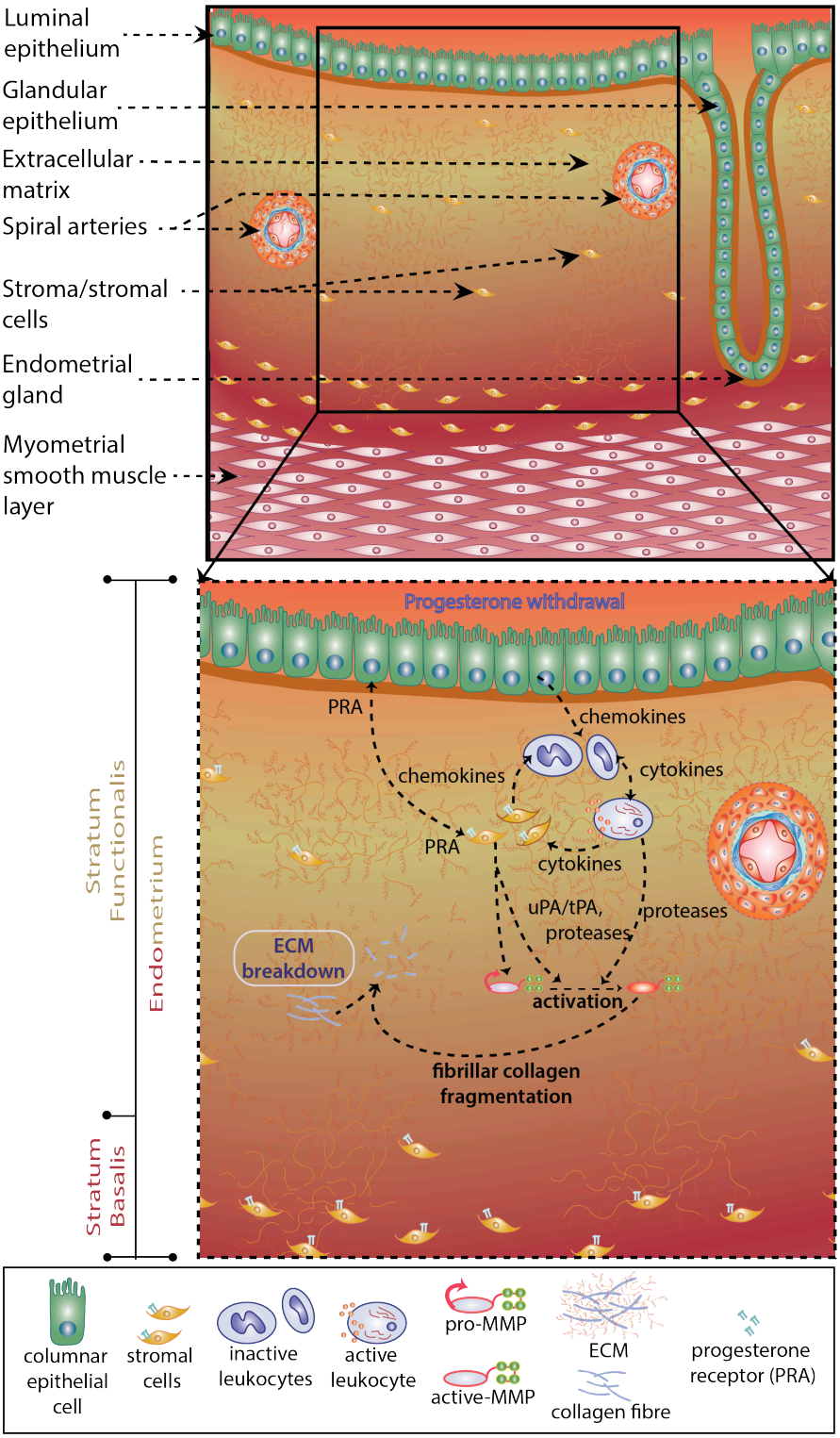


Figure 1.7: Tissue destruction at menstruation. Progesterone withdrawal affects epithelial cells to stimulate chemokine production, which activates leukocytes. Leukocytes produce cytokines, which stimulate production of latent (pro) matrix metalloproteinases (MMPs), chemokines and other mediators. Leukocytes also produce proteases that start the activation cascade of MMPs. Activation of pro-MMPs can also be triggered by other proteases or by the plasmin system (uPA/tPA) released either by stromal cells or by inflammatory cells. An increase in MMPs leads to an imbalance between the activators and inhibitors of tissue breakdown, leading to breakdown of extracellular matrix (ECM).

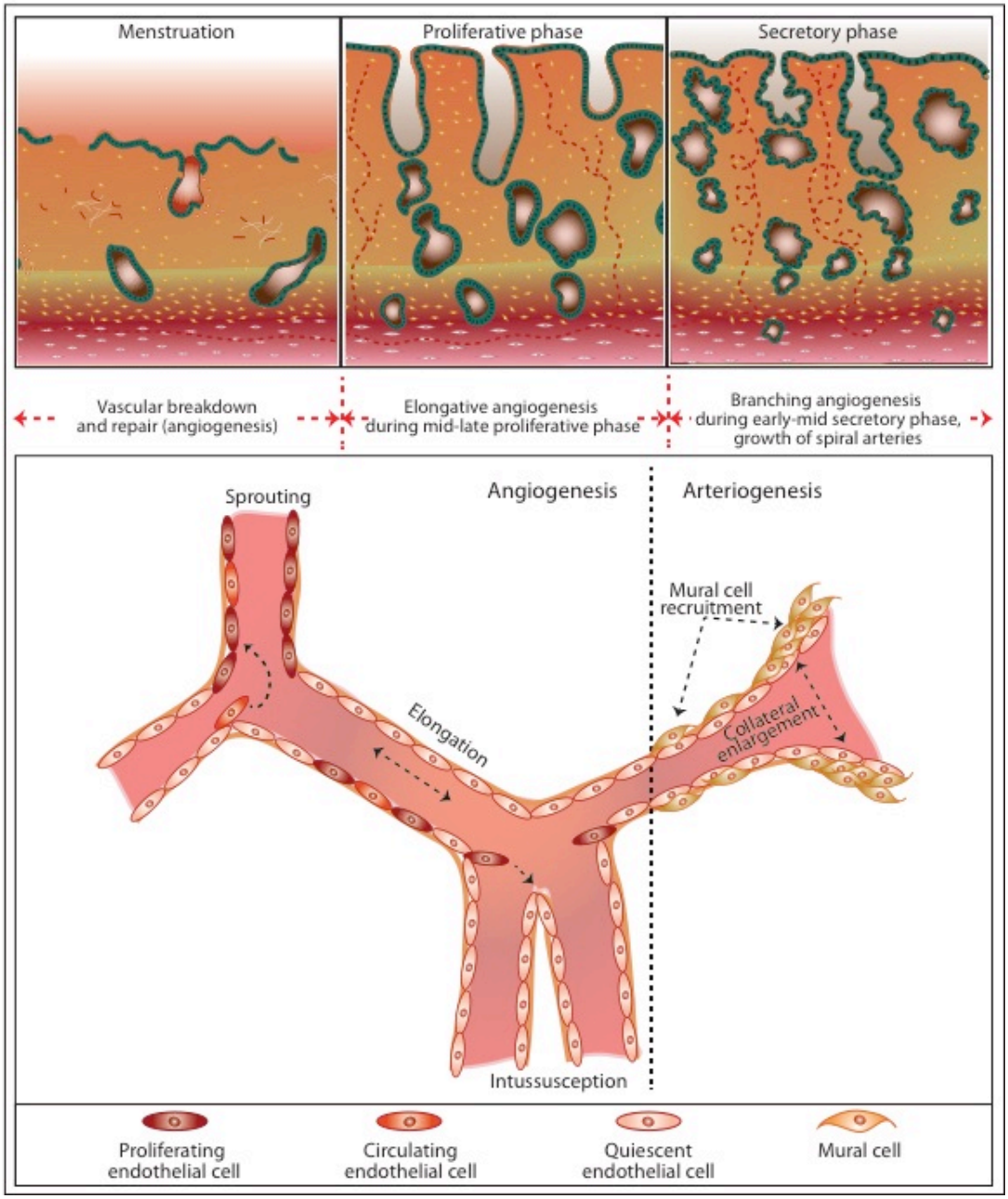


Figure 1.8: Mechanisms of angiogenesis and arteriogenesis. While angiogenesis involves sprouting, intussusception or elongation, arteriogenesis involves *de-novo* arteriole formation from new or pre-existing capillaries by recruitment of pericytes or vascular smooth muscle cells (mural cells) and by collateral enlargement. Elongative angiogenesis occurs in the mid-late proliferative phase while branching angiogenesis is common in the early-mid secretory phase of the menstrual cycle. Diagram re-drawn by author with reference to Aplin *et al.* (2008a).

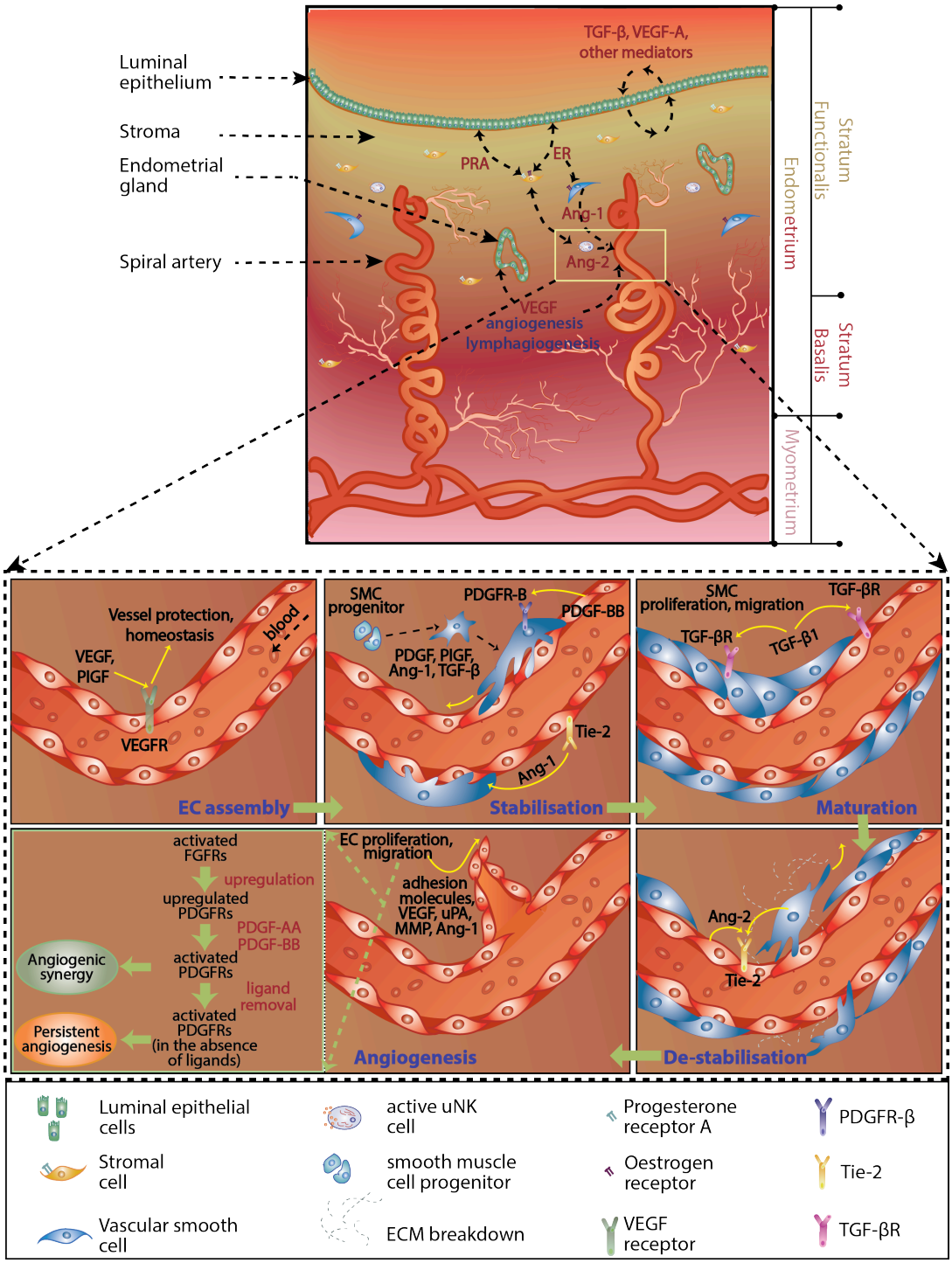


Figure 1.9: Major pathways involved in angiogenesis and arteriogenesis. Angiogenic factors bind to their receptors and activate the endothelial cells (ECs). EC activation releases proteases, which dissolve basement membrane and start the process of EC assembly via proliferation and migration. While the VEGF receptors maintain normal vasculature, platelet derived growth factor (PDGF) helps to recruit smooth muscle cells (SMCs). Following this transforming growth factor (TGF-β) mediates proliferation and migration of VSMCs to form layers around the EC tube. Once a vessel is mature, a network is formed via destabilization, EC proliferation and migration under actions of VEGF, matrix metalloproteinases (MMPs), and adhesion molecules.

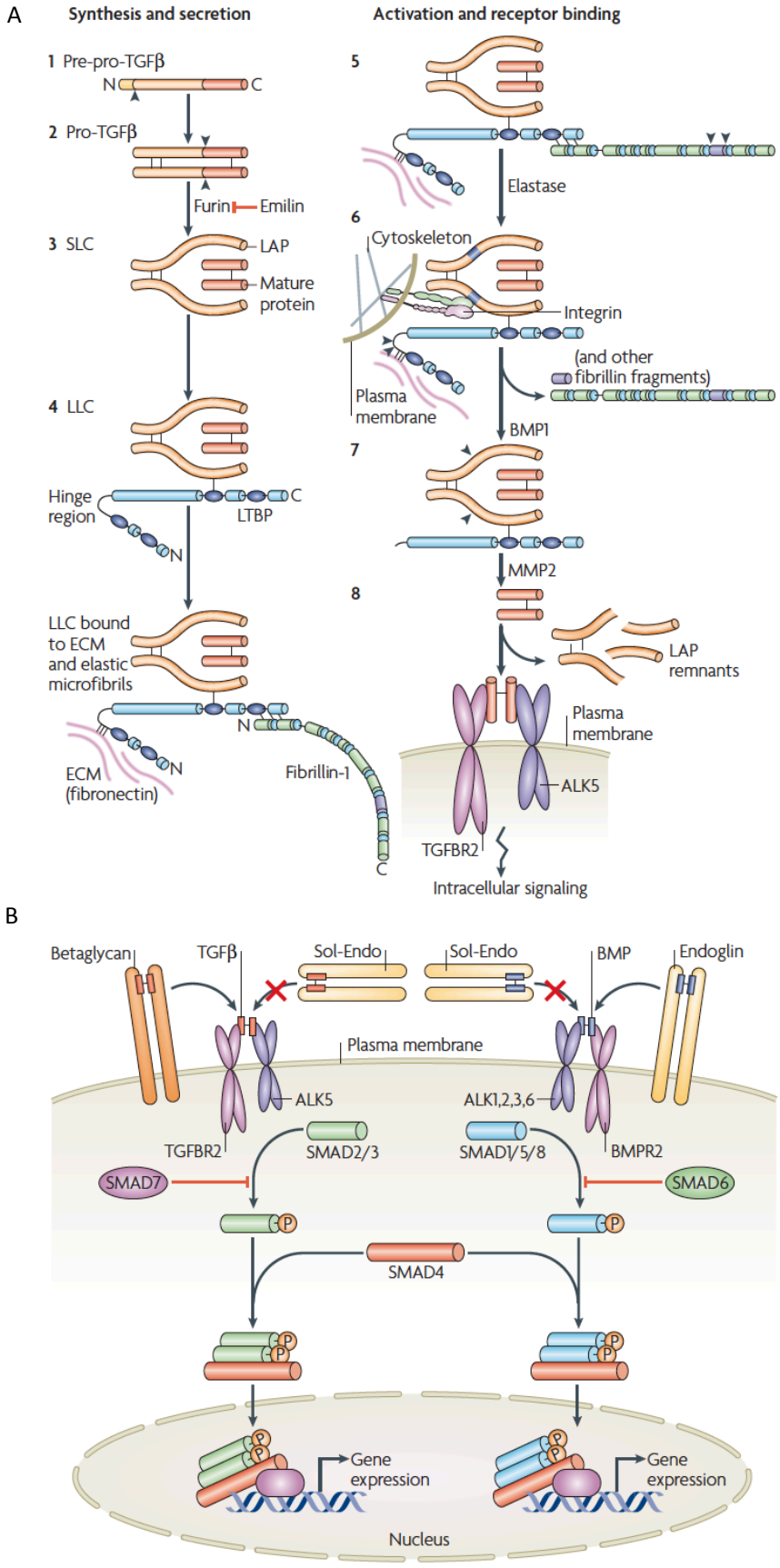


Figure 1.10: The TGFβ regulatory pathway. (**A**) Regulation of TGFβ bioavailability and (**B**) the TGFβ signal transduction pathway. Diagram adapted from ten Dijke and Arthur (2007).

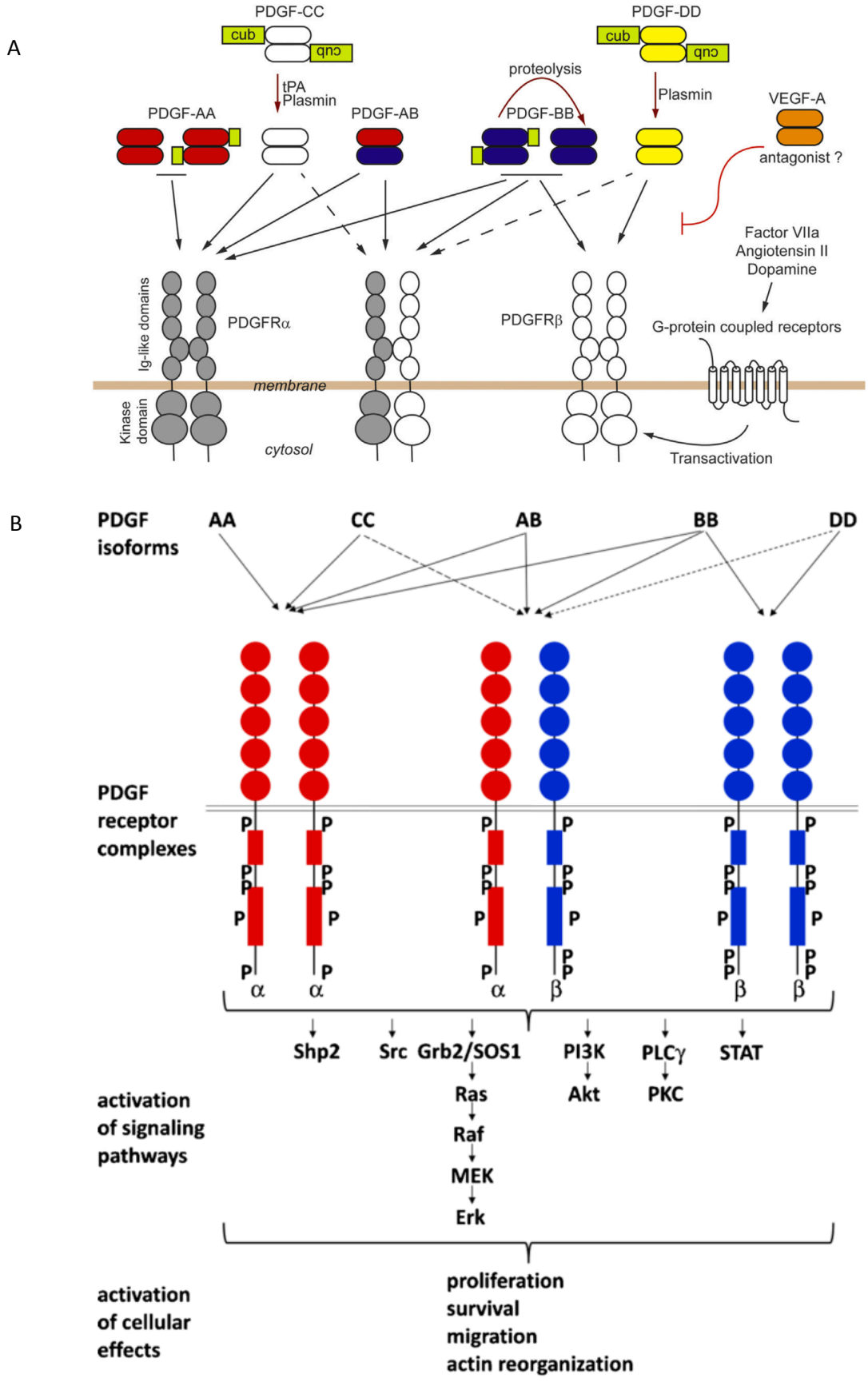


Figure 1.11: The PDGF regulatory pathway. (**A**) Regulation of PDGF bioavailability and (**B**) the PDGF signal transduction pathway. Diagrams (**A**, **B**) adapted from Demoulin and Essaghir (2014), Heldin (2014) respectively.

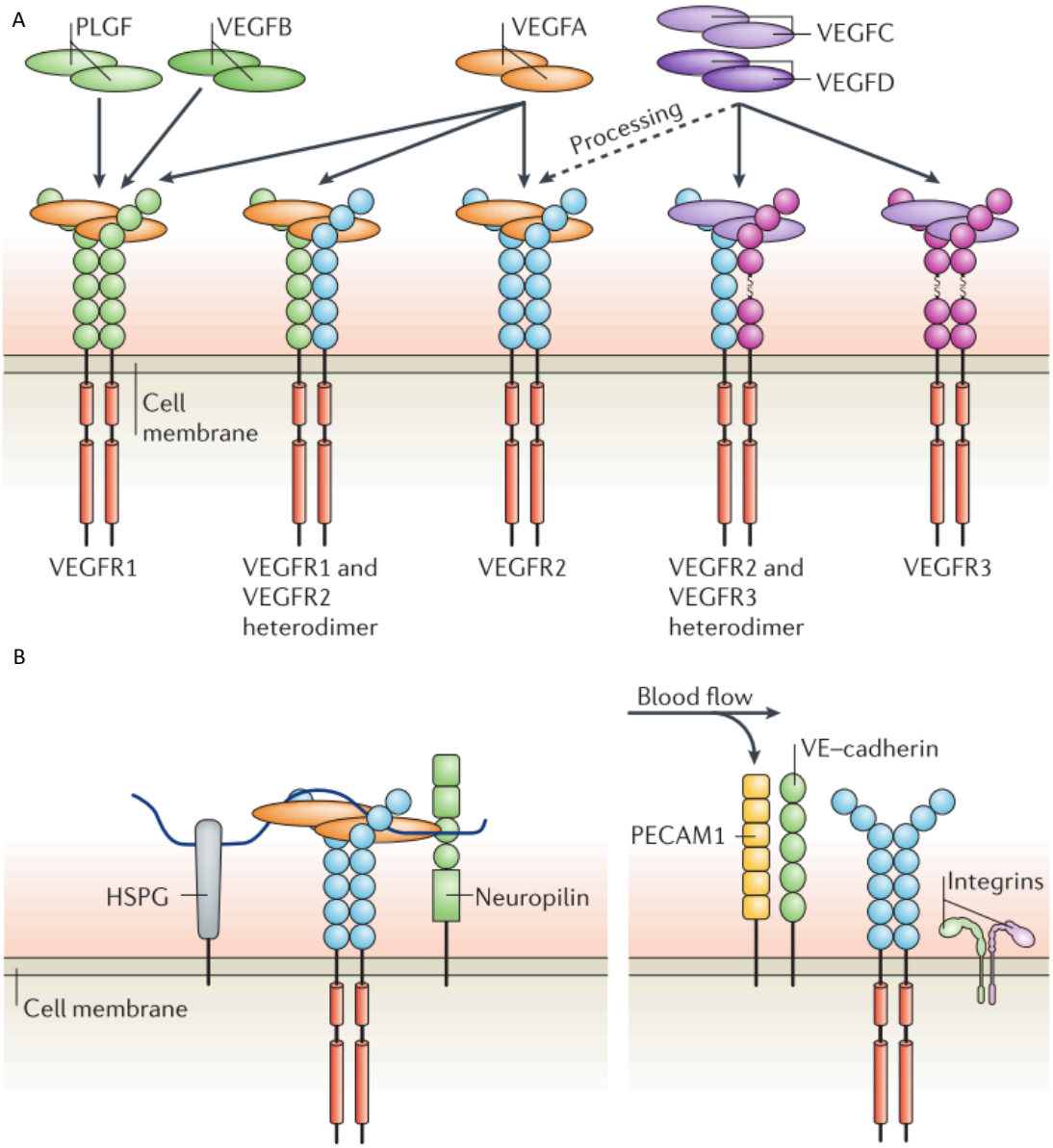


Figure 1.12: The VEGF family. (**A**) The VEGF family of receptors and ligands and (**B**) co-receptors involved in VEGF pathway. Diagram adapted from Olsson *et al.* (2006).

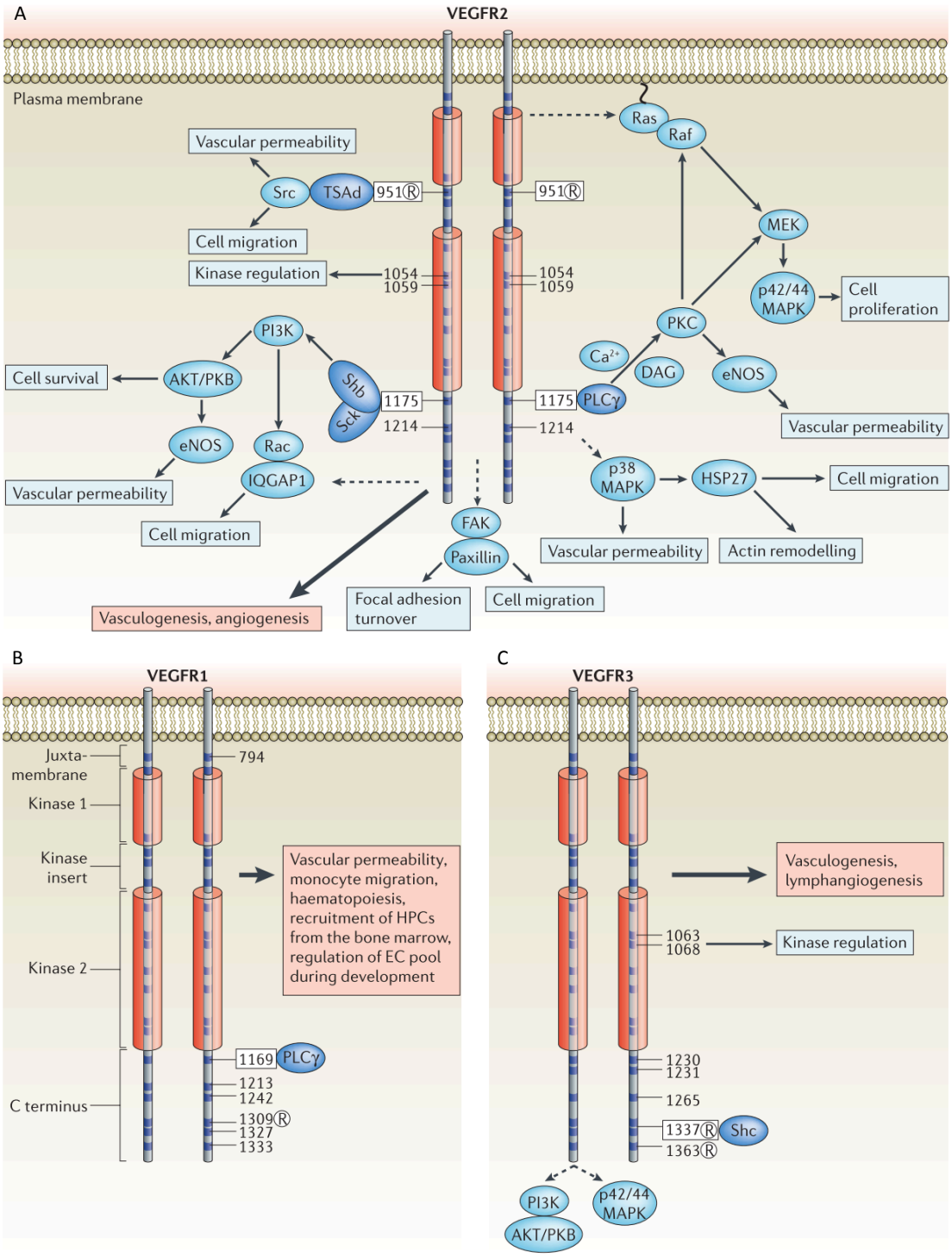


Figure 1.13: The VEGF regulatory pathway via (**A**) VEGFR1, (**B**) VEGFR2 and (**C**) VEGFR3. Diagram adapted from Olsson *et al.* (2006).

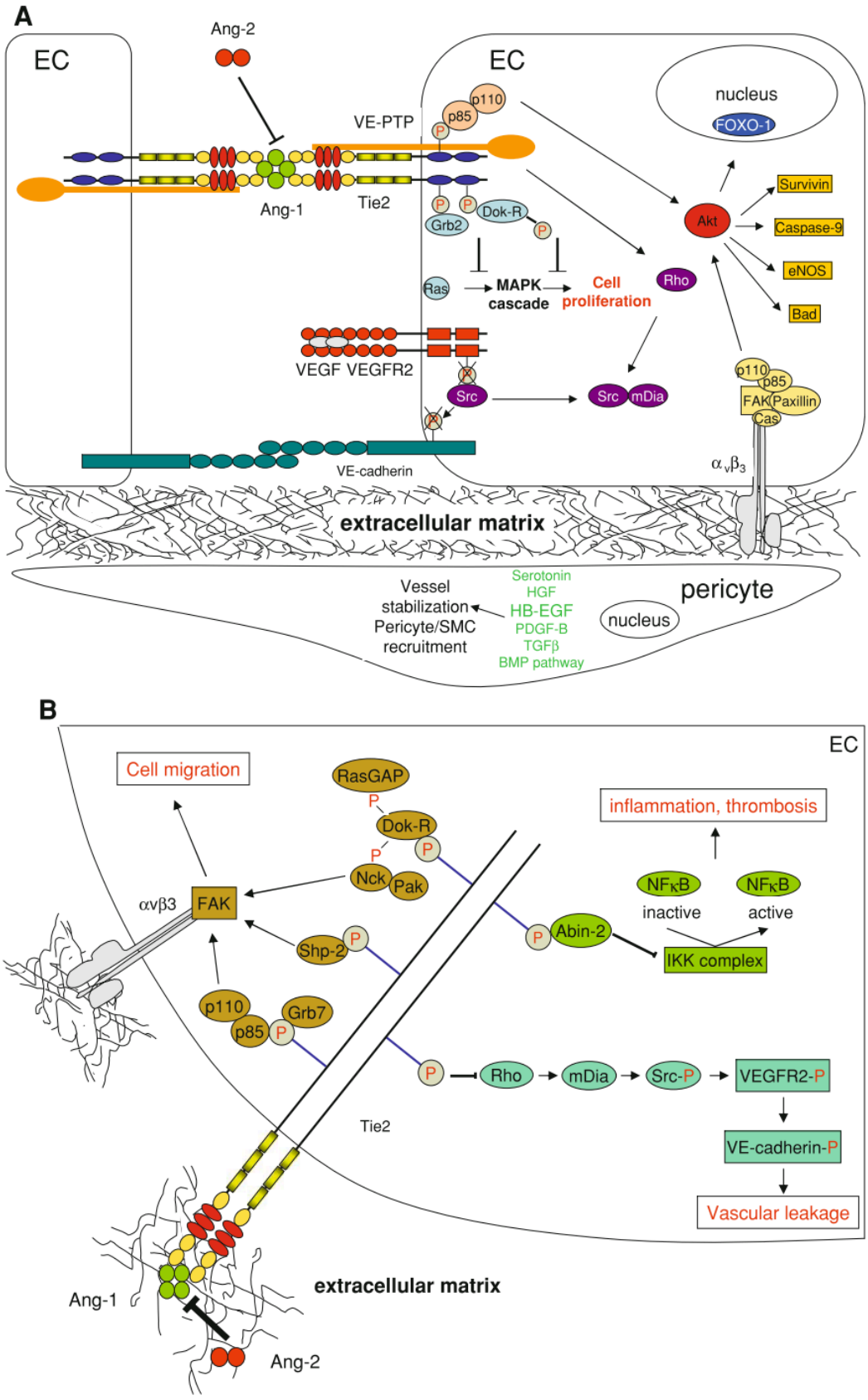


Figure 1.14: The angiopoietin regulatory pathway. Angiopoietin signaling pathways involved in (**A**) cell proliferation and (**B**) cell migration, vascular leakage and inflammation. Diagram adapted from Thomas and Augustin (2009).

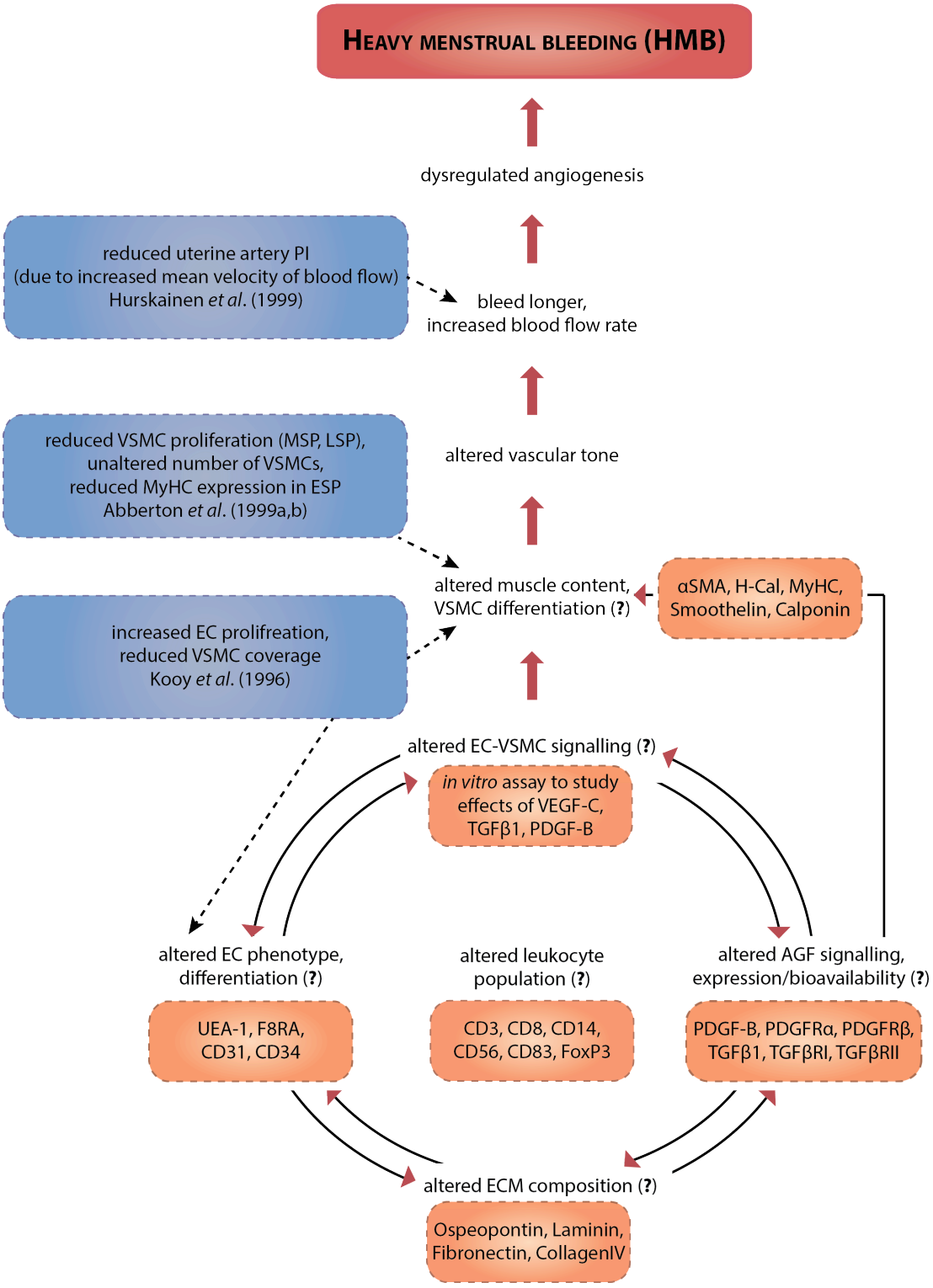


Figure 1.15: Factors involved in dysregulation of angiogenesis underlying HMB. This study aims to investigate the factors highlighted in orange. ESP-early secretory phase; MSP-mid secretory phase; LSP-late secretory phase; PI- pulsatility index.

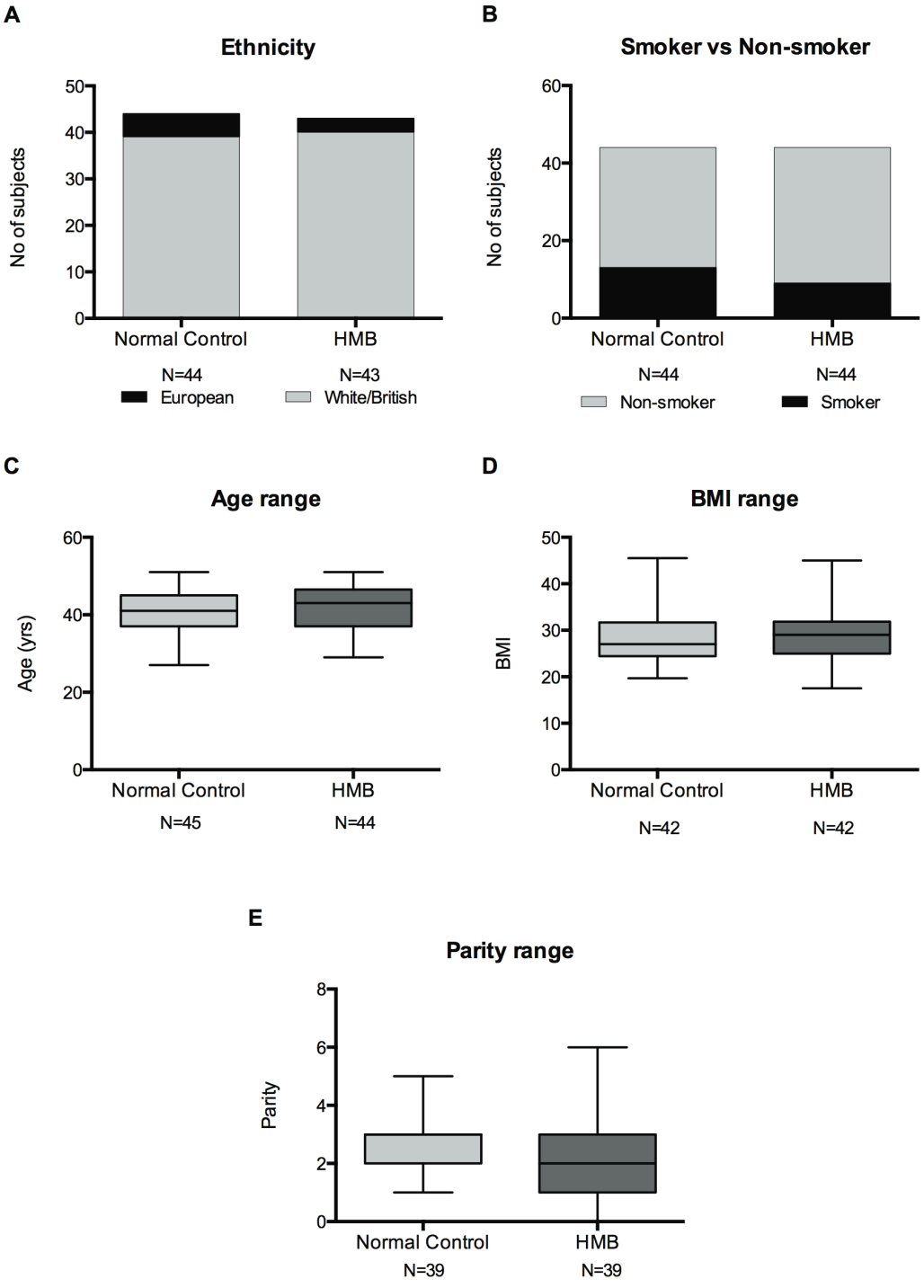


Figure 2.1: Demographic details of control and menorrhagia groups. In **A** and **B** the stacked bars represent number of patients in each of control and heavy menstrual bleeding (HMB) groups, while the different colours represent their ethnic origin or smoking history, respectively. In **C**, **D** and **E** the box plots (median indicated with black line, within each box) compares the age range, body mass index (BMI) and parity between control and HMB groups, respectively. Chi-square test (ethnicity, smoking history), Fisher's test followed by unpaired Student's t-test (age and BMI) and Mann-Whitney test (parity) indicated no statistical significance ($P>0.05$). Variation in patient number (N) in (**A**-**E**) is due to availability of different information.

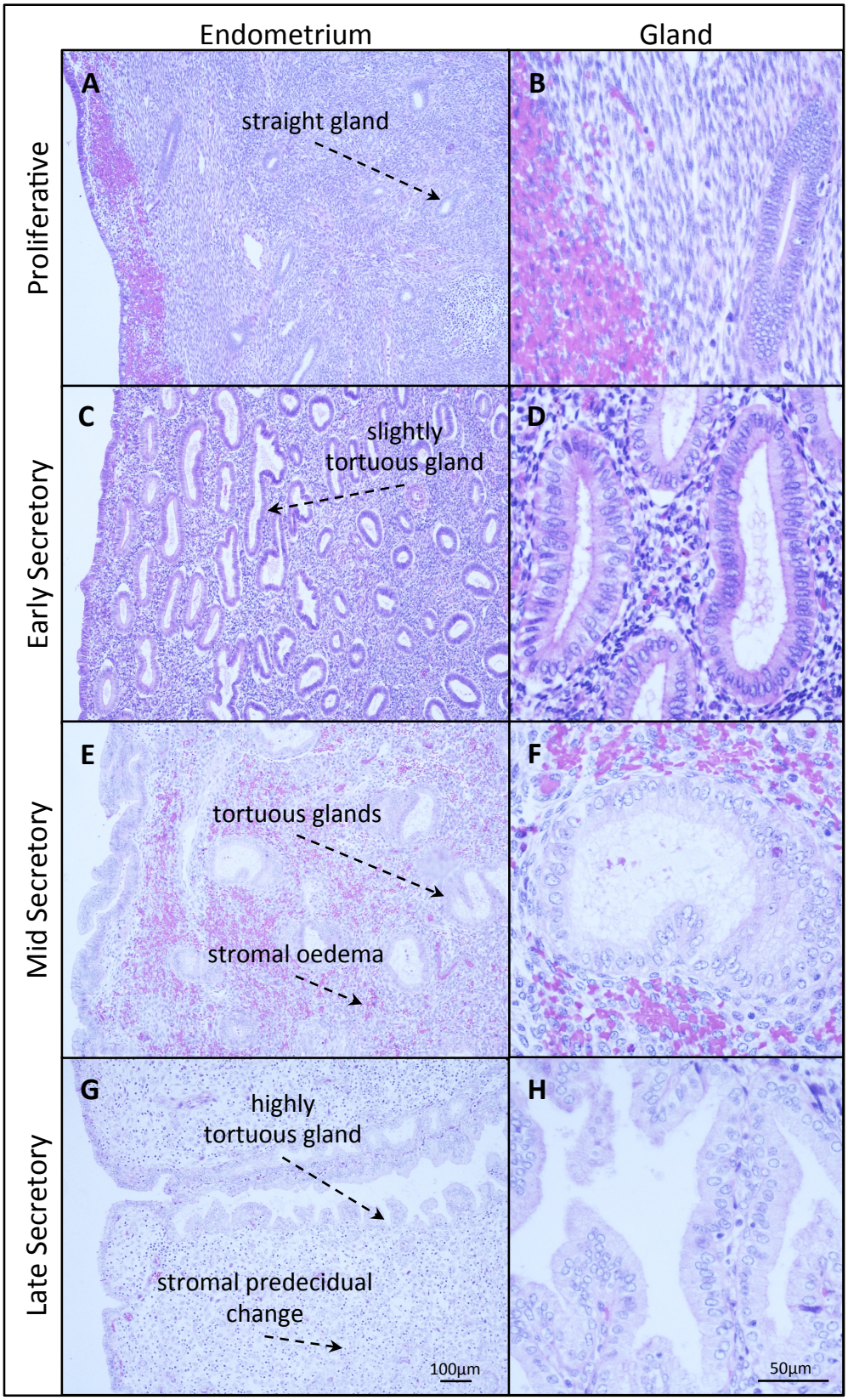


Figure 2.2: Haematoxylin and eosin stained human endometrium (**A**, **C**, **E**, **G**; 100x original magnification) and endometrial glands (**B**, **D**, **F**, **H**; 400x original magnification). Arrows indicate respective changes at the different stages of the menstrual cycle.

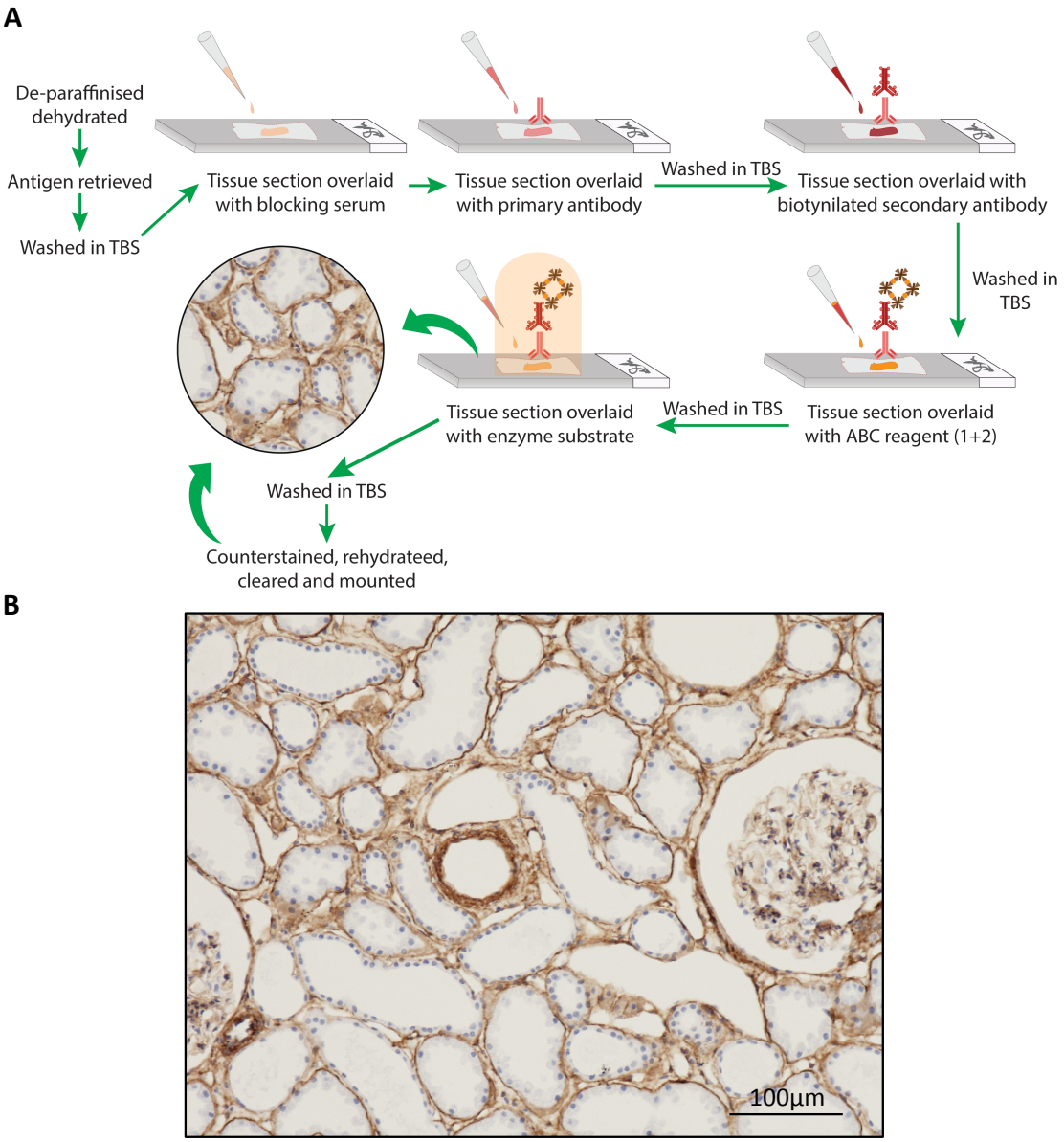


Figure 2.3: (**A**) The avidin-biotin complex (ABC) method for immunohistochemical staining. (**B**) Formalin fixed paraffin embedded 3µm section of human kidney positively stained for collagen-IV using ABC method (200x original magnification).

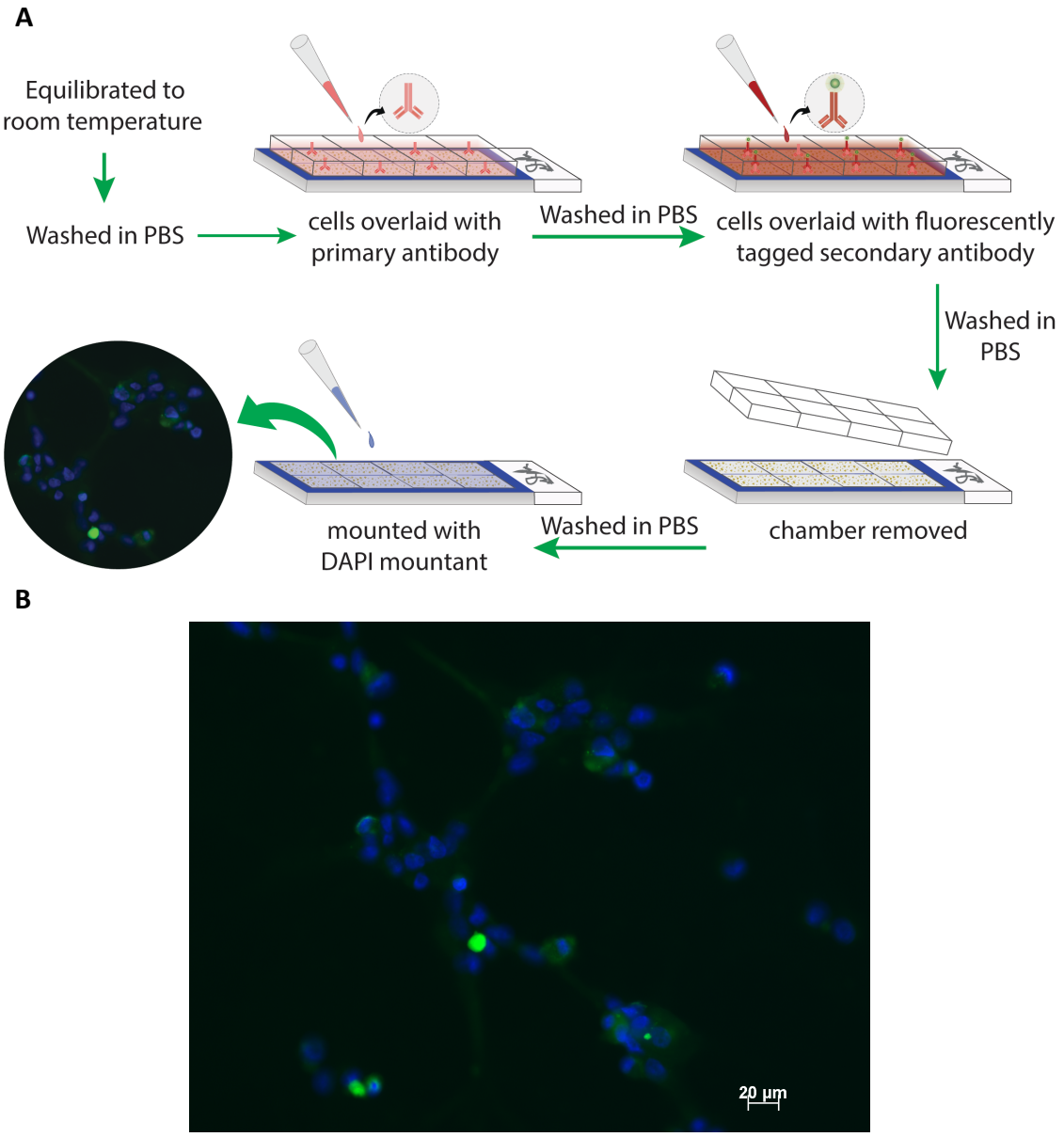


Figure 2.4: (**A**) Immunofluorescent staining of 8-well chamber slides. (**B**) Ethanol fixed, frozen human saphenous vein derived vascular smooth muscle cells positively stained for αSMA (FITC-green) and nuclei (DAPI-blue), 200x original magnification.

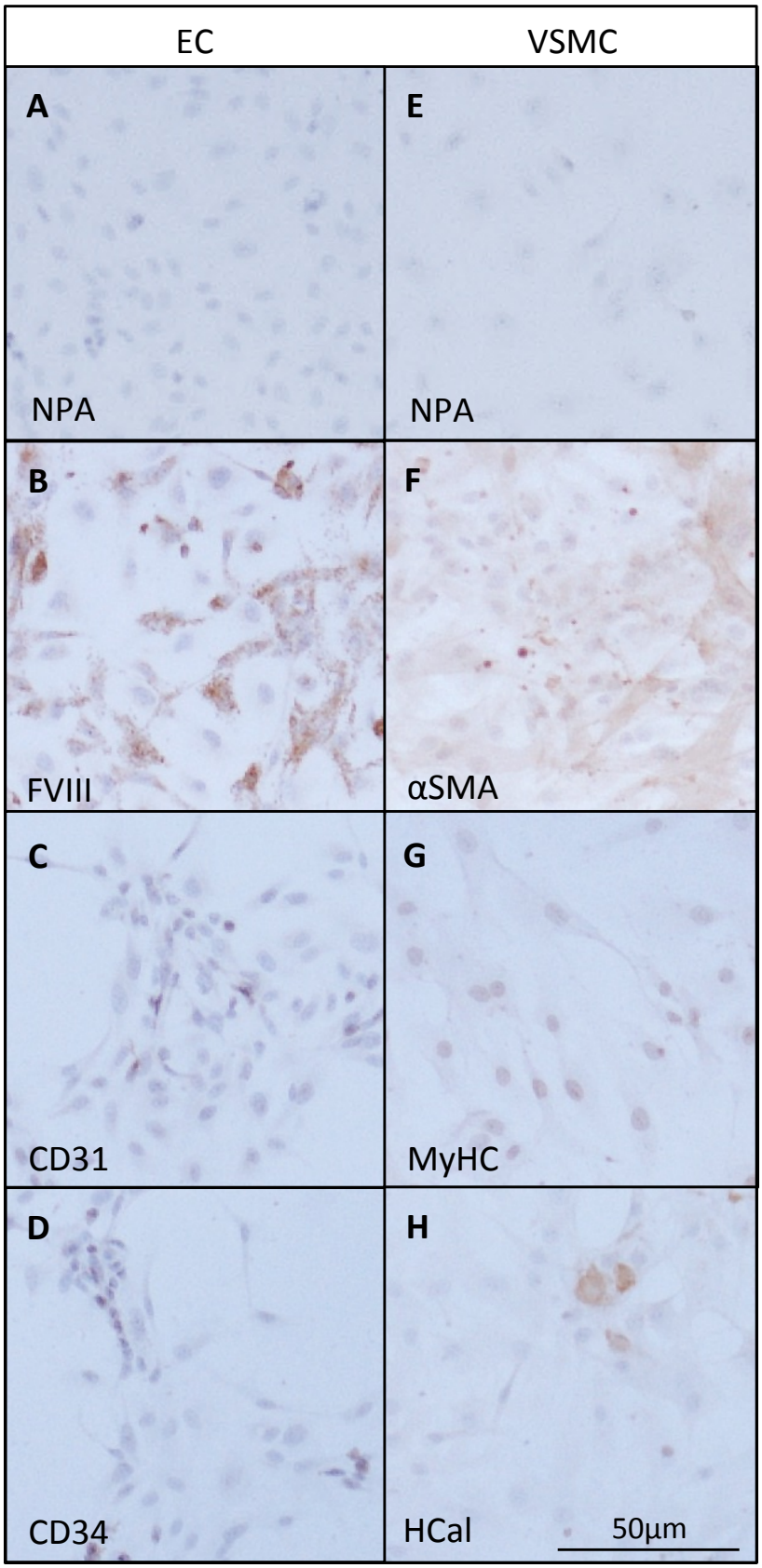


Figure 2.5: Characterisation of saphenous vein derived cells. Ethanol fixed, frozen human saphenous vein derived endothelial cells (**A**-**D**) and vascular smooth muscle cells (**E**-**H**) characterised for their respective markers at passage 4 (200x original magnification).

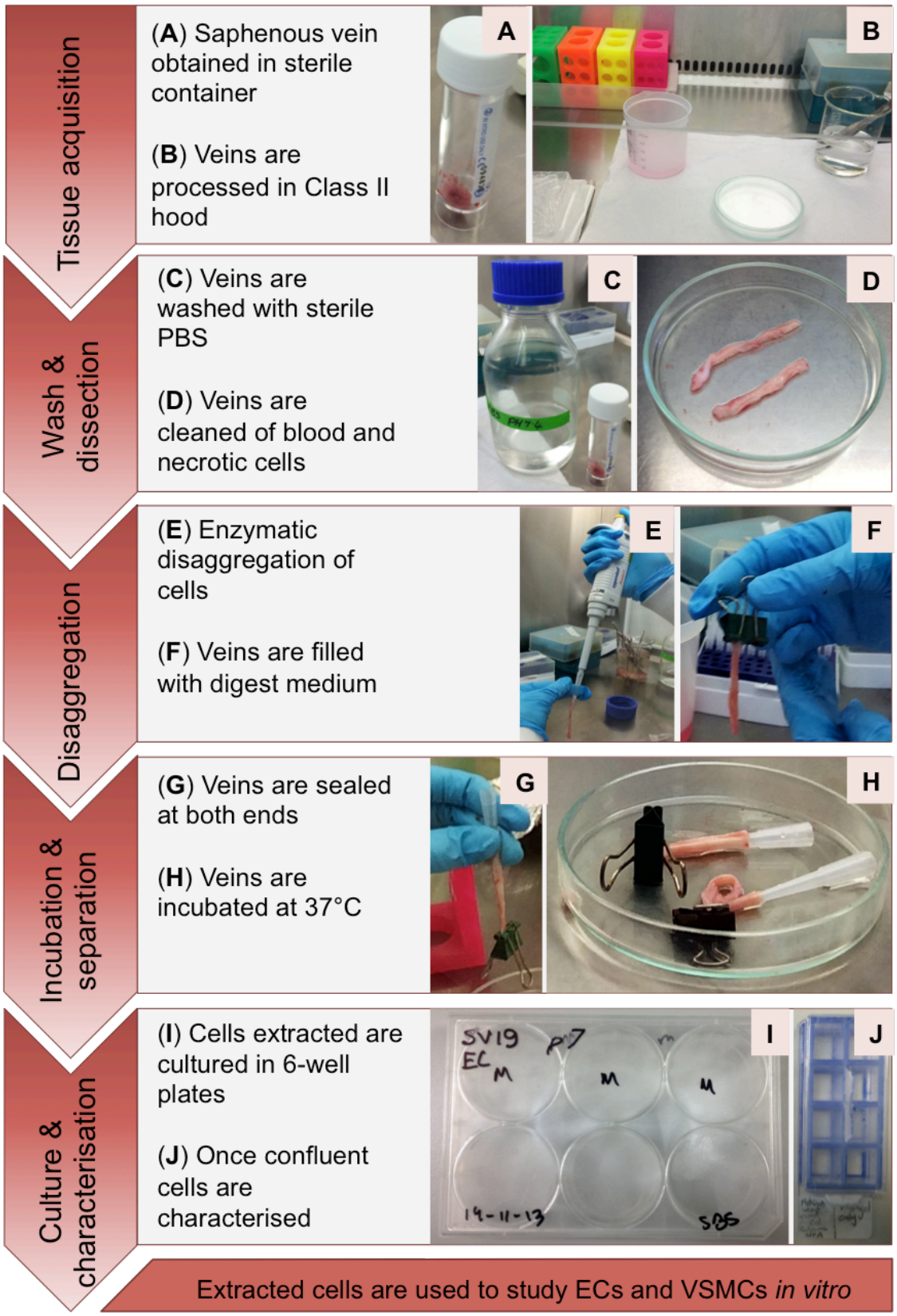


Figure 2.6: Enzymatic disaggregation for ECs or VSMCs from human saphenous veins. The incubation and separation and culture and characterisation steps are repeated two additional times for collection of VSMCs.

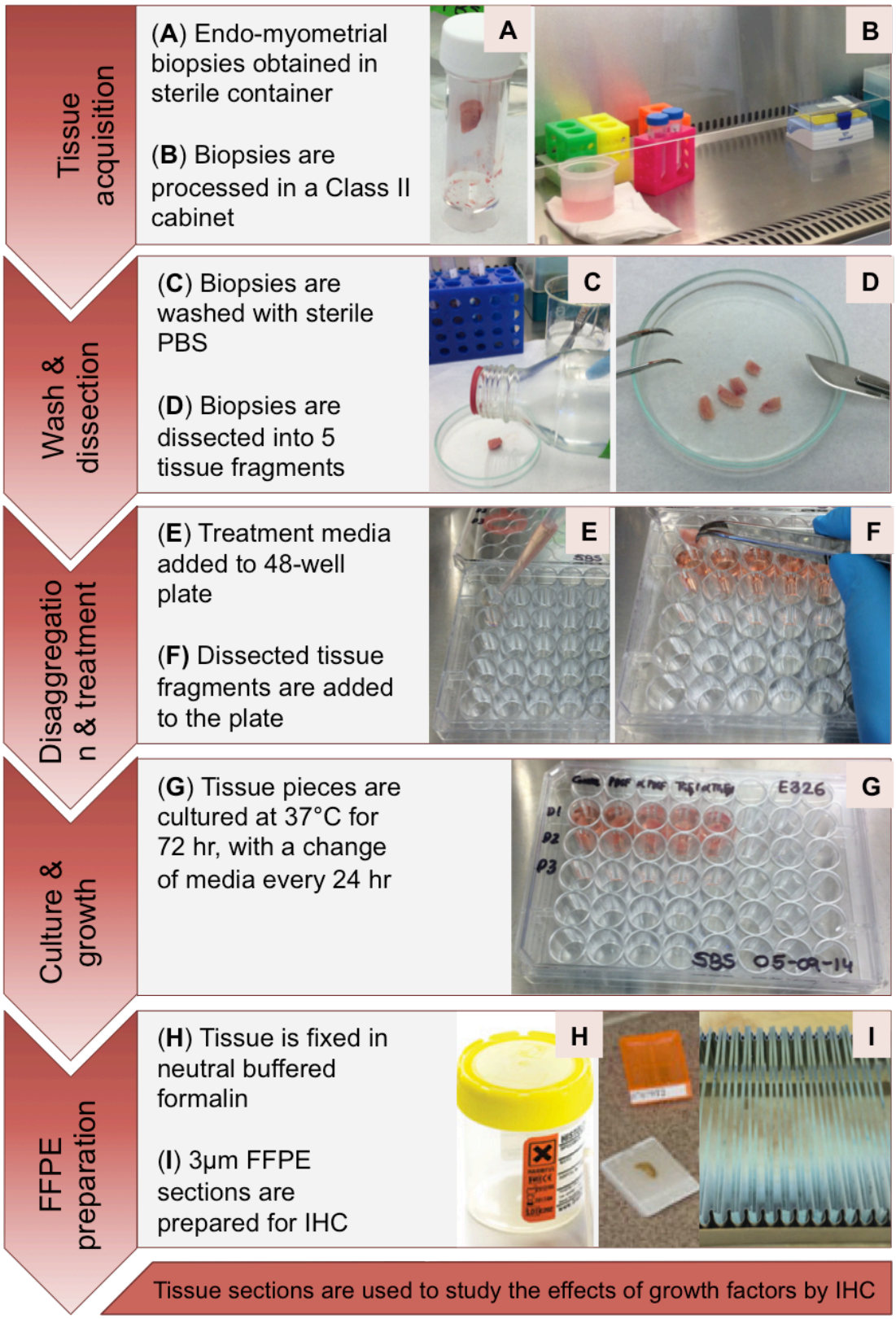


Figure 2.7: Human endometrial explant culture.

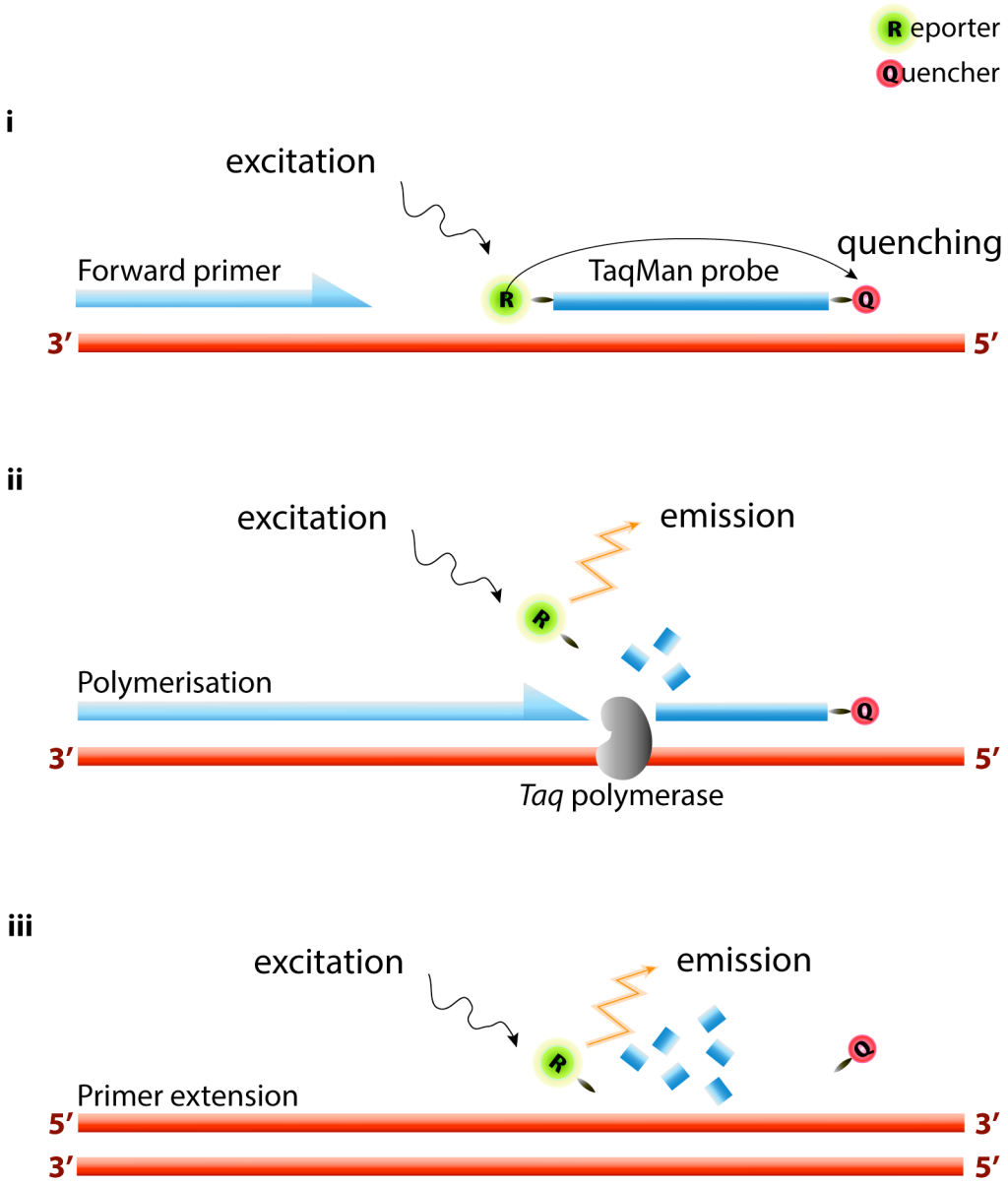


Figure 2.8: Principle behind TaqMan® chemistry. During PCR amplification; (**i**) the TaqMan® probe anneals to the complementary target DNA strand, (**ii**) *Taq* polymerase enzyme cleaves the 5' end of the probe, separating the fluorescent dye from the quencher resulting in an increase in reporter dye signal and (**iii**) removes the probe from the target strand leading to primer extension.

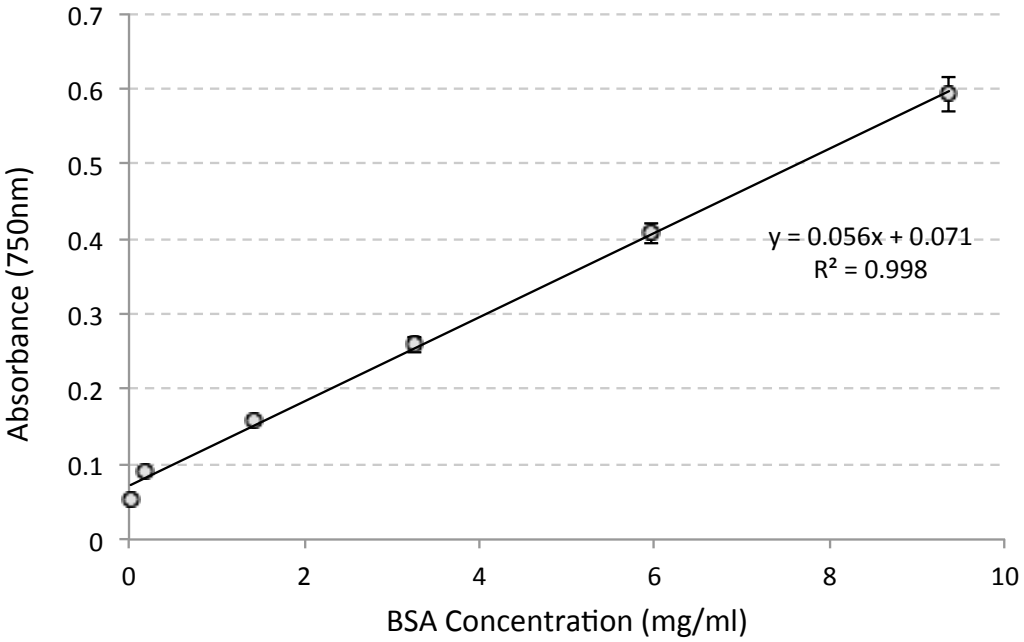


Figure 2.9: Representative standard curve to determine protein concentration. The standard curve was prepared by serially diluting BSA between 0mg/ml and 10mg/ml. The protein concentration in test samples was determined from the standard curve. Error bars are representative of mean ± standard deviation (N=2).

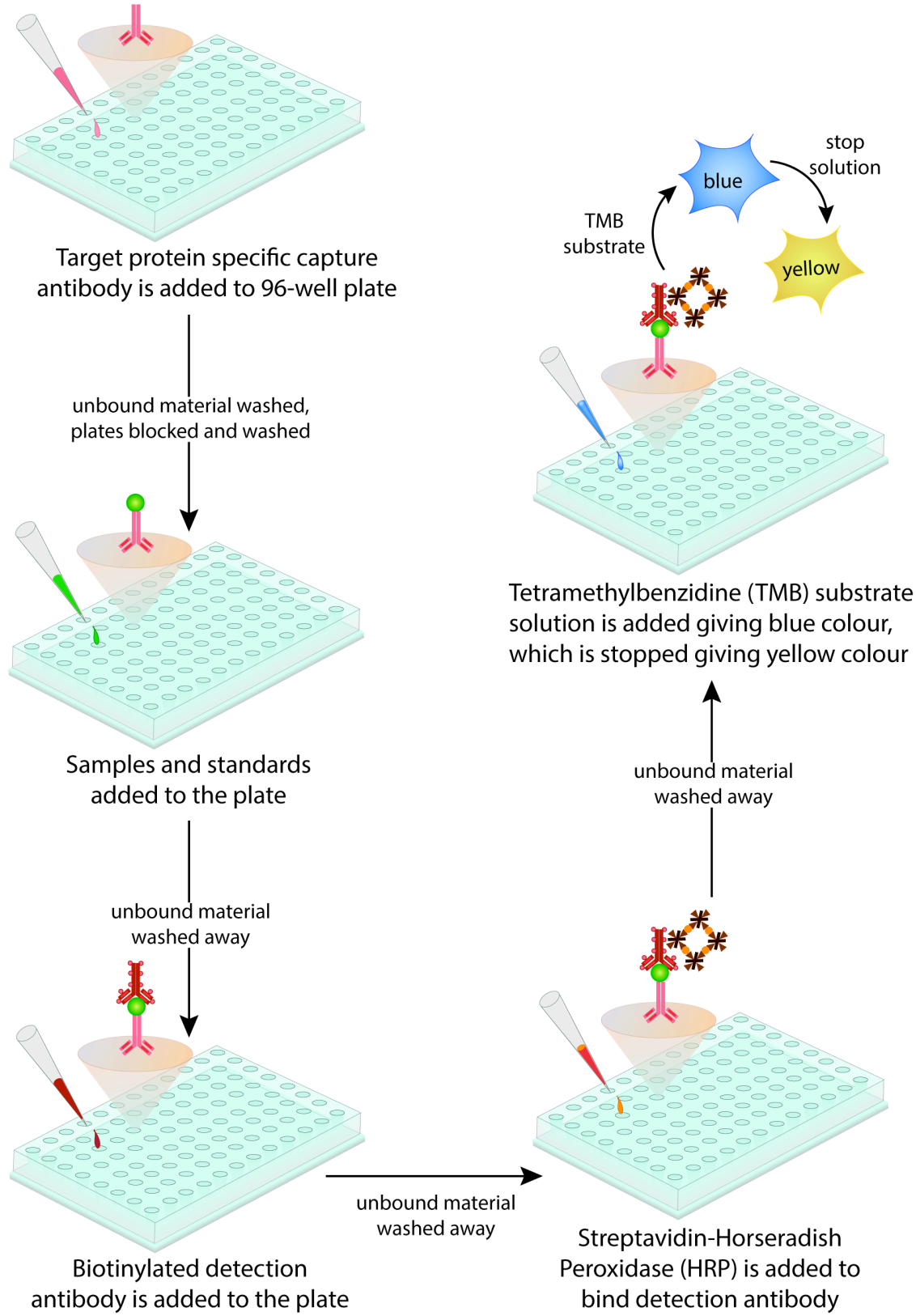


Figure 2.10: Principle behind DuoSet® Sandwich ELISA development system.

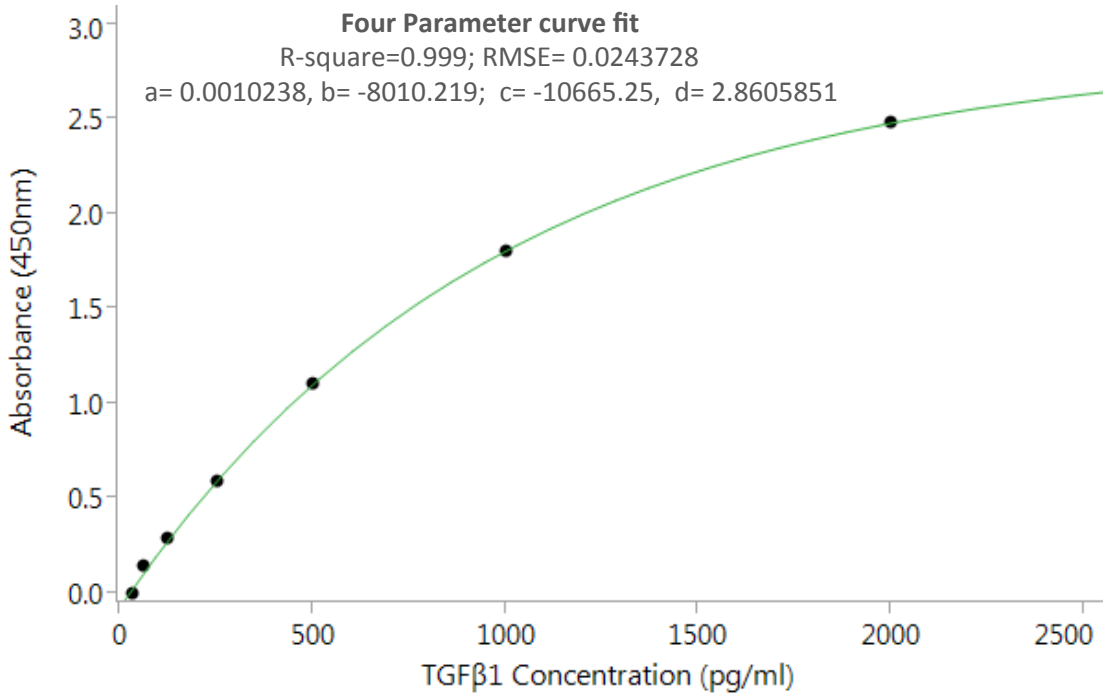


Figure 2.11: Representative standard curve to determine protein concentration using the R&D DuoSet® ELISA kit. The standard curve was prepared for human TGFβ1 ranging from 0pg/ml - 2000pg/ml. Protein concentrations in test samples were determined from the standard curve.

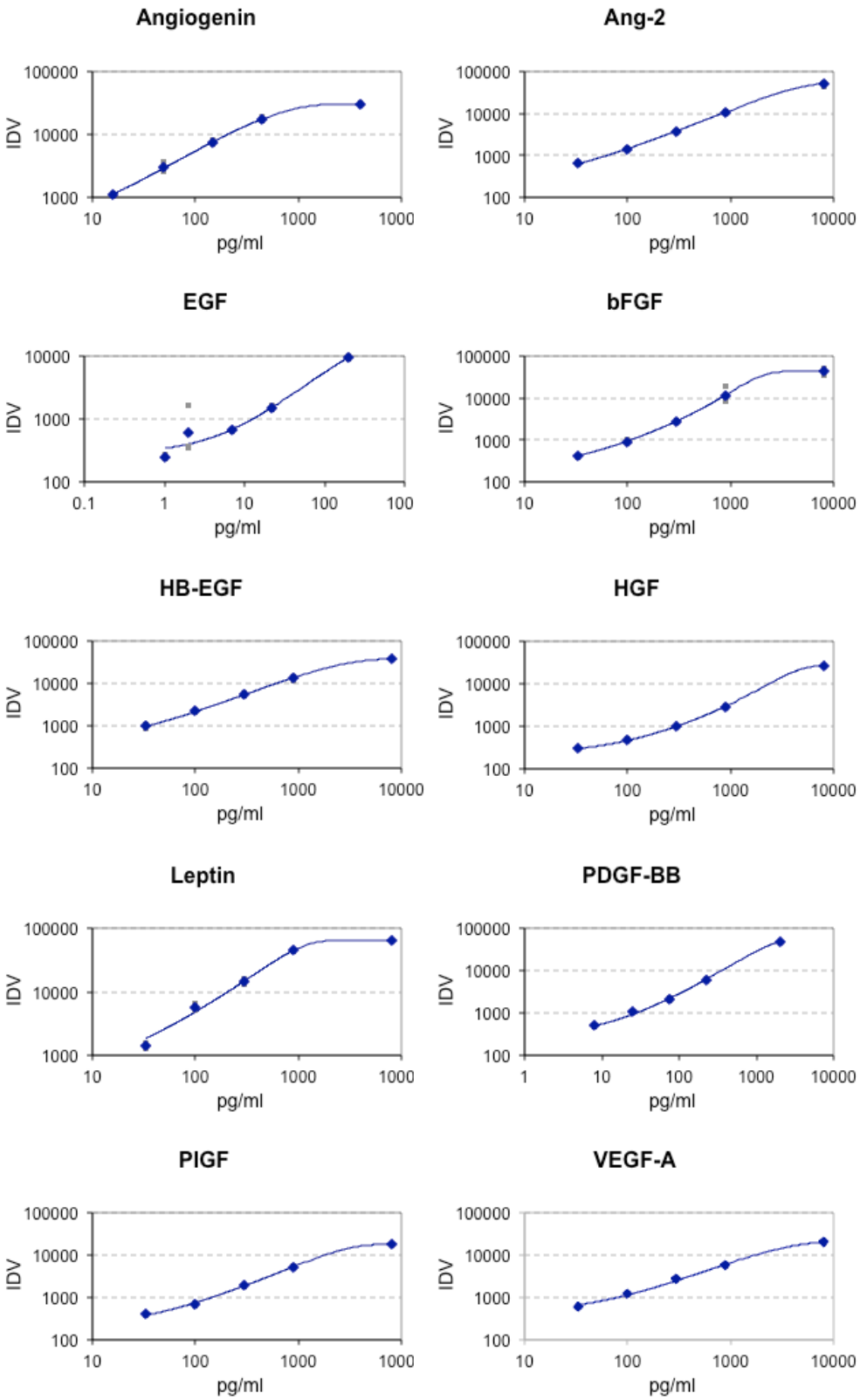


Figure 2.12: Representative standard curves to determine protein concentration using the Quantibody® human angiogenesis array kit. Protein concentrations in test samples were determined from the standard curve.

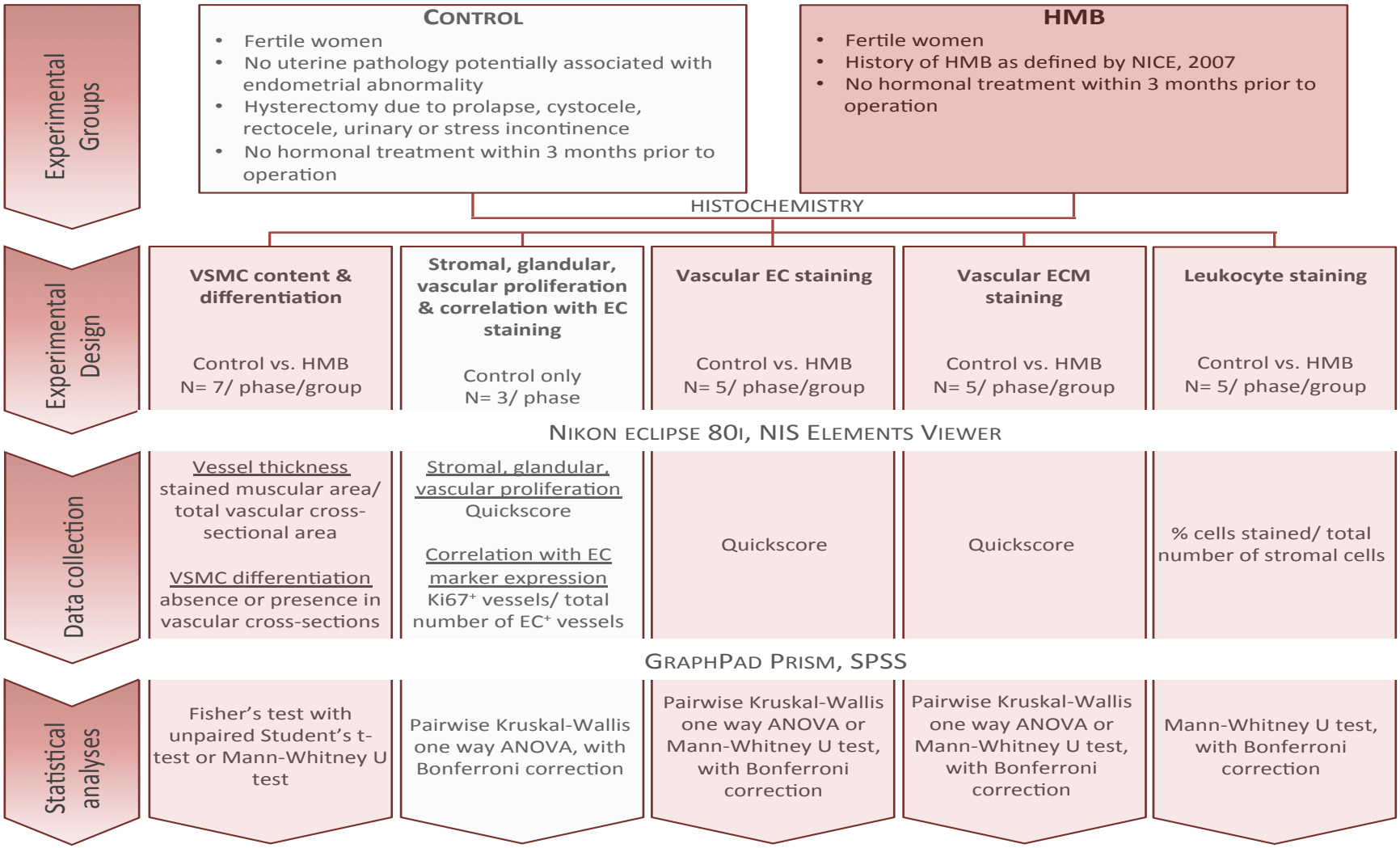


Figure 3.1: Experimental design to investigate histochemical changes in the uterine vasculature of women with HMB.

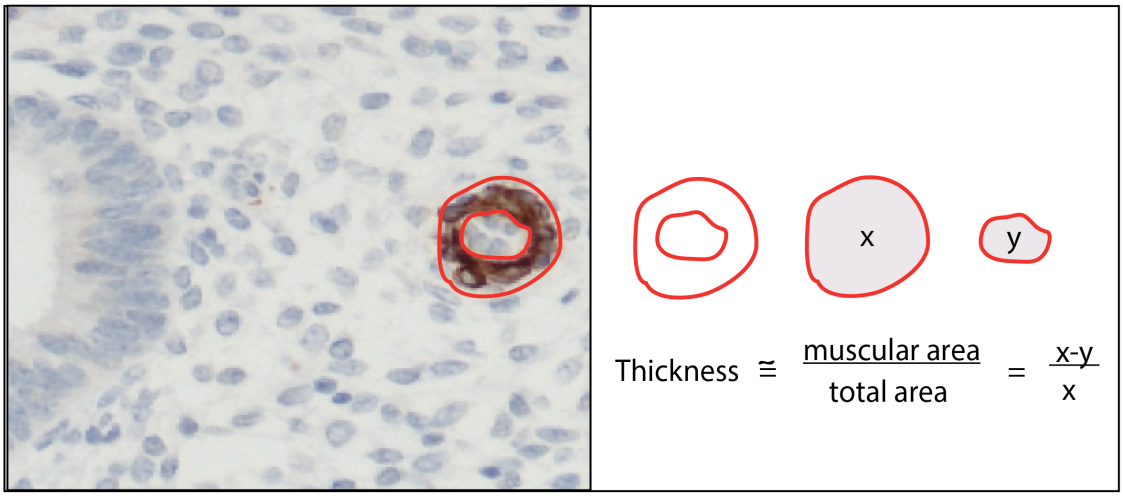


Figure 3.2: Measurement of endometrial vascular wall thickness. Vessel thickness was expressed as the ratio of the outer stained muscular area (x-y) to the total area (x= stained area + inner luminal area) of the vascular cross-section.

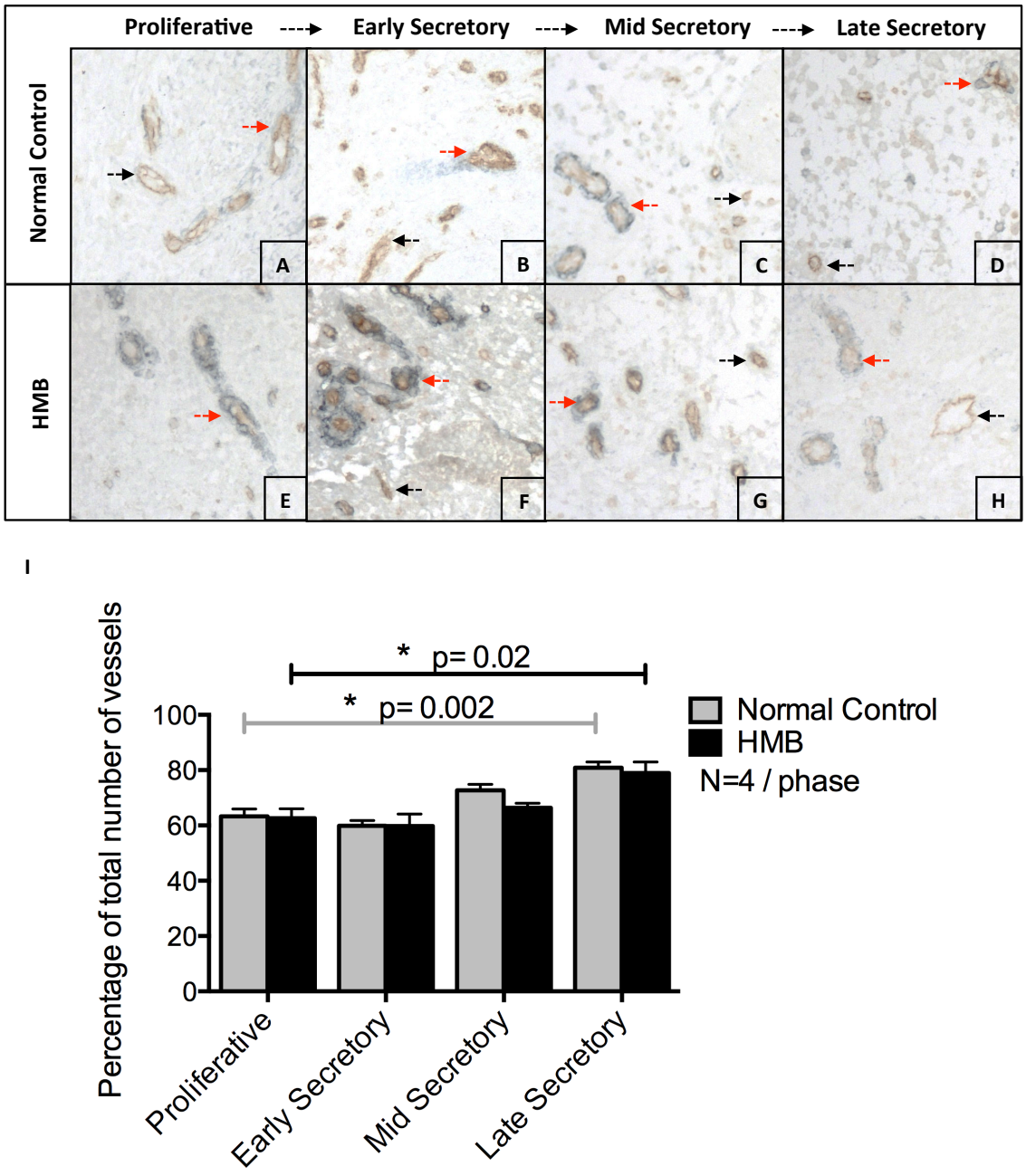
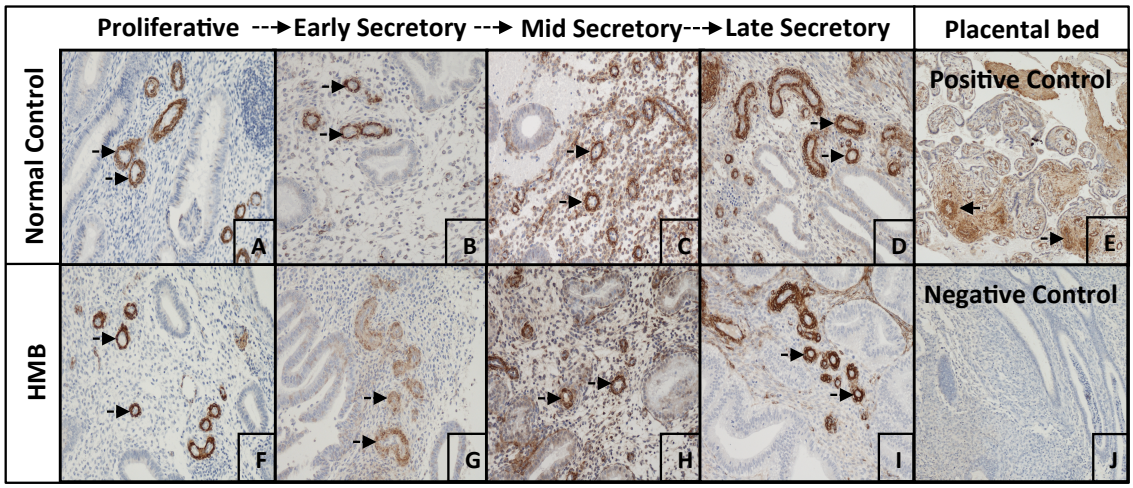


Figure 3.3: The proportion of vessels stained with αSMA in the control menstrual cycle and in heavy menstrual bleeding (HMB). **A-H** shows representative double immunostaining CD31/αSMA (brown/silver grey) of blood vessels in control (**A-D**) and HMB (**E-H**). The red and black arrows indicate CD31+/αSMA+ (brown/silver) vessels and CD31+/αSMA- vessels, respectively. Images were captured at 200x magnification. Bar chart with a standard error of mean (SEM) represents the percentage of αSMA+ vessels in each phase of the menstrual cycle for control and HMB groups (**I**). Fisher's test followed by unpaired Student's t-test was used (denoted by '*').



K

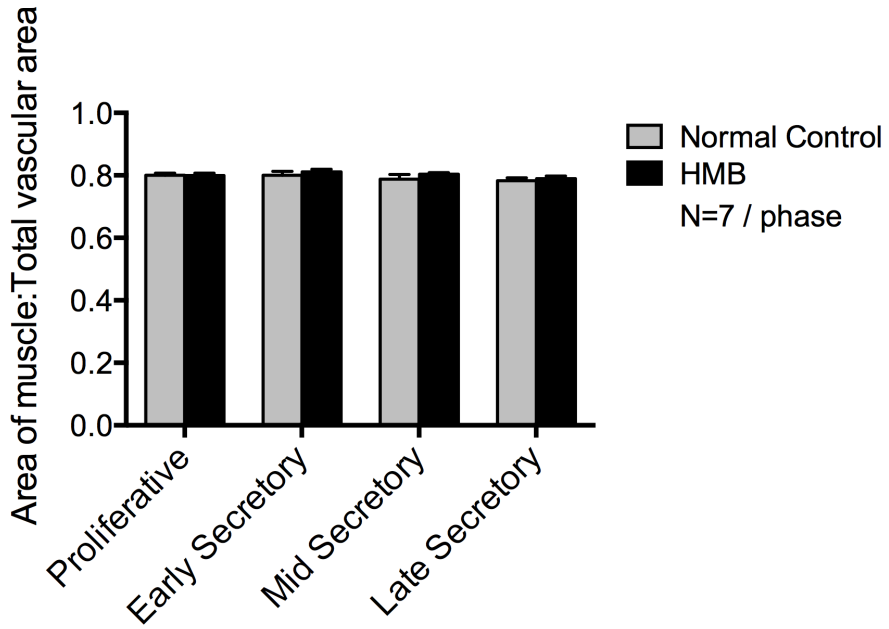


Figure 3.4: Vascular smooth muscle content did not differ between control and heavy menstrual bleeding (HMB) endometrium. **A-J** show vessels (arrowed) immunopositive for αSMA in control (**A-D**) and HMB (**F-J**) endometrium in the proliferative, early secretory, mid secretory and late secretory phases of the menstrual cycle. Images were captured at 200x magnification. Bar chart with a standard error of mean (SEM) represents the mean muscle content in each phase of the menstrual cycle for both control and HMB groups (**K**). Fisher's test followed by unpaired multiple Student's t-test, with Holm-Sidak correction method to account for multiple comparisons (P>0.05).

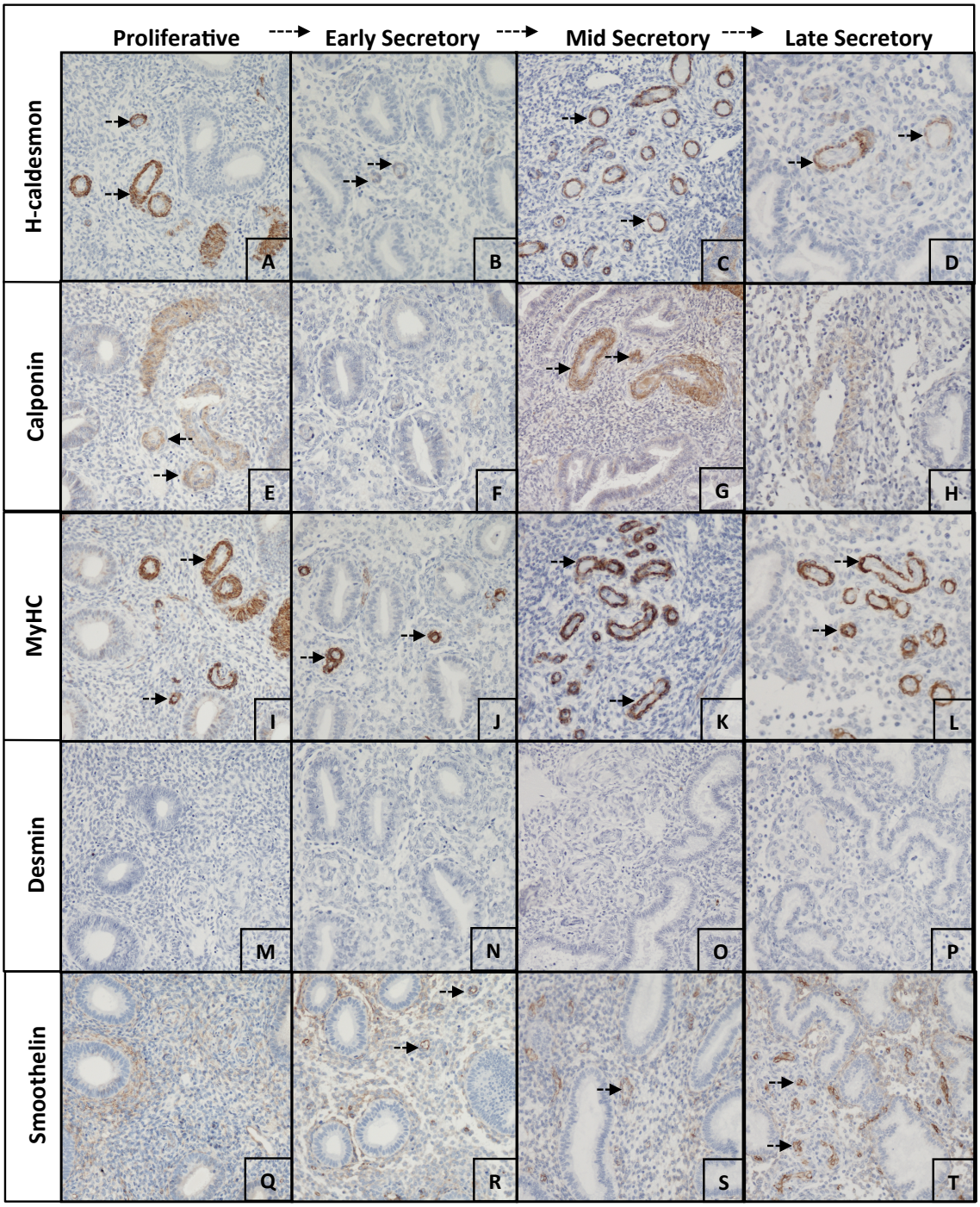


Figure 3.5: VSMC differentiation markers during the menstrual cycle in heavy menstrual bleeding (HMB). Arrows indicate vessels immunopositive for (**A-D**) H-Caldesmon, (**E-H**) calponin, **(I-L)** MyHC, (**M-P**) desmin and (**Q-T**) smoothelin. Images were captured at 200x original magnification.

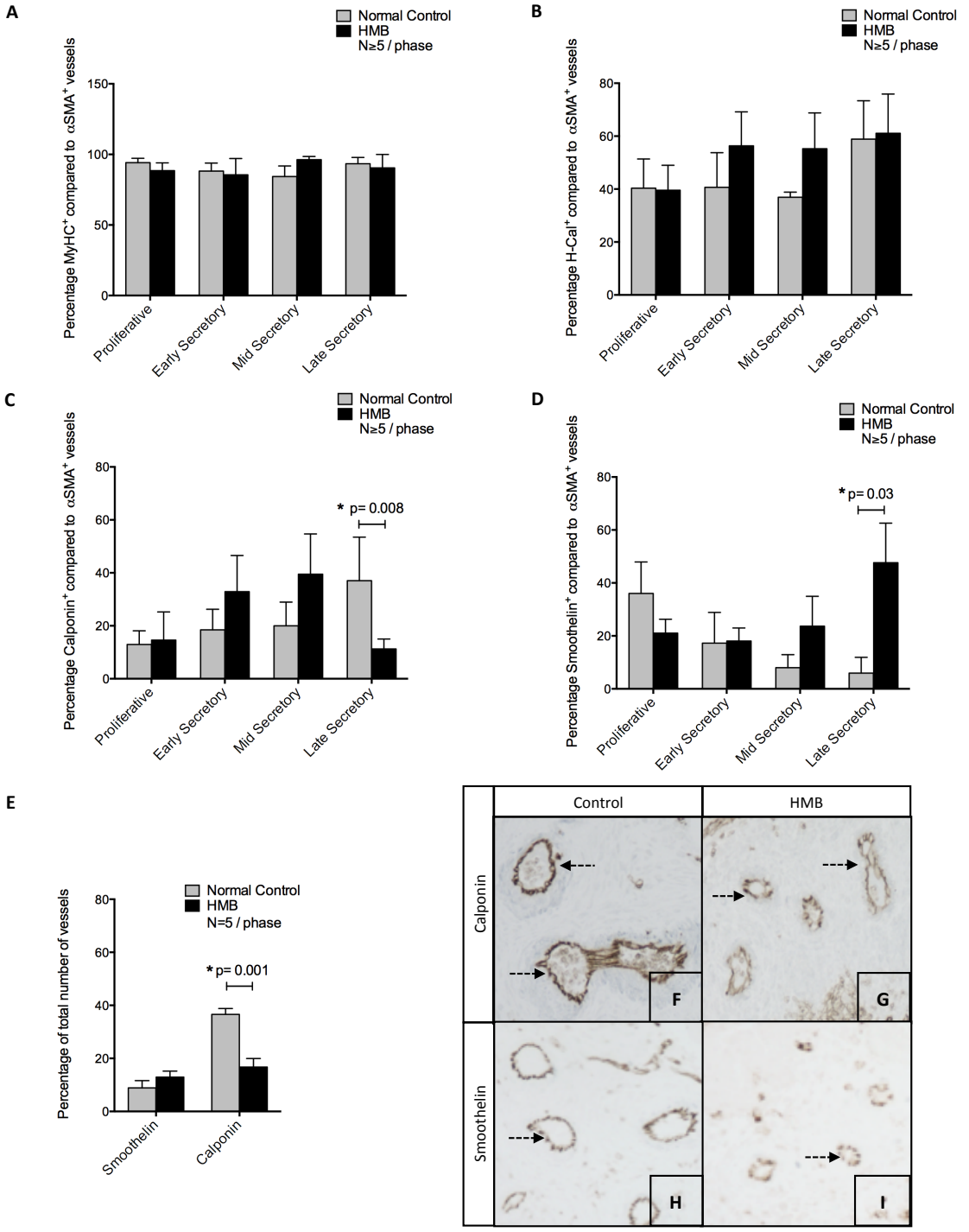


Figure 3.6: Vascular smooth muscle cell (VSMC) differentiation markers in control and HMB endometrium across the menstrual cycle. **(A-D)** Bar charts represent mean percentage of vessels immunopositive for different VSMC markers in each phase of the menstrual cycle for control and HMB. **(E)** Bar chart represents mean (±SEM) percentage of smoothelin+ or calponin+ vessels respectively in the LSP for both control and HMB. Double immunolabeling of endometrial blood vessels in **(F, H)** control and **(G, I)** HMB. **(F, G)** Calponin and **(H, I)** smoothelin are silver/grey and endothelial cells, **(F, G)** UEA-1 and **(H, I)** CD31 in brown. Black arrows indicate calponin$^+$/UEA-1$^+$ and smoothelin$^+$/CD31$^+$ vessels. Images were captured at 200x original magnification.

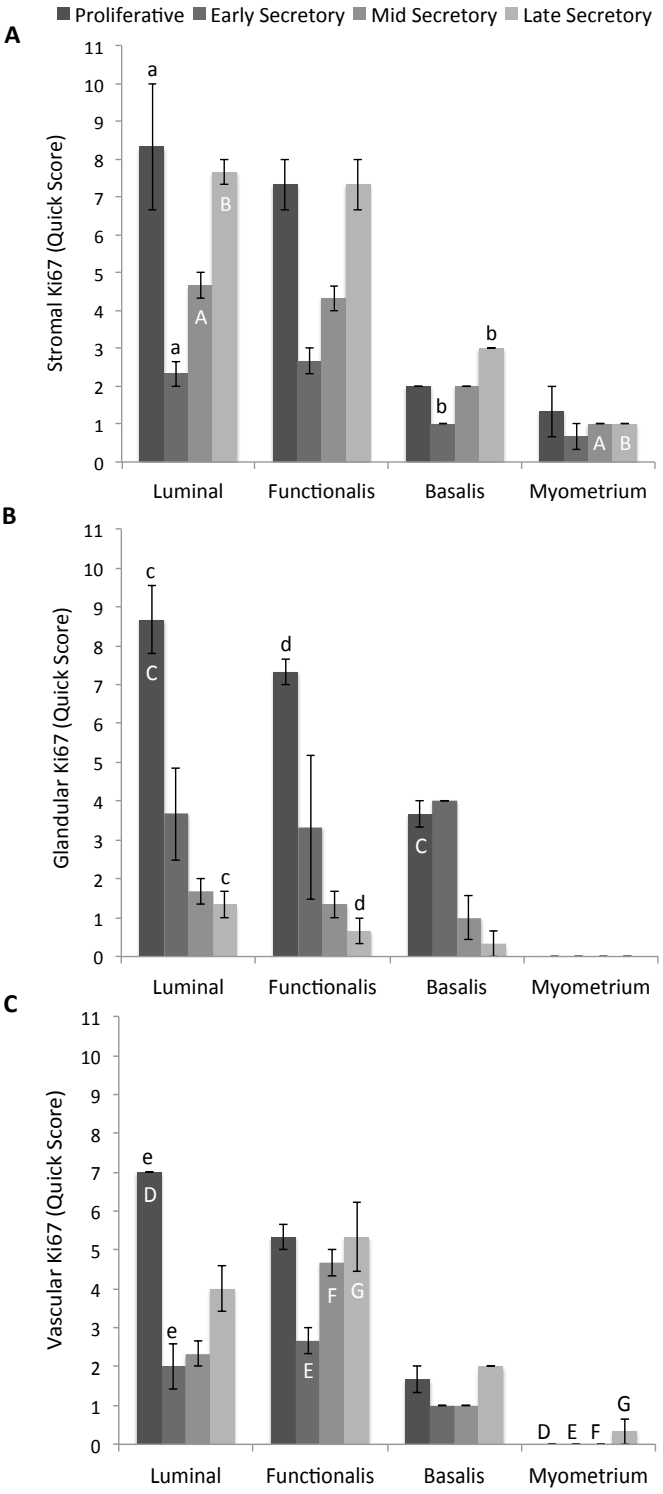


Figure 3.7: Graphical representation (mean ± SEM) of pattern of immunohistochemical staining for proliferation marker Ki67. Ki67 staining between phases (N=3, each phase) of the control menstrual cycle (proliferative, early secretory, mid secretory, late secretory) and in the different tissue layers (luminal, stratum functionalis, stratum basalis, myometrium) for **(A)** stroma, **(B)** glands **(C)** and vessels. Bars labelled with the same letter are significantly different from each other. (a-e) represent differences between phases within each layer, (A-G) represent differences between layers, within each phase. $^{a,\ e}P$=0.008, ^{b}P=0.001, $^{c,\ d}P$=0.006; ^{A}P=0.005, ^{B}P=0.007, ^{C}P=0.015, $^{D,\ F}P$=0.002, $^{E,\ G}P$=0.004. Pairwise Kruskal-Wallis one way ANOVA, with Bonferroni correction determined significant difference.

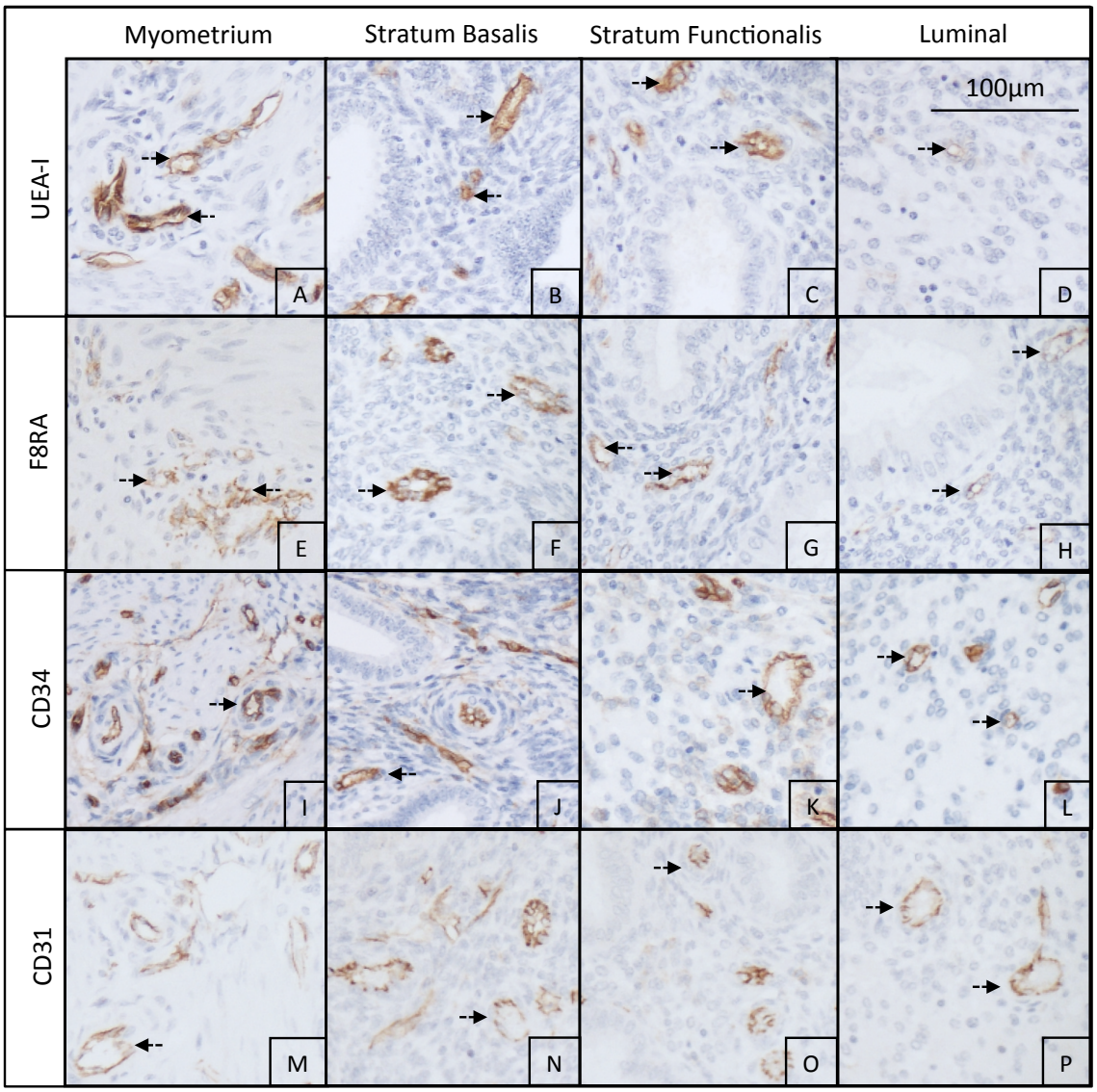


Figure 3.8: Staining for endothelial cell (EC) markers in the uterus. Layers of the uterus (myometrium, stratum basalis, stratum functionalis, luminal) showing vessels stained positive for (**A-D**) UEA-I, (**E-H**) F8RA, (**I-L**) CD34 and (**M-P**) CD31 during the mid secretory phase of the control menstrual cycle. Images were captured at 200x original magnification.

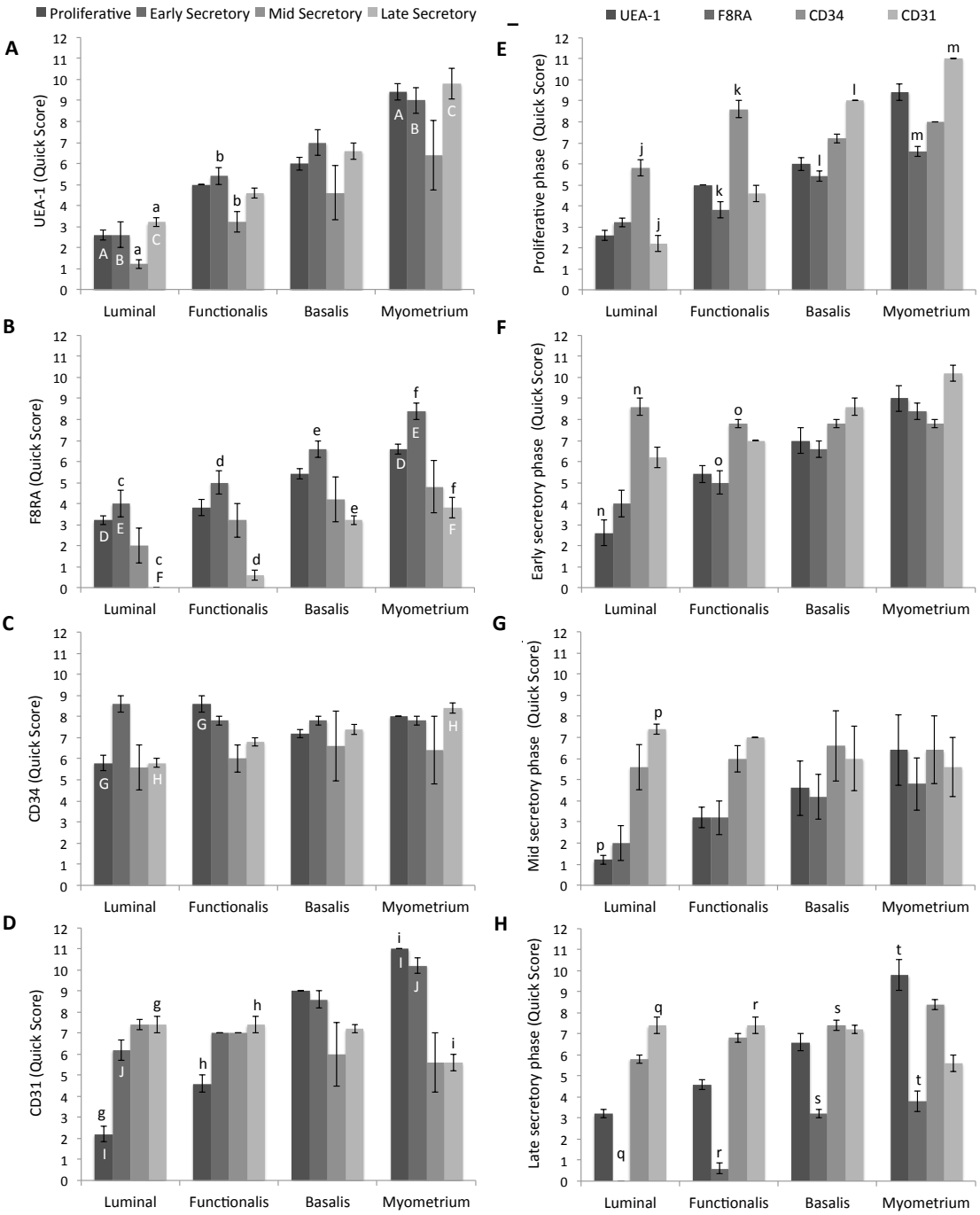


Figure 3.9: Graphical representation (mean ± SEM) of Quickscore assessment of immunohistochemical staining for endothelial cell (EC) marker staining between phases (N=5, each phase) of the normal menstrual cycle in the tissue layers (luminal, stratum functionalis, stratum basalis, myometrium) for each EC marker (**A-D**) and between the different EC markers (UEA-1, F8RA, CD34, CD31) in the tissue layers for each menstrual cycle phase (**E-H**). Bars labelled with the same letter are significantly different from each other. (a-t) represent differences between phases or factors, within each layer, (A-J) represent differences between layers, within each phase. $^{a, c}P$=0.006, $^{b, f, h, t}P$=0.002, $^{d, e, l, j, s}P$=0.003, ^{g}P=0.007, $^{k, l, n, r}P$=0.001, $^{m, q}P$<0.001, ^{o}P=0.005, ^{p}P=0.008; $^{A, I}P$<0.001, $^{B, C, H}P$=0.001, $^{D, E, G, J}P$=0.002, ^{F}P=0.004. Pairwise Kruskal-Wallis one way ANOVA, with Bonferroni correction determined significant difference.

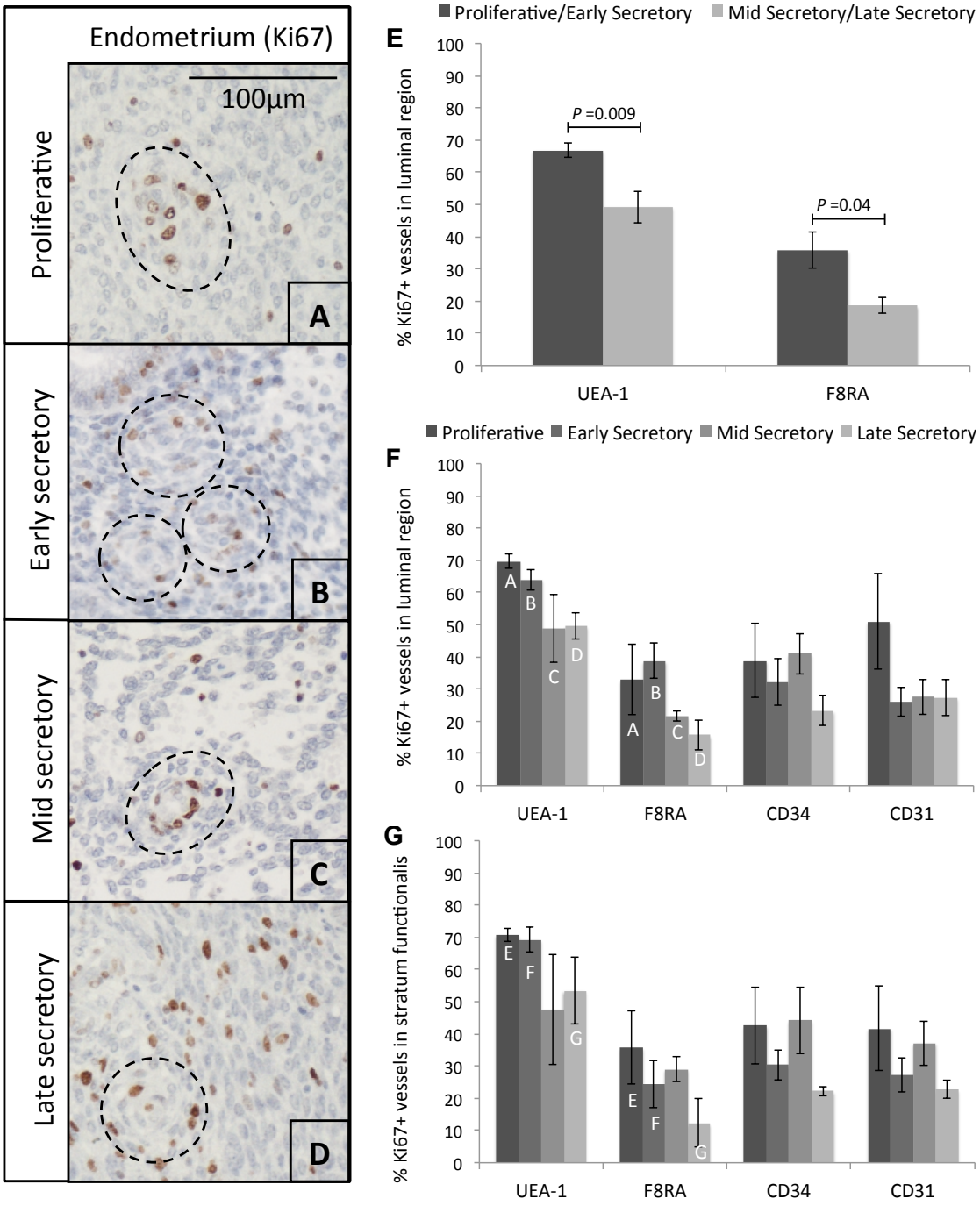


Figure 3.10: Staining for vascular Ki67 in the control menstrual cycle. (**A-D**) Ki67^{+} vessels indicated by the dotted circles in proliferative, early secretory, mid secretory and late secretory phase. Images were captured at 200x original magnification. Graphical representation (mean ± SEM) of the percentage assessment of immunohistochemical staining for proliferation (Ki67, N=3, each phase) in vessels expressing UEA-1, F8RA, CD34 and CD31 in the control menstrual cycle in (**E, F**) luminal region and (**G**) stratum functionalis. (**E**) Mann-Whitney U test determined statistical significance between PP/ESP and MSP/LSP. Pairwise Kruskal-Wallis one way ANOVA, with Bonferroni correction determined significant difference between factors. (A-G) represent differences between factors, within each phase. $^{A,B,C,E,F,G}P$=0.05, ^{D}P=0.046.

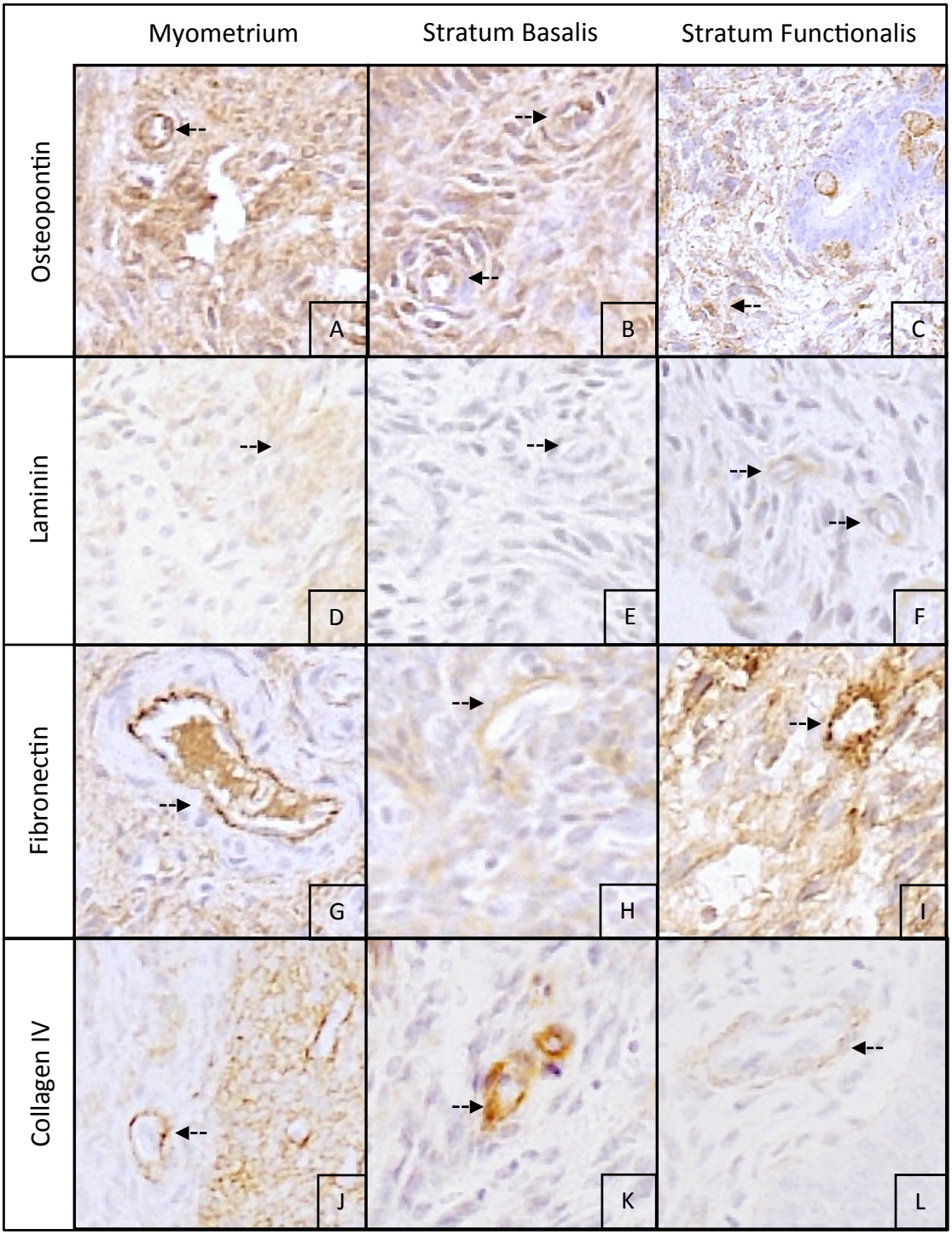


Figure 3.11: Staining for extracellular matrix components in the uterus. Uterine layers (myometrium, stratum basalis, stratum functionalis), showing vessels immunopositive for (**A-C**) osteopontin, (**D-F**) laminin, (**G-I**) fibronectin and (**J-L**) collagen IV during the mid secretory phase of the control menstrual cycle. Arrows indicate vascular extracellular matrix components. Images were captured at 200x original magnification.

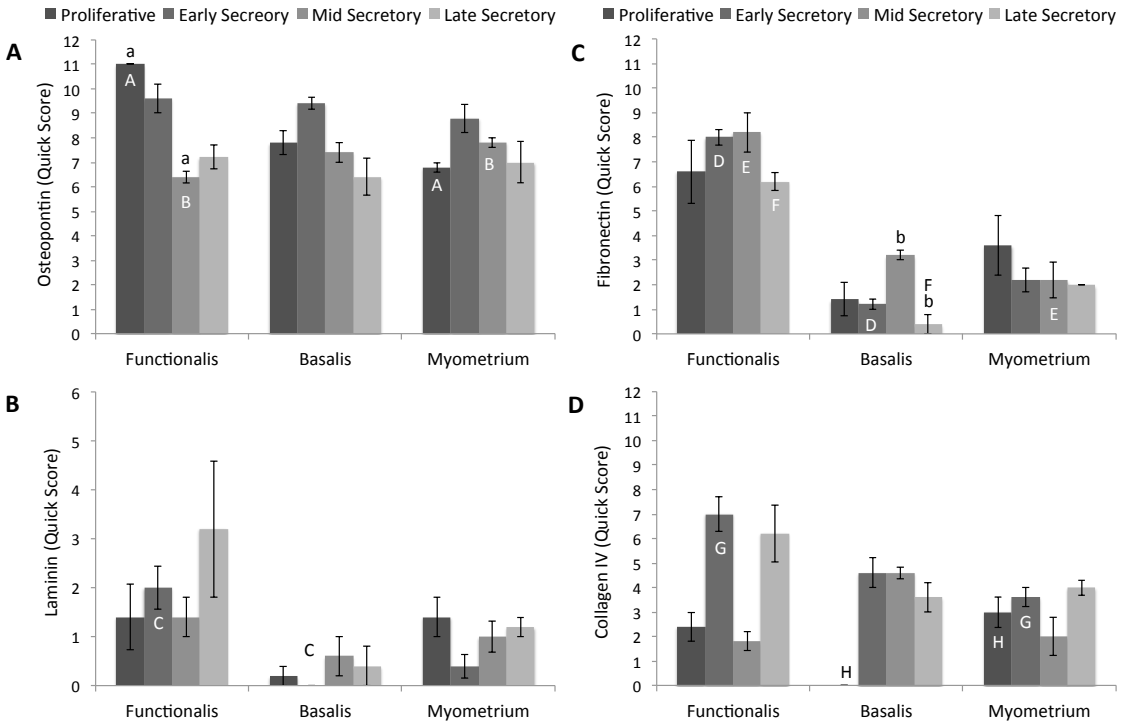


Figure 3.12: Immunohistochemical staining for pattern of staining for vascular extracellular matrix (ECM) markers in the control menstrual cycle. Graphical representation (mean ± SEM) of Quickscore assessment of ECM markers between phases (N=5, each phase) of the control menstrual cycle (proliferative, early secretory, mid secretory, late secretory) in the tissue layers (stratum functionalis, stratum basalis, myometrium) for each ECM marker (osteopontin, laminin, fibronectin, collagen IV) **(A-D)**. (*a*, *b*) represent differences between phases or factors, within each layer, (A-H) represent differences between layers, within each phase. ^{a}P=0.003, ^{b}P=0.005; ^{A}P=0.002, ^{B}P=0.02, ^{C}P=0.005, ^{D}P=0.003, ^{E}P=0.004, ^{F}P=0.001, ^{G}P=0.01, ^{H}P=0.01. Pairwise Kruskal-Wallis one way ANOVA, with Bonferroni correction determined significant difference.

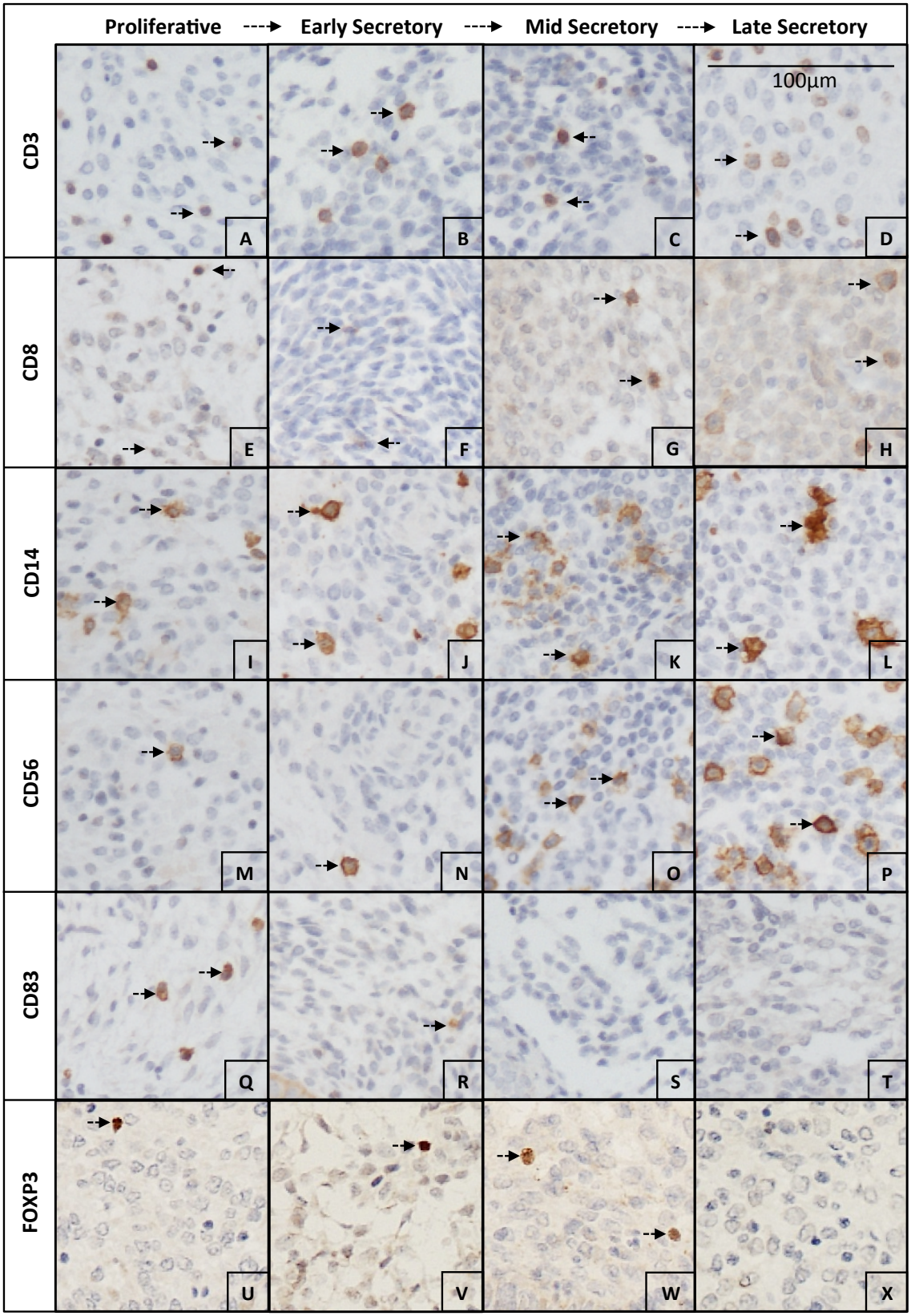


Figure 3.13: Immunohistochemical labeling for leukocytes in the stratum functionalis of endometrium in HMB. Arrows indicate $CD3^+$ cells (**A-D**), $CD8^+$ T cells (**E-H**), $CD14^+$ macrophages (**I-L**), $CD56^+$ uNK cells (**M-P**), $CD83^+$ dendritic cells (**Q-T**), and $FOXP3^+$ regulatory T cells (**U-X**), during the proliferative, early secretory, mid secretory and late secretory phases of the menstrual cycle. Images were captured at 200x original magnification.

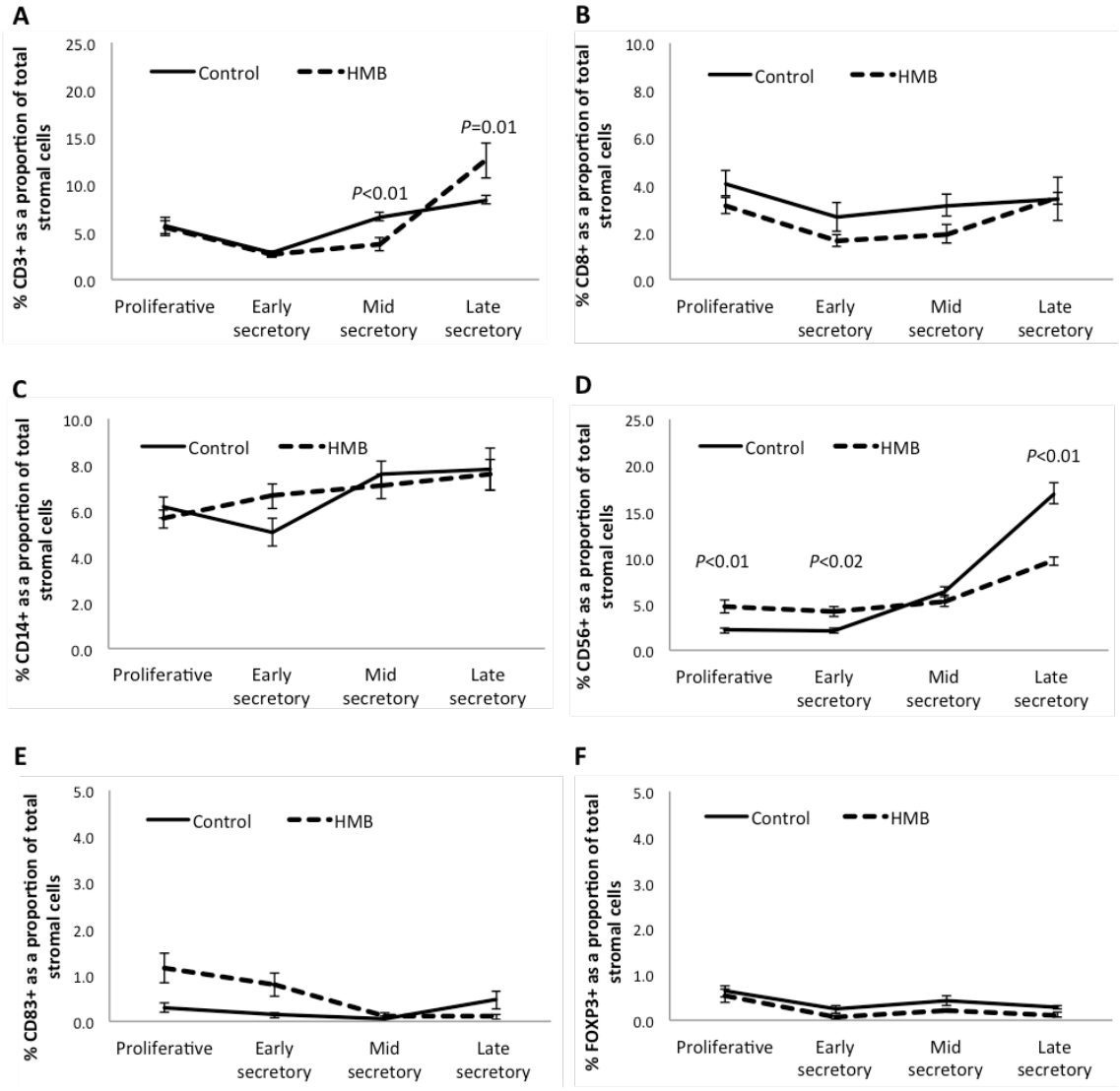


Figure 3.14: Endometrial leukocyte population as a proportion of the total stromal cells at each phase of the menstrual cycle in controls and in HMB. Proportion of $CD3^+$ cells (**A**), $CD8^+$ T cells (**B**), $CD14^+$ macrophages (**C**), $CD56^+$ uNK cells (**D**), $CD83^+$ dendritic cells (**E**) and $FOXP3^+$ regulatory T cells (**F**) in stratum functionalis of the endometrium across the phases of the menstrual cycle in controls and in HMB (N=5 in each phase). The line graphs show mean ± standard error of mean (SEM) of the percentage population of leukocytes as a proportion of total stromal cells at each phase of the menstrual cycle. Non-parametric Mann-Whitney U test, with Bonferroni correction for multiple comparisons was used to determine significance.

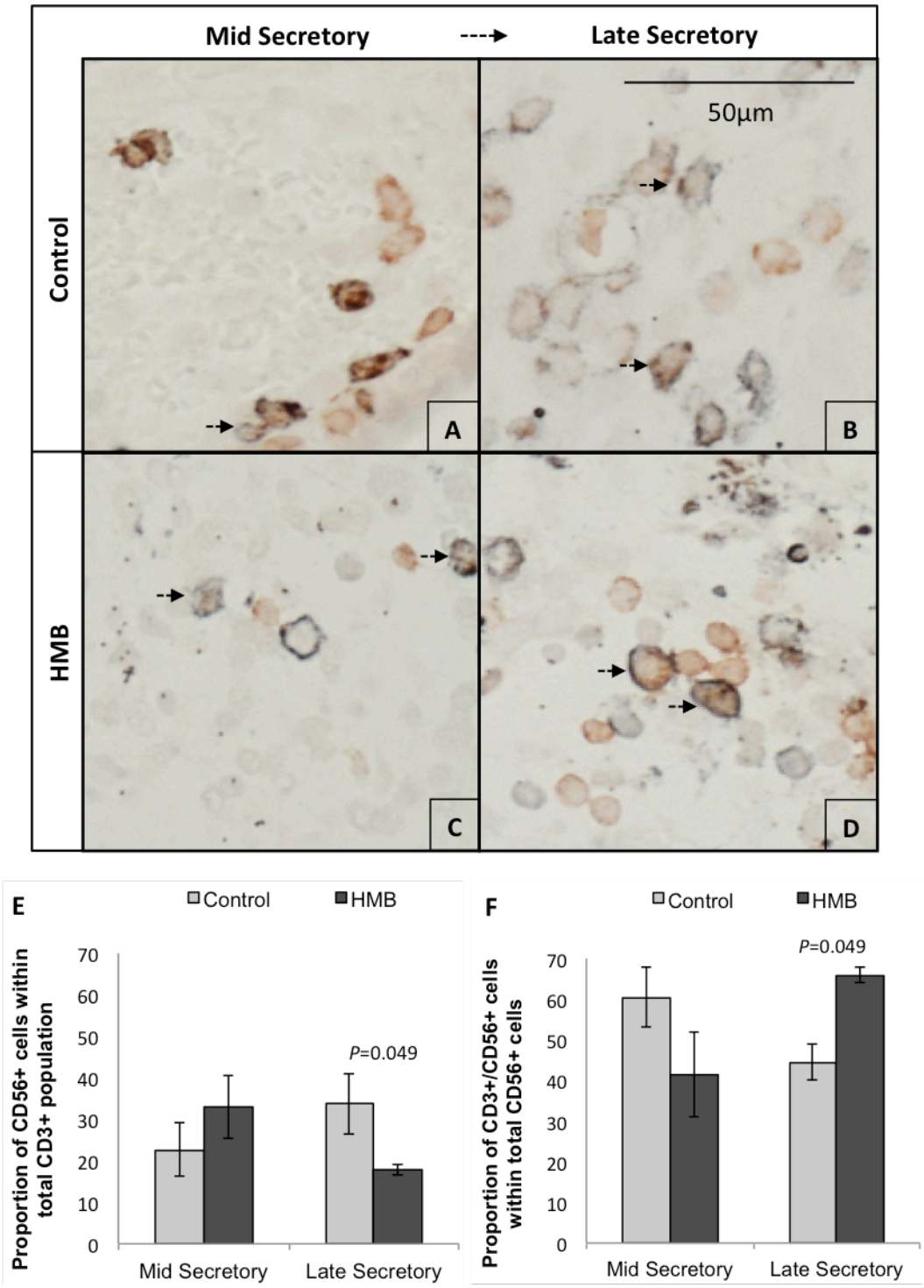


Figure 3.15: Double immunolabeling for $CD3^+$ cells and $CD56^+$ uNK cells in the mid secretory and late secretory phases in stratum functionalis of control (**A, B**) and HMB samples (**C, D**). $CD3^+$ cells are red and $CD56^+$ cells are silver. The black arrows indicate $CD3^+CD56^+$ cells. Images were captured at 400x original magnification. Bar chart with a standard error mean (SEM) represents the mean percentage of $CD3^+CD56^+$ cells as a proportion of all $CD3^+$ cells (**E**) and that of $CD3^+CD56^+$ cells as a proportion of all $CD56^+$ cells (**F**) in control and HMB samples. Mann-Whitney U test was used to determine statistical significance.

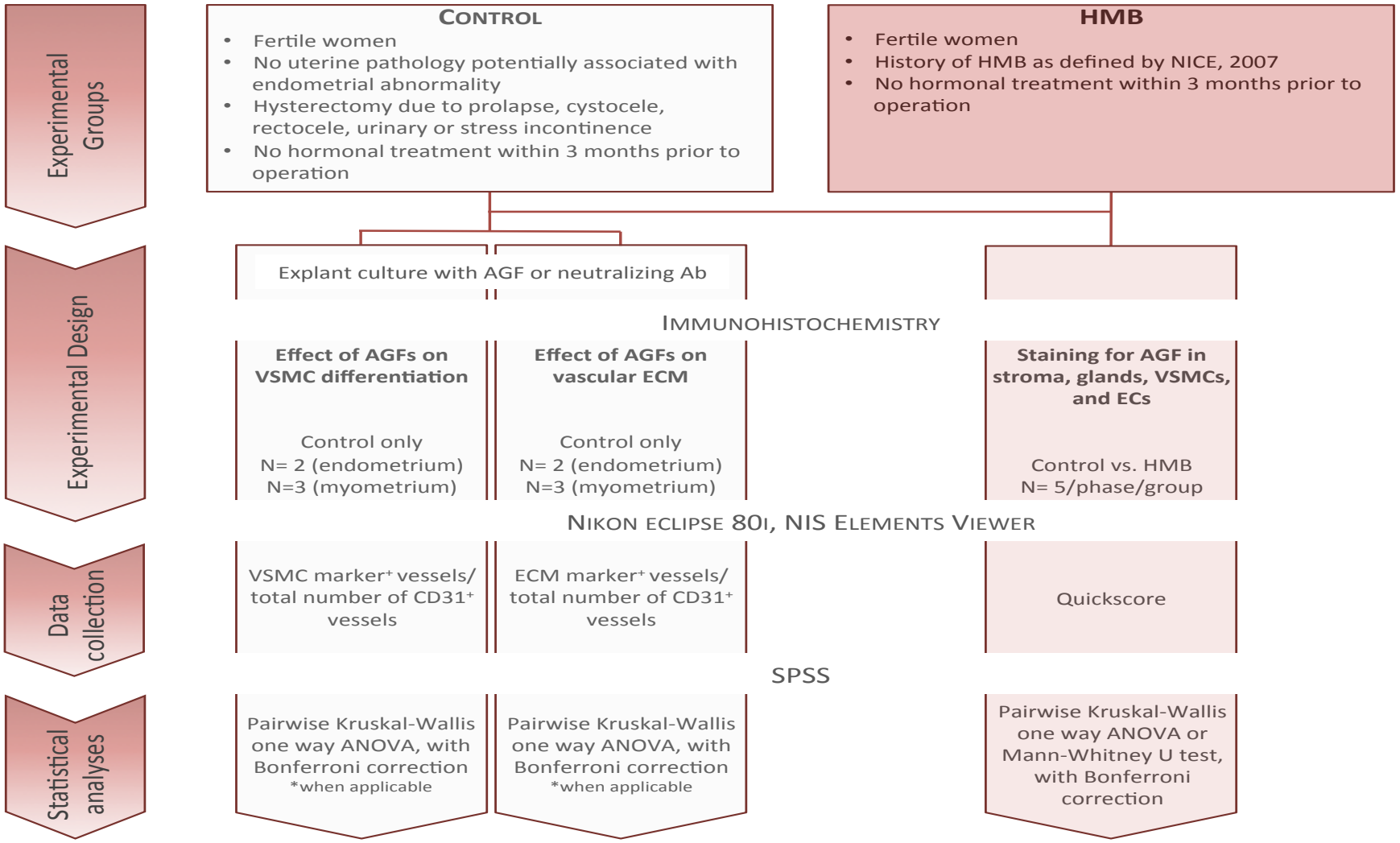


Figure 4.1: Experimental design to investigate angiogenic growth factors and blood vessel development in women with HMB.

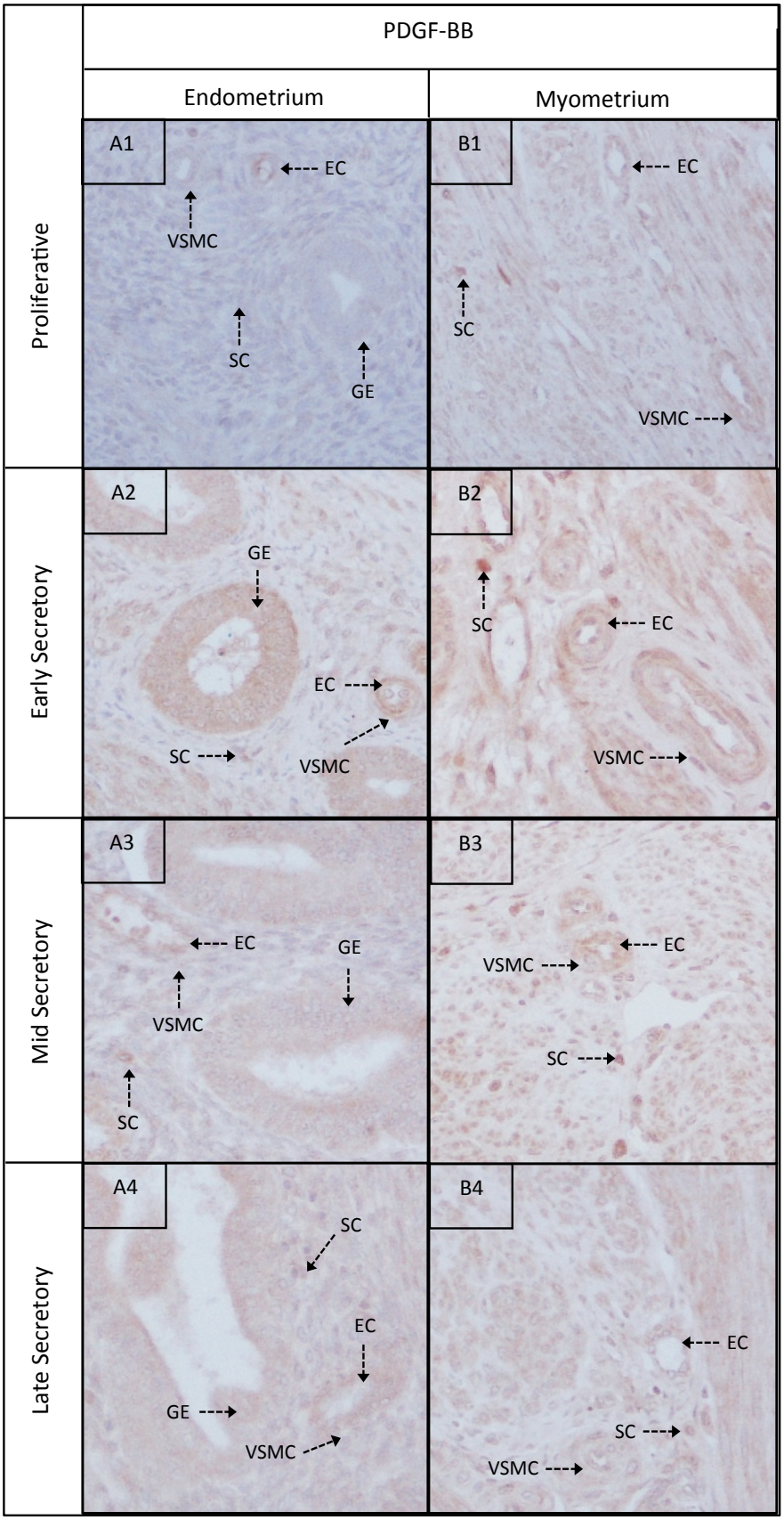


Figure 4.2a: Staining for PDGF-BB in the endometrium and myometrium during the menstrual cycle. Stromal cells (SC), glandular epithelial cells (GE), VSMCs and ECs were stained positive for PDGF-BB (**A1**-**A4**, **B1**-**B4**). Images were captured at 200x original magnification.

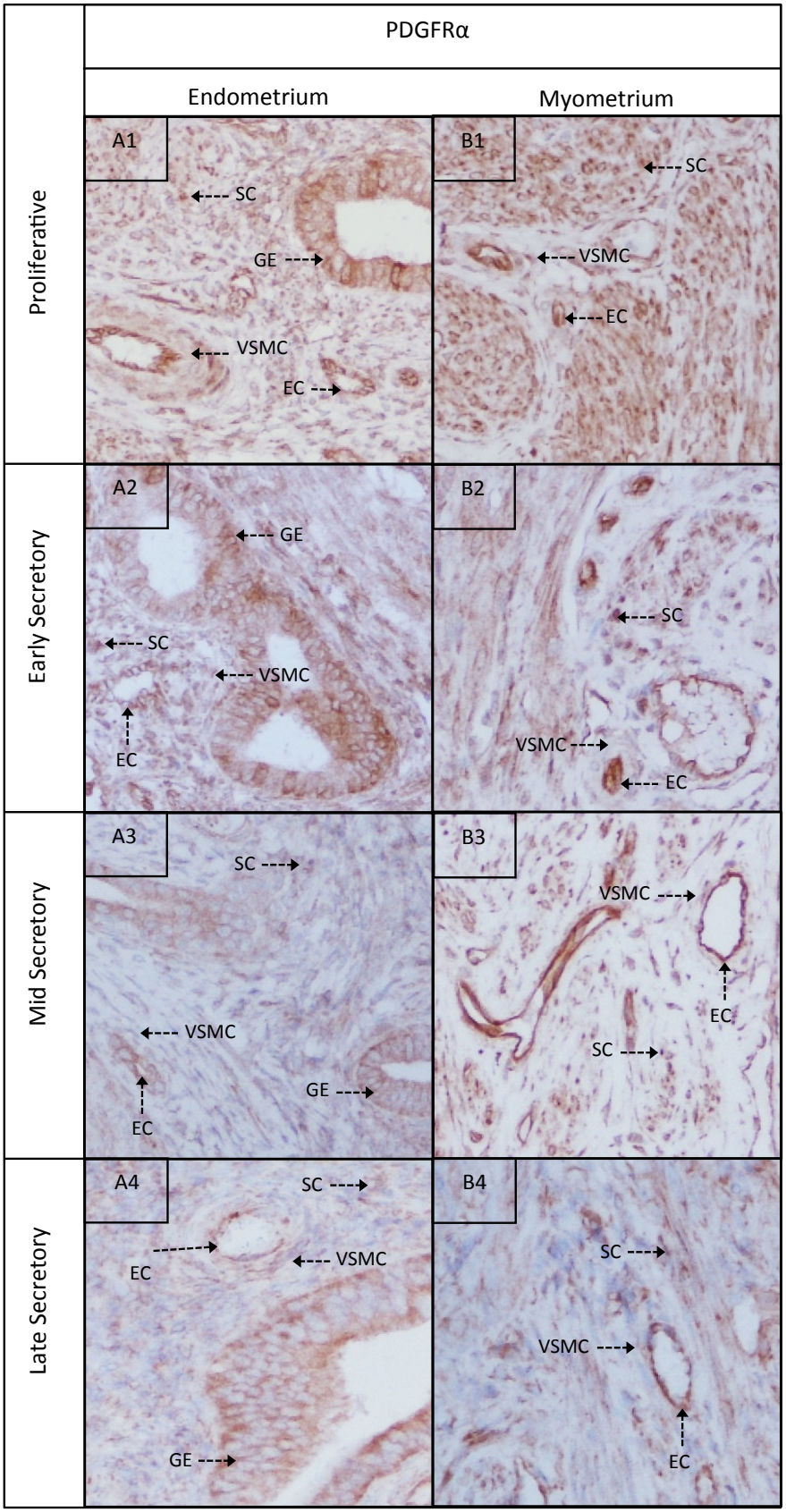


Figure 4.2b: Staining for PDGFRα in the endometrium and myometrium during the menstrual cycle. Stromal cells (SC), glandular epithelial cells (GE), VSMCs and ECs were stained positive for PDGFRα (**A1**-**A4**, **B1**-**B4**). Images were captured at 200x original magnification.

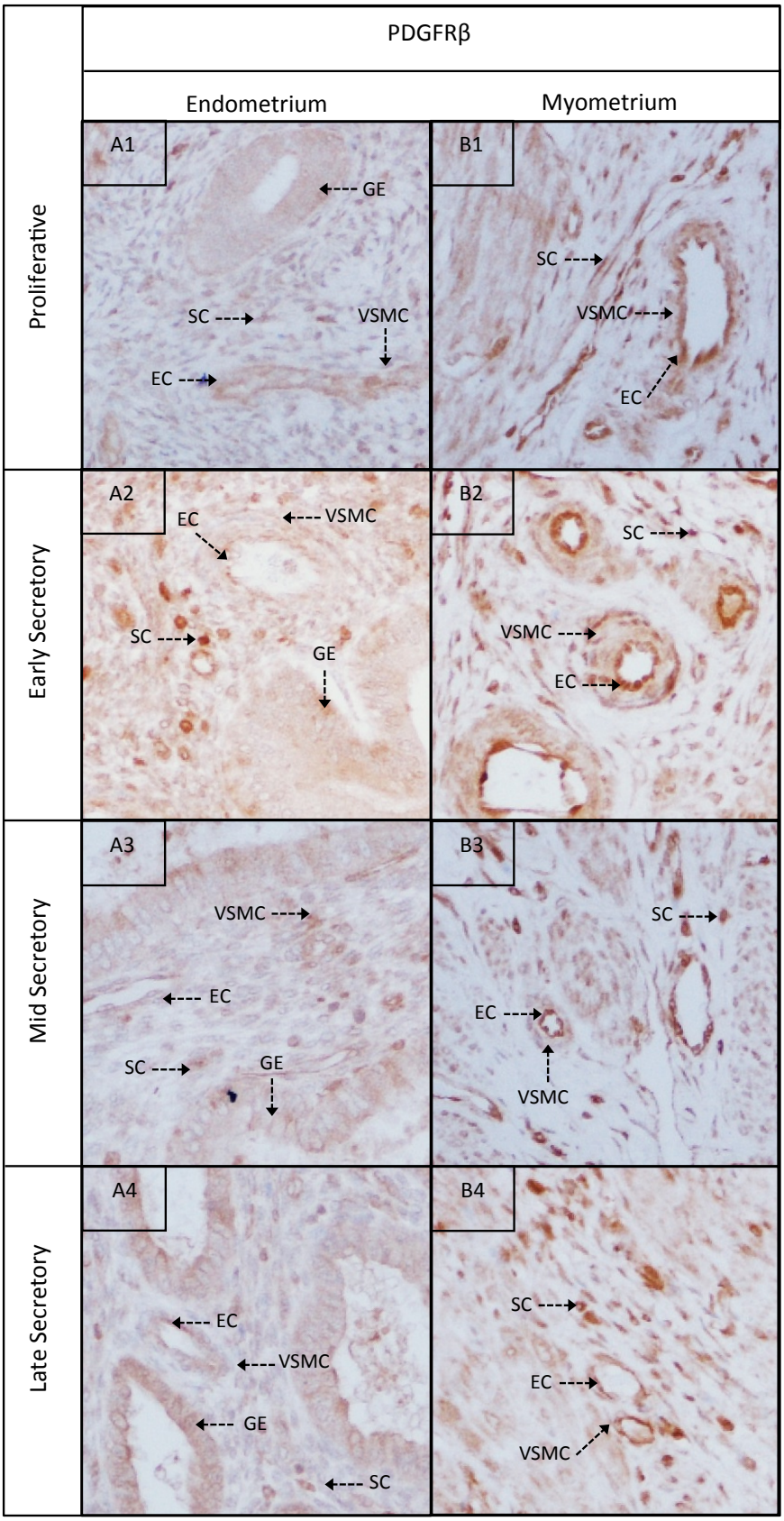


Figure 4.2c: Staining for PDGFRβ in the endometrium and myometrium during the menstrual cycle. Stromal cells (SC), glandular epithelial cells (GE), VSMCs and ECs were stained positive for PDGFRβ (**A1**-**A4**, **B1**-**B4**). Images were captured at 200x original magnification.

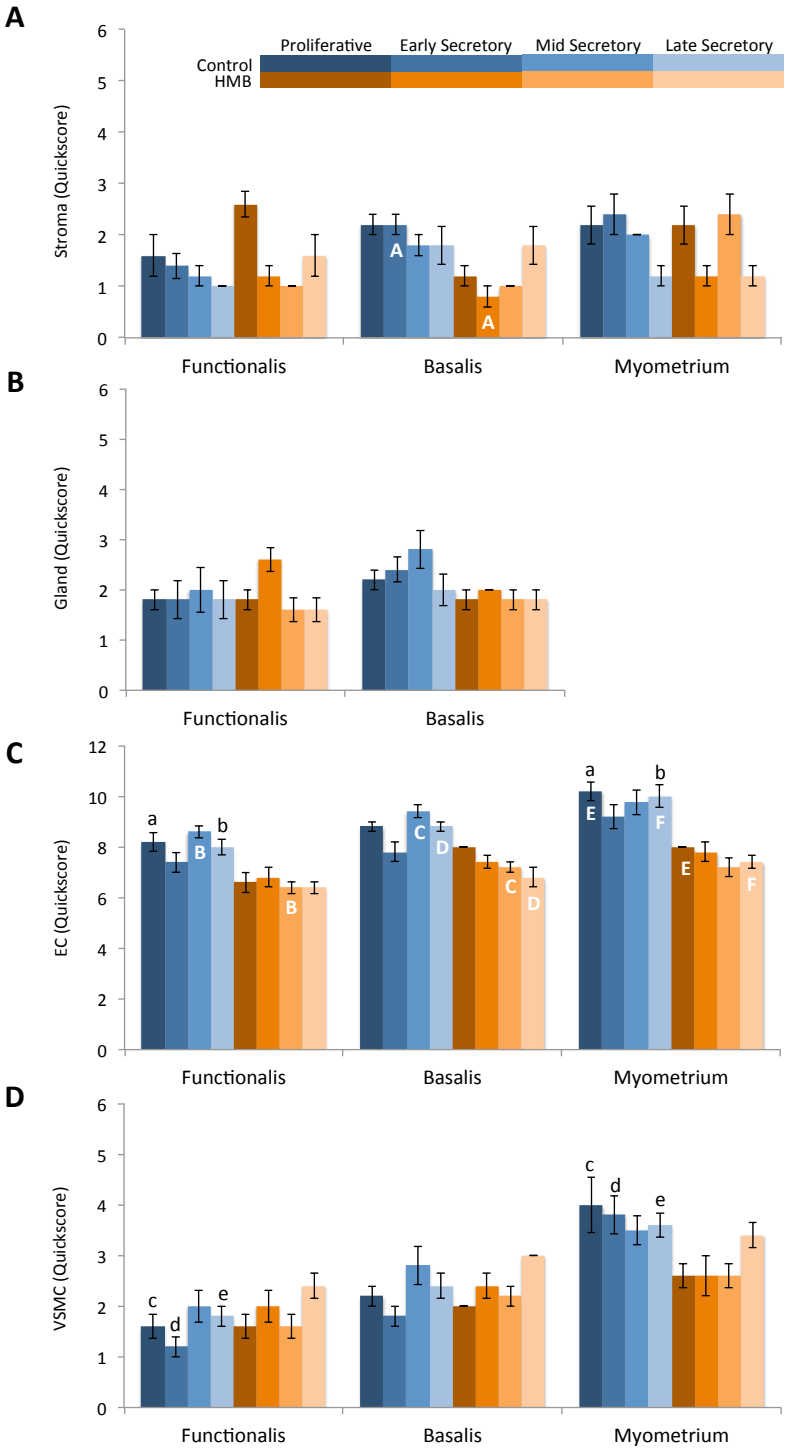


Figure 4.3: Graphical representation of immunohistochemical staining for PDGF-BB during the menstrual cycle. (**A-D**) Quickscore assessment (mean ± SEM) of PDGF-BB expression (N=5, each phase, each group) in controls and in HMB for stromal cells (**A**), glandular epithelial cells (**B**), ECs (**C**) and VSMCs (**D**). Bars labelled with the same letter are significantly different from each other. (a-e) represent differences between layers, within each phase; ^{a}P=0.01, ^{b}P=0.009, $^{c,e}P$=0.004, ^{d}P=0.003. (A-F) represent differences between control and HMB; $^{A\text{-}F}P$=0.008. Pairwise Kruskal-Wallis one way ANOVA, with Bonferroni correction determined significant differences between phases or layers in control. Mann-Whitney U test, with Bonferroni correction determined significant differences between control and HMB.

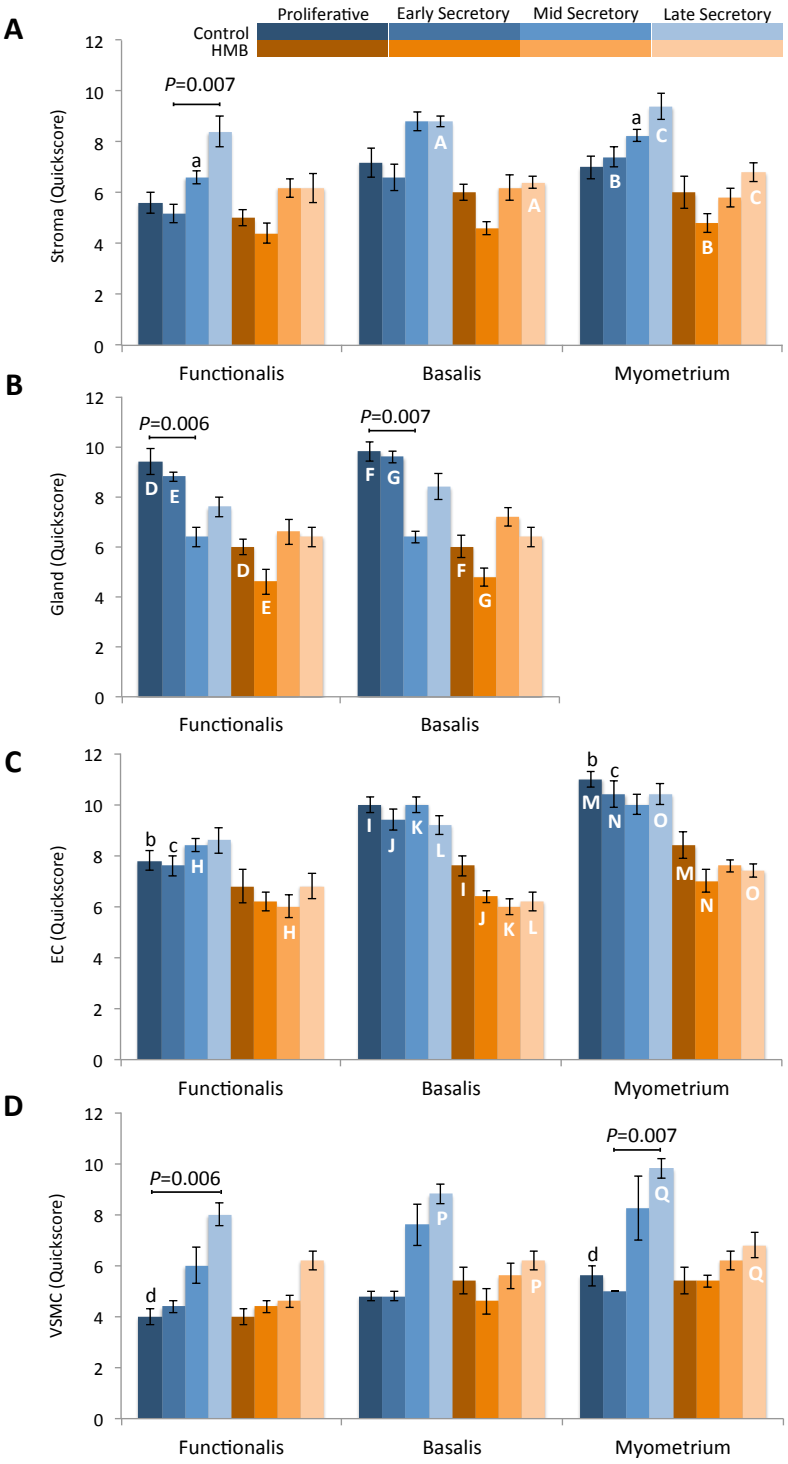


Figure 4.4: Graphical representation of immunohistochemical staining for PDGFRα during the menstrual cycle. (**A-D**) Quickscore assessment (mean ± SEM) of PDGFRα (N=5, each phase, each group) in controls and in HMB for stromal cells (**A**), glandular epithelial cells (**B**), ECs (**C**) and VSMCs (**D**). '*P*' values shown in graph represent significant differences between phases within each layer. Bars labelled with the same letter are significantly different from each other. (a-d) represent differences between layers, within each phase; ^{a}P=0.007, ^{b}P=0.003, ^{c}P=0.01, ^{d}P=0.014. (A-Q) represent differences between control and HMB; $^{A\text{-}Q}P$=0.008. Pairwise Kruskal-Wallis one way ANOVA, with Bonferroni correction determined significant differences between phases or layers in control. Mann-Whitney U test, with Bonferroni correction determined significant differences between control and HMB.

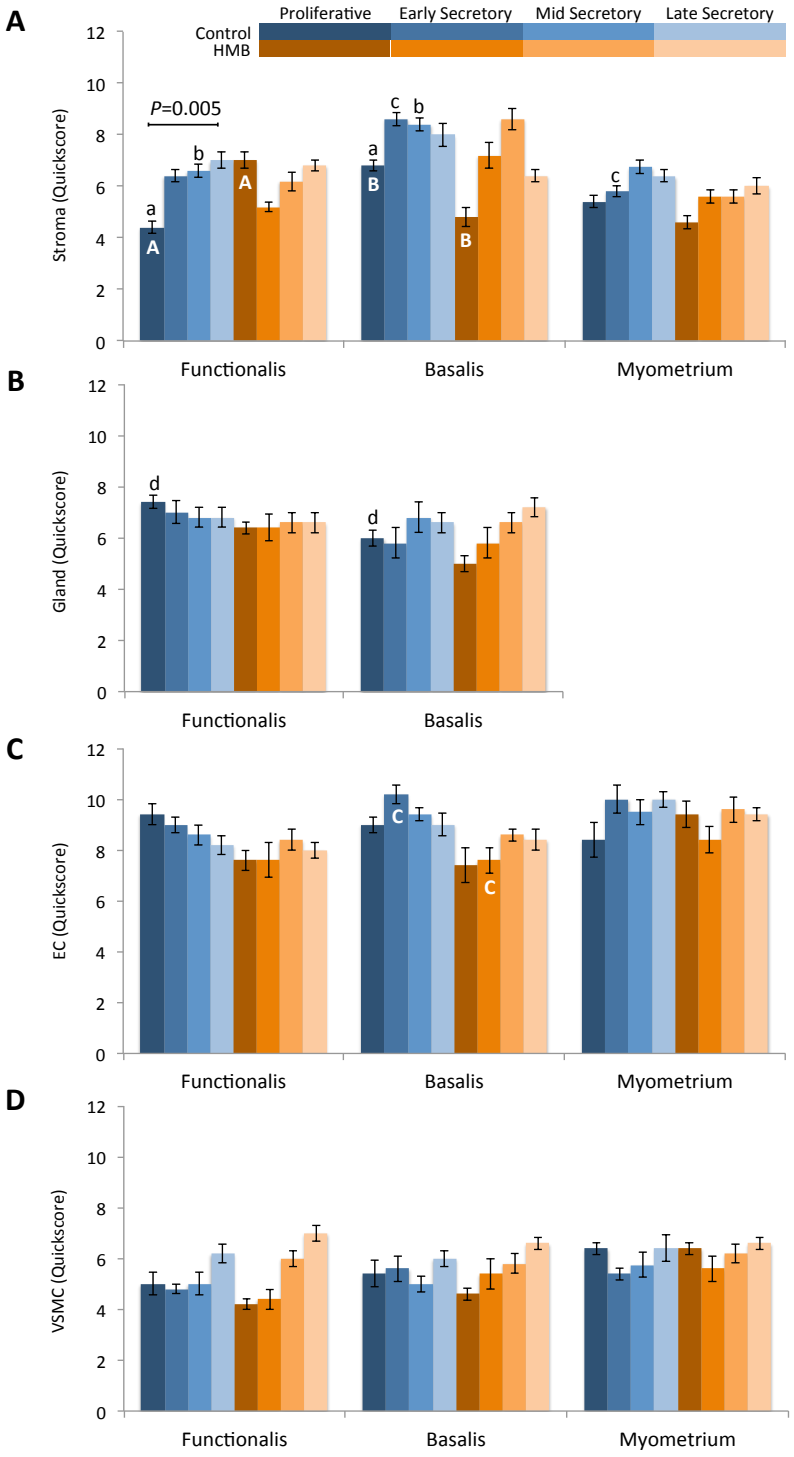


Figure 4.5: Graphical representation of immunohistochemical staining for PDGFRβ during the menstrual cycle. (**A-D**) Quickscore assessment (mean ± SEM) of PDGFRβ staining (N=5, each phase, each group) in controls and in HMB for stromal cells (**A**), glandular epithelial cells (**B**), ECs (**C**) and VSMCs (**D**). '*P*' value shown in graph represents significant difference between phases within each layer. Bars labelled with the same letter are significantly different from each other. (a-d) represent differences between layers, within each phase; ^{a}P=0.002, ^{b}P=0.011, ^{c}P=0.003, ^{d}P=0.016. (A-C) represent differences between control and HMB; $^{A\text{-}C}P$=0.008. Pairwise Kruskal-Wallis one way ANOVA, with Bonferroni correction determined significant differences between phases or layers in control. Mann-Whitney U test, with Bonferroni correction determined significant differences between control and HMB.

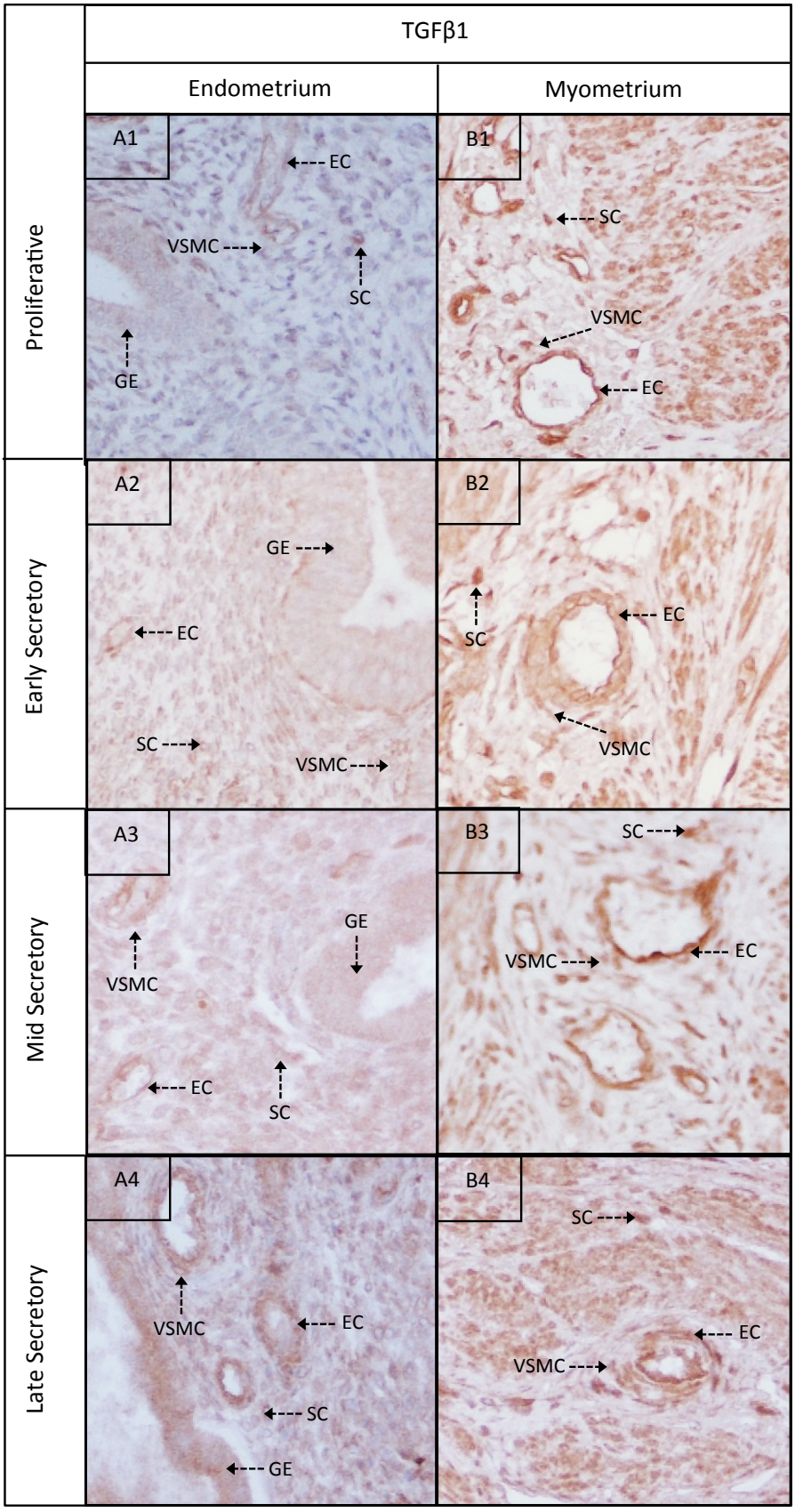


Figure 4.6a: Staining for TGFβ1 in the endometrium and myometrium during the menstrual cycle. Stromal cells (SC), glandular epithelial cells (GE), VSMCs and ECs were stained positive for TGFβ1 (**A1**-**A4**, **B1**-**B4**). Images were captured at 200x original magnification.

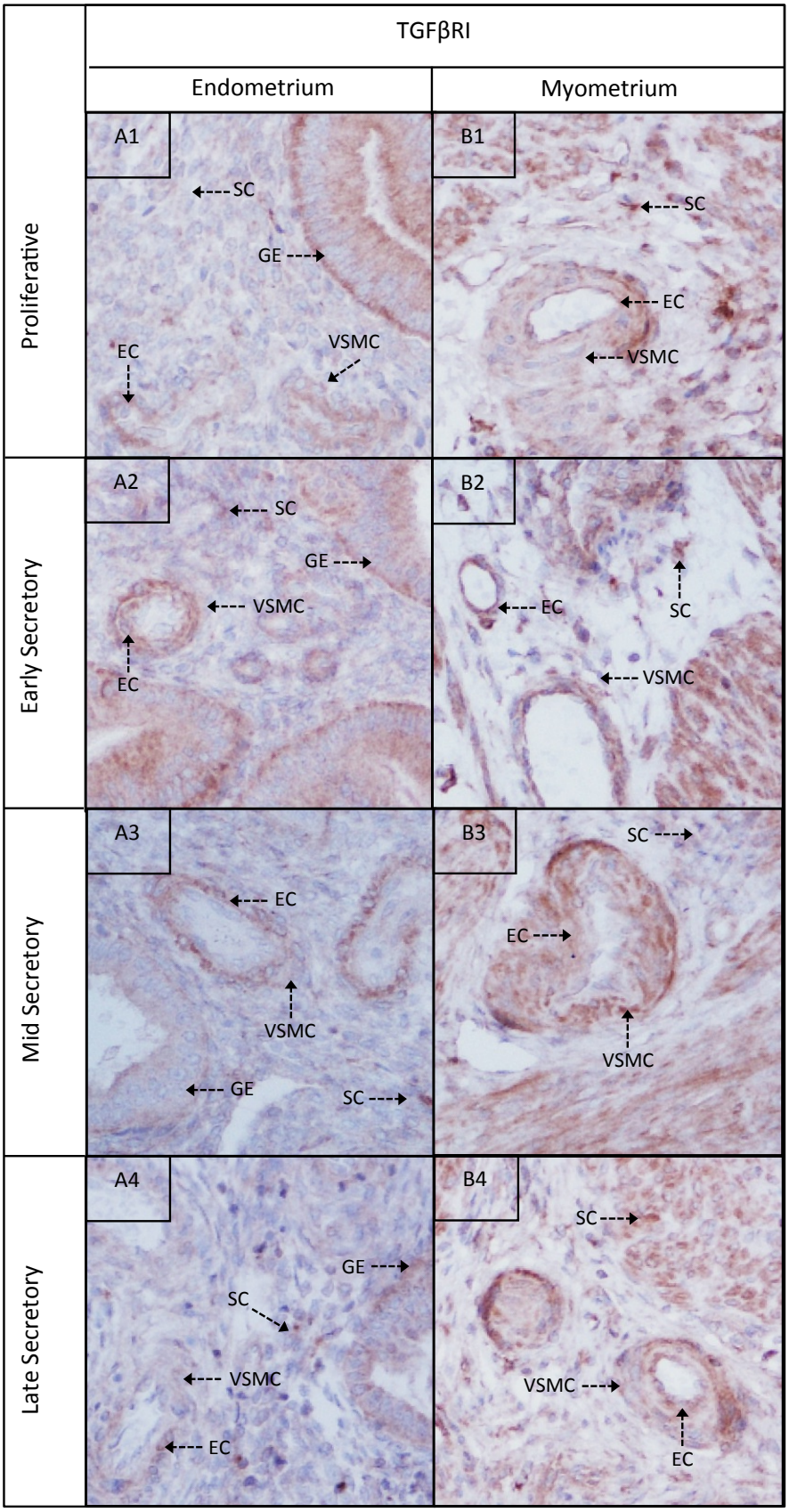


Figure 4.6b: Staining for TGFβRI in the endometrium and myometrium during the menstrual cycle. Stromal cells (SC), glandular epithelial cells (GE), VSMCs and ECs were stained positive for TGFβRI (**A1**-**A4**, **B1**-**B4**). Images were captured at 200x original magnification.

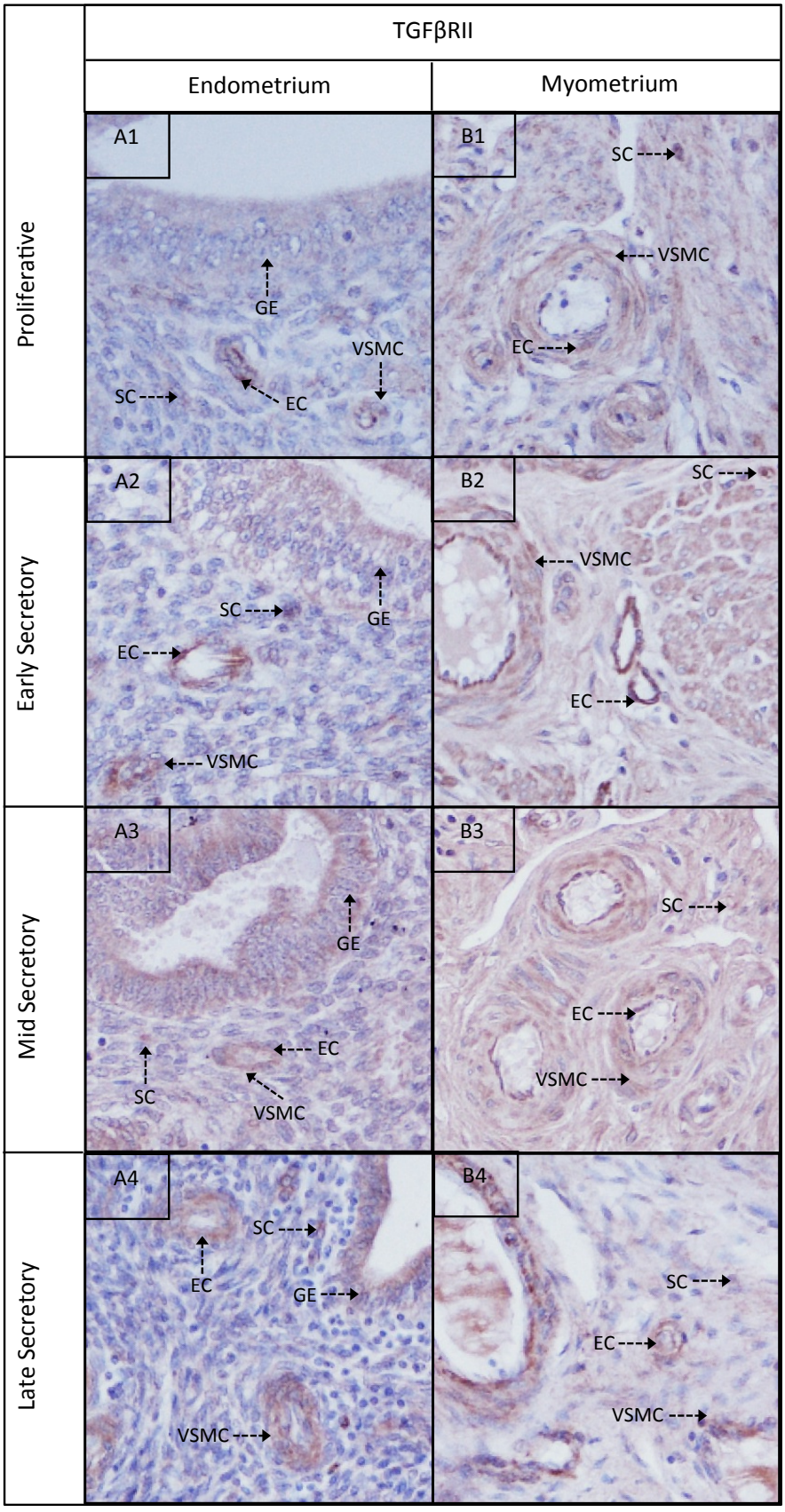


Figure 4.6c: Staining for TGFβRII in the endometrium and myometrium during the menstrual cycle. Stromal cells (SC), glandular epithelial cells (GE), VSMCs and ECs were stained positive for TGFβRII (**A1**-**A4**, **B1**-**B4**). Images were captured at 200x original magnification.

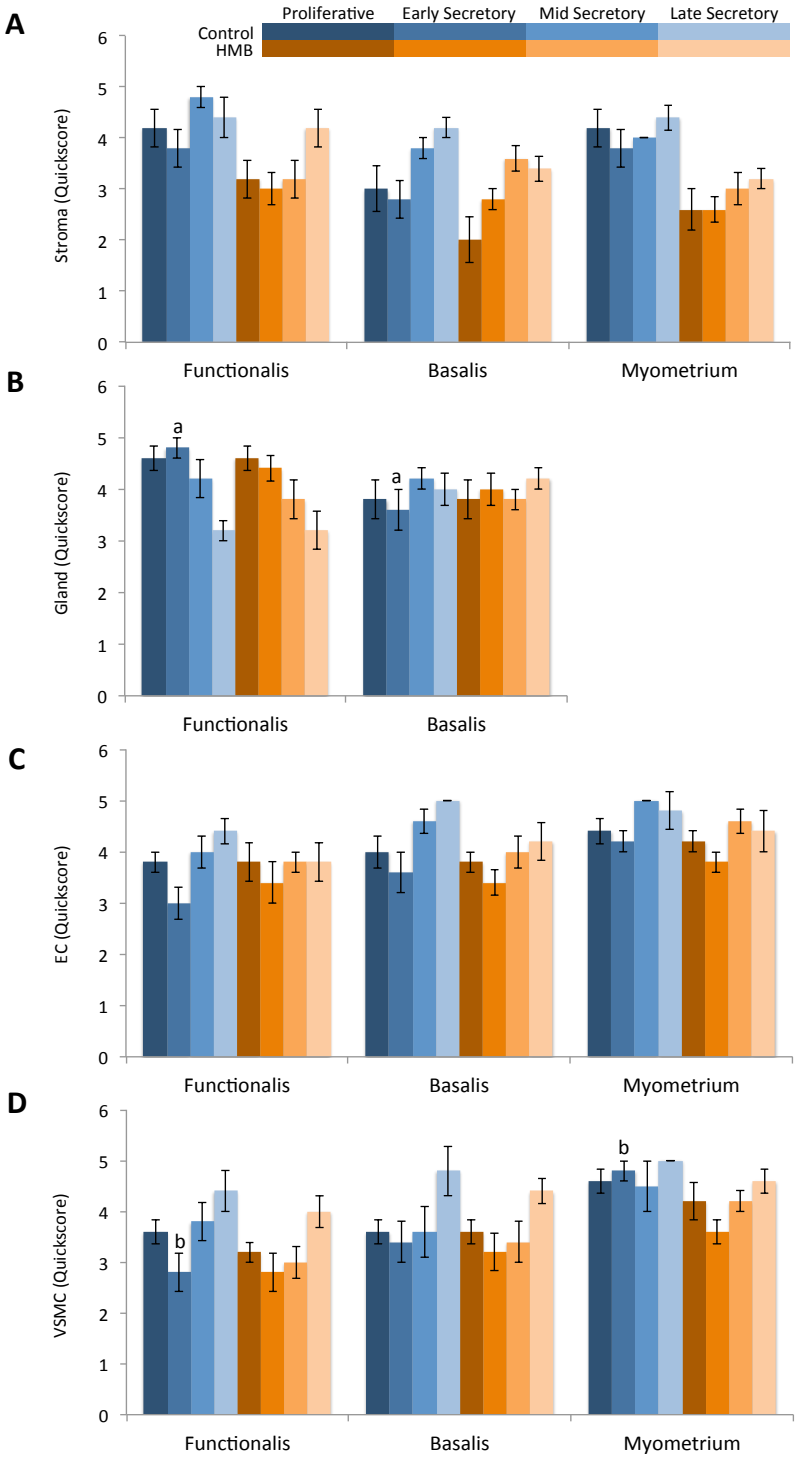


Figure 4.7: Graphical representation of immunohistochemical staining for TGFβ1 during the menstrual cycle. (**A-D**) Quickscore assessment (mean ± SEM) of TGFβ1 staining (N=5, each phase, each group) in controls and in HMB for stromal cells (**A**), glandular epithelial cells (**B**), ECs (**C**) and VSMCs (**D**). Bars labelled with the same letter are significantly different from each other. (a, b) represent differences between layers, within each phase; ^{a}P=0.015, ^{b}P=0.010. Pairwise Kruskal-Wallis one way ANOVA, with Bonferroni correction determined significant differences between phases or layers in control. Mann-Whitney U test, with Bonferroni correction determined significant differences between control and HMB.

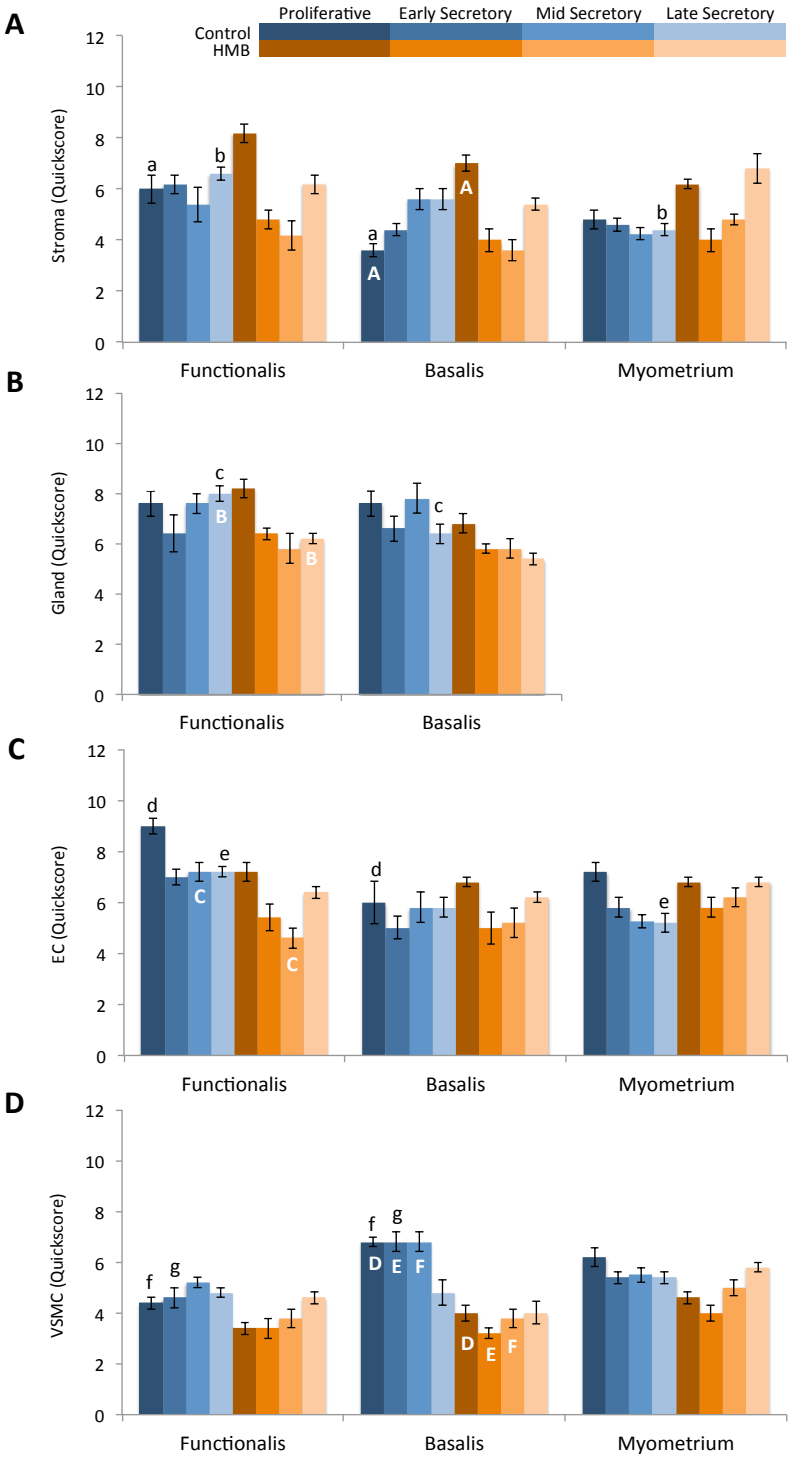


Figure 4.8: Graphical representation of immunohistochemical staining for TGFβRI during the menstrual cycle. (**A-D**) Quickscore assessment (mean ± SEM) of TGFβRI staining (N=5, each phase, each group) in controls and in HMB for stromal cells (**A**), glandular epithelial cells (**B**), ECs (**C**) and VSMCs (**D**). Bars labelled with the same letter are significantly different from each other. (a-g) represent differences between layers, within each phase; ^{a}P=0.012, $^{b, f}P$=0.006, ^{c}P=0.016, $^{d, g}P$=0.009, ^{e}P=0.010. (A-F) represent differences between control and HMB; $^{A\text{-}F}P$=0.008. Pairwise Kruskal-Wallis one way ANOVA, with Bonferroni correction determined significant differences between phases or layers in control. Mann-Whitney U test, with Bonferroni correction determined significant differences between control and HMB.

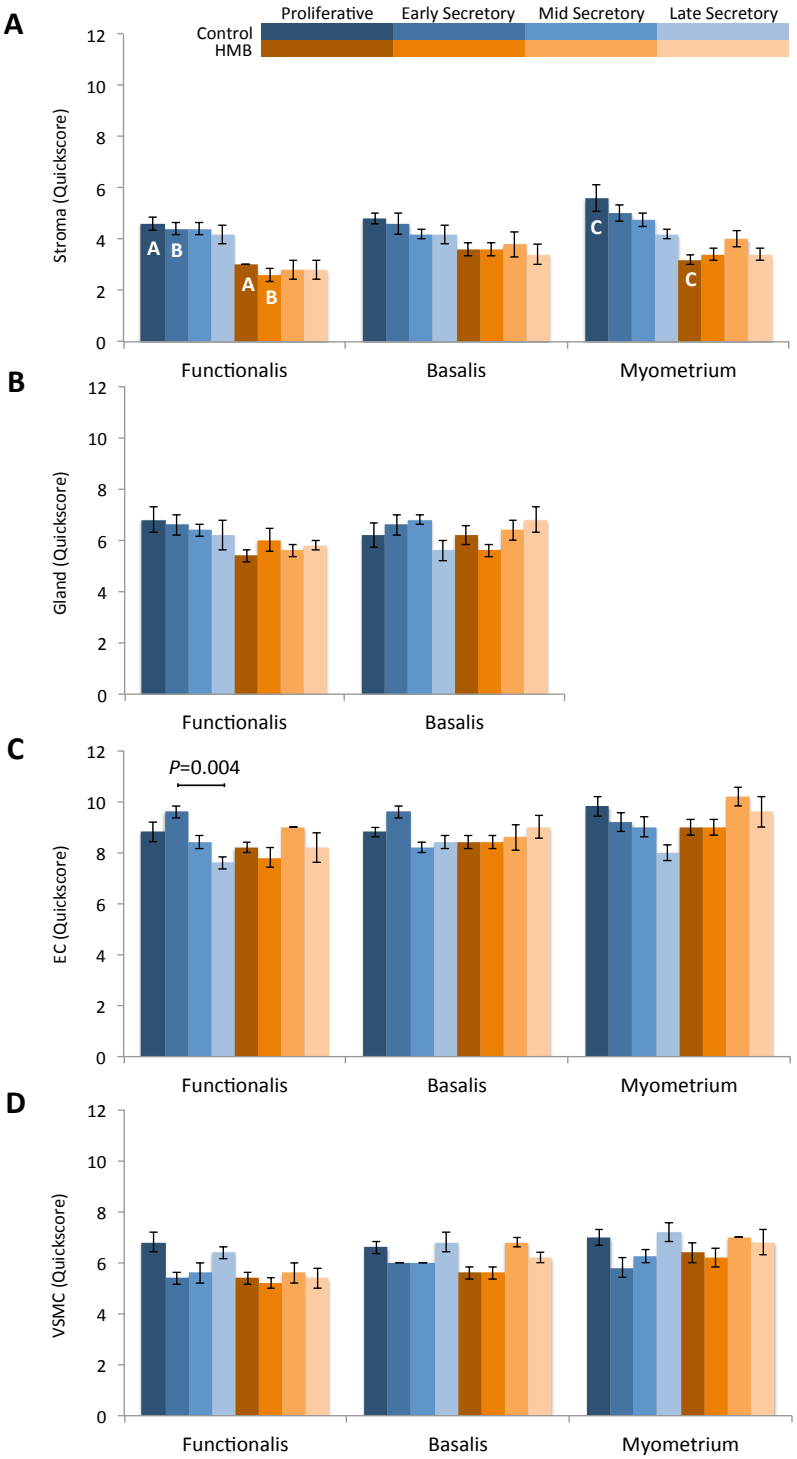


Figure 4.9: Graphical representation of immunohistochemical staining for TGFβRII during the menstrual cycle. (**A-D**) Quickscore assessment (mean ± SEM) of TGFβRII staining (N=5, each phase, each group) in controls and in HMB for stromal cells (**A**), glandular epithelial cells (**B**), ECs (**C**) and VSMCs (**D**). '*P*' value shown in graph represents significant difference between phases within each layer. Bars labelled with the same letter are significantly different from each other. (A-C) represent differences between control and HMB; $^{A\text{-}C}P$=0.008. Pairwise Kruskal-Wallis one way ANOVA, with Bonferroni correction determined significant differences between phases or layers in control. Mann-Whitney U test, with Bonferroni correction determined significant differences between control and HMB.

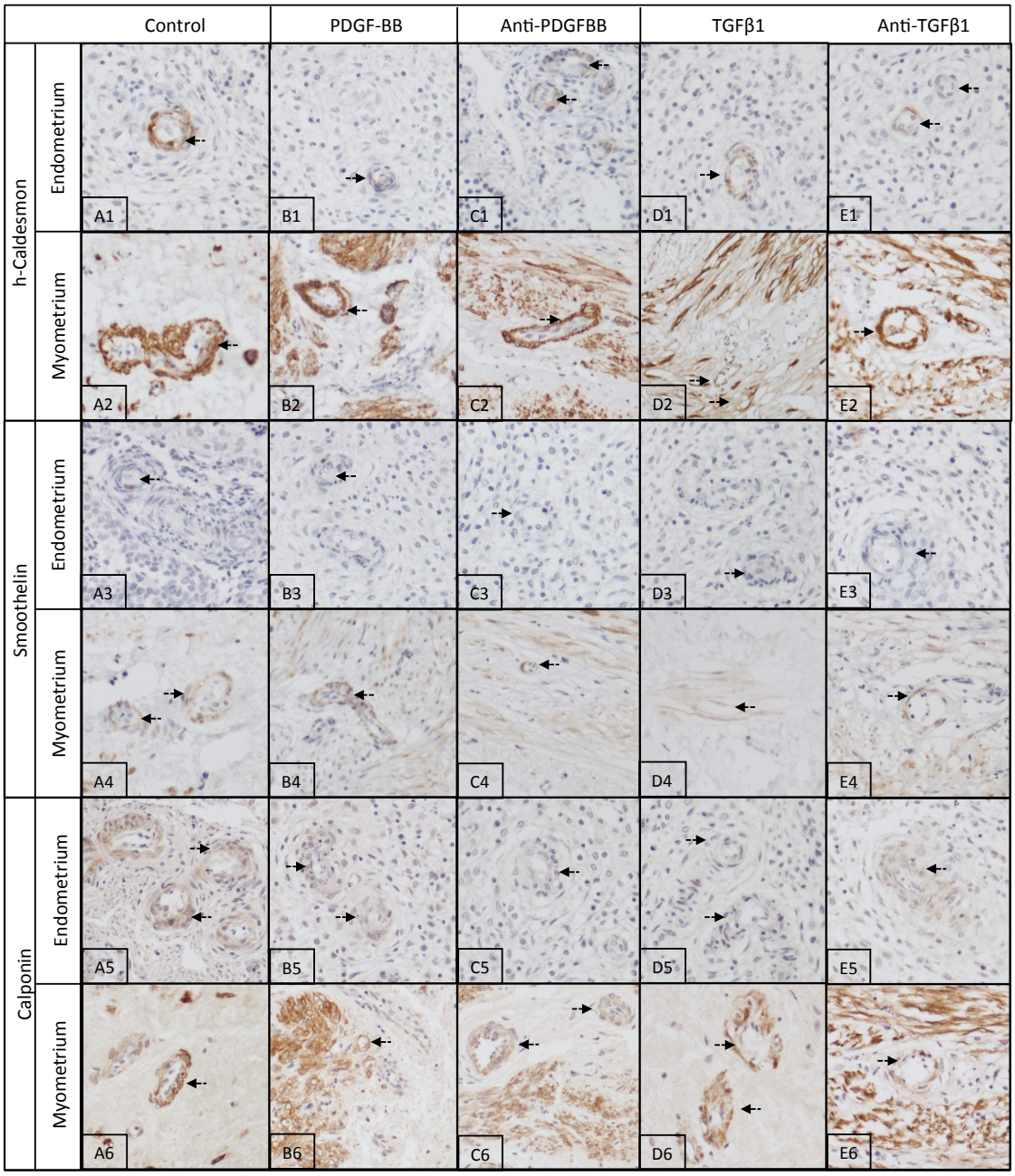


Figure 4.10: Staining for VSMC differentiation markers h-Caldesmon, smoothelin and calponin in endometrial and superficial myometrial explants. Arrows indicate vessels in untreated control endometrium and myometrium (**A1**-**A6**) or after treatment with 10ng/ml of PDGF-BB (**B1**-**B6**), anti-PDGFBB (**C1**-**C6**), TGFβ1 (**D1**-**D6**) and anti-TGFβ1 (**E1**-**E6**). Images were captured at 200x original magnification.

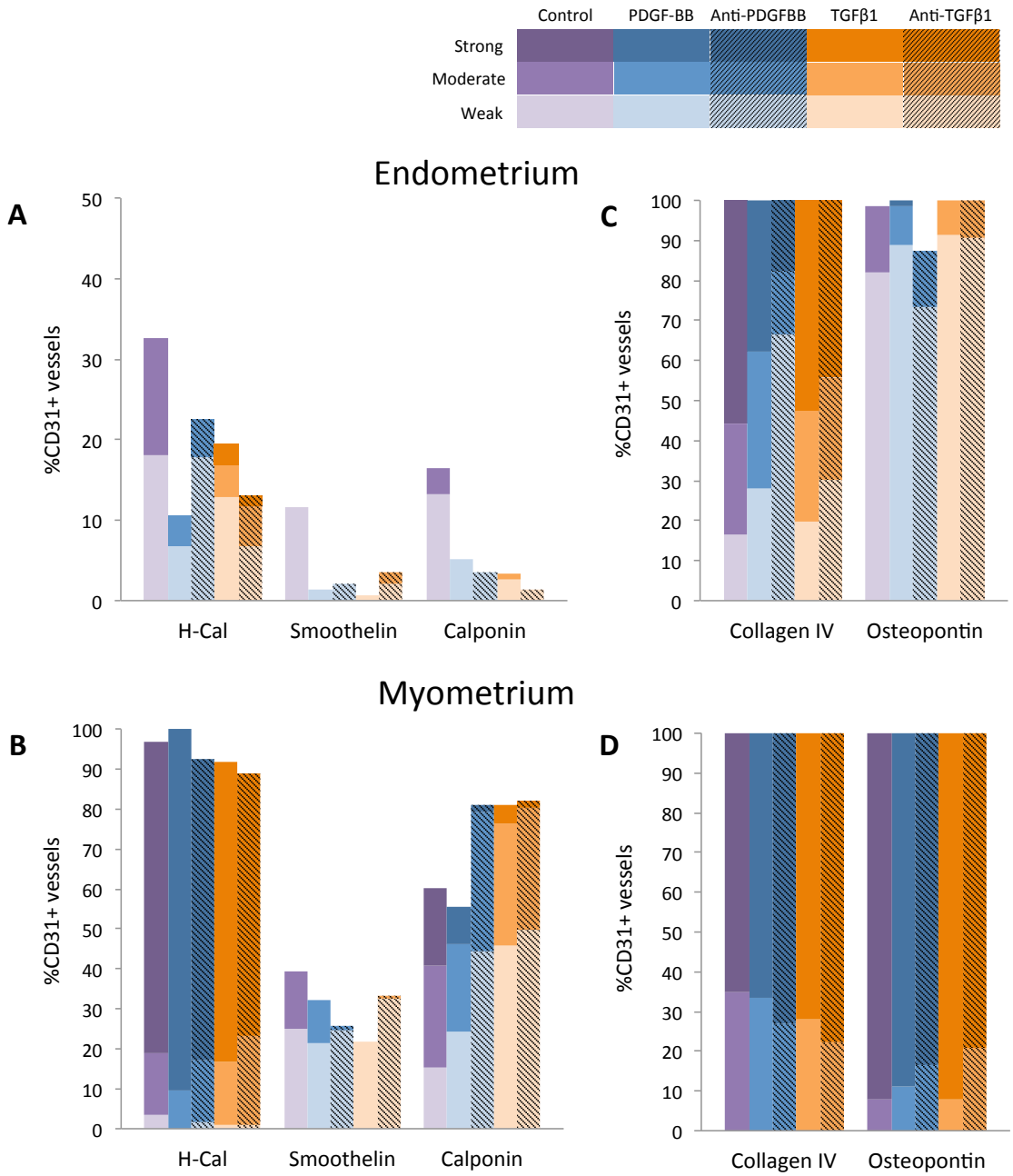


Figure 4.11: Stacked cluster chart showing % CD31 positive vessels stained for VSMC differentiation markers and ECM components in endometrial and superficial myometrial explants. h-Caldesmon, smoothelin, calponin (**A**,**B**) and collagen IV and osteopontin (**C**,**D**) in the endometrium (**A**,**C**; N=2) and myometrium (**B**,**D**; N=3) of untreated control or treated for 72 hr with 10ng/ml of each of PDGF-BB, anti-PDGFBB, TGFβ1 and anti-TGFβ1. Pairwise Kruskal-Wallis one way ANOVA, with Bonferroni correction was used to determine significant differences between control and treated groups for myometrium; no significant differences were observed.

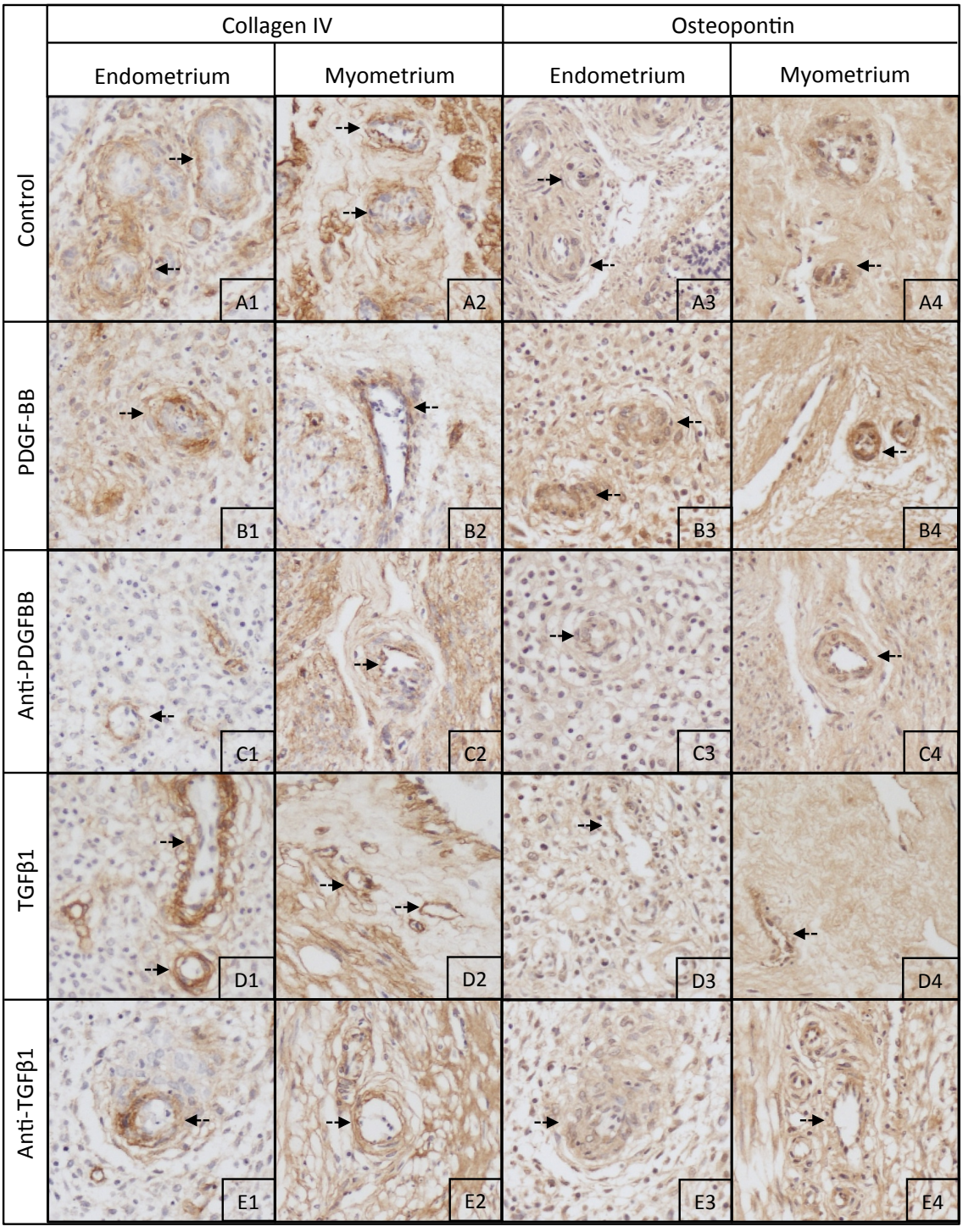


Figure 4.12: Staining for ECM components collagen IV and osteopontin in endometrial and superficial myometrial explants. Arrows indicate vessels in untreated control endometrium and myometrium (**A1**-**A4**) or treated for 72 hr with 10ng/ml of each of PDGF-BB (**B1**-**B4**), anti-PDGFBB (**C1**-**C4**), TGFβ1 (**D1**-**D4**) and anti-TGFβ1 (**E1**-**E4**). Images were captured at 200x original magnification.

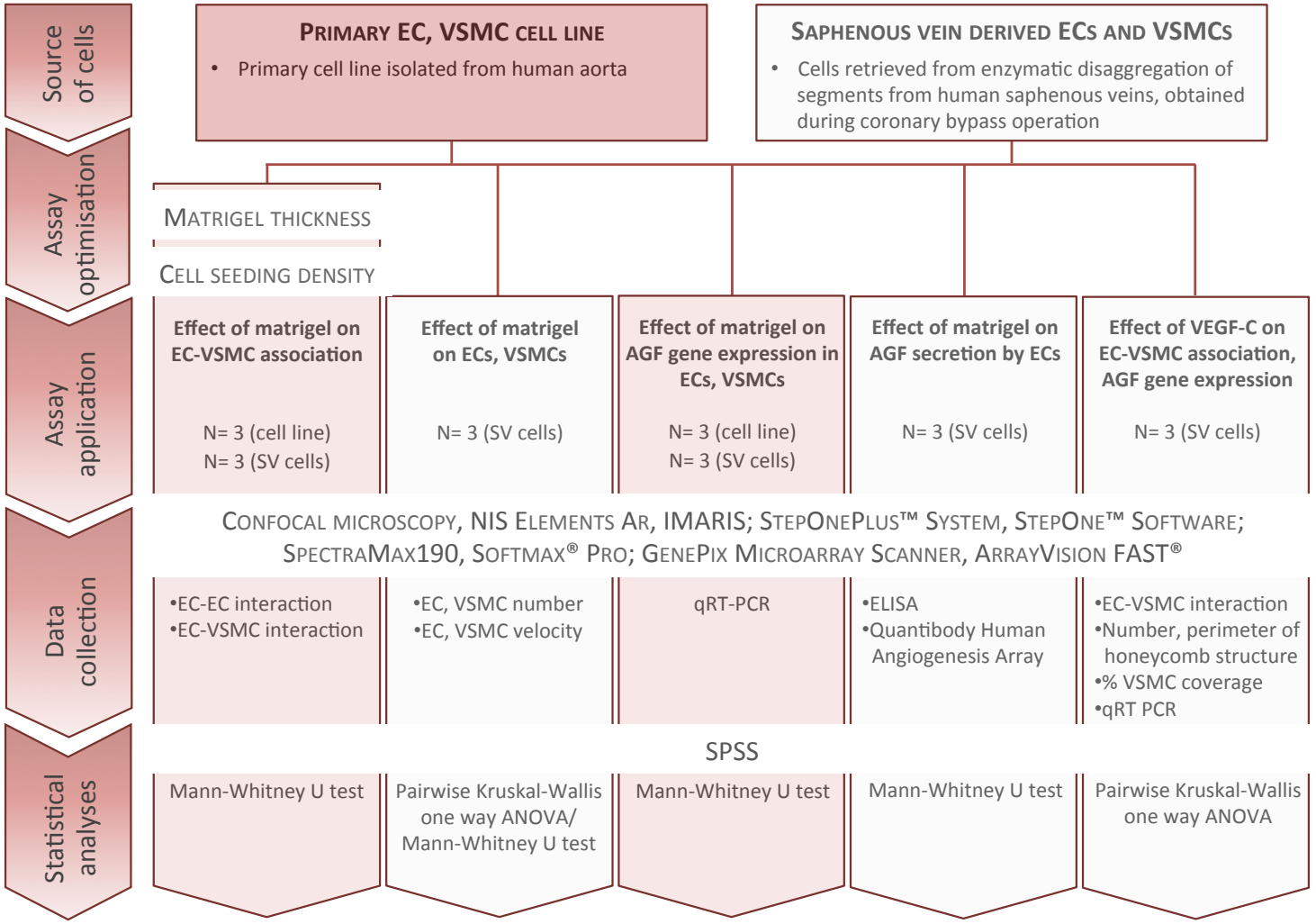


Figure 5.1: Experimental design to develop and optimise an *in vitro* assay aiding investigation of EC-VSMC association and how this process is affected by angiogenic growth factors.

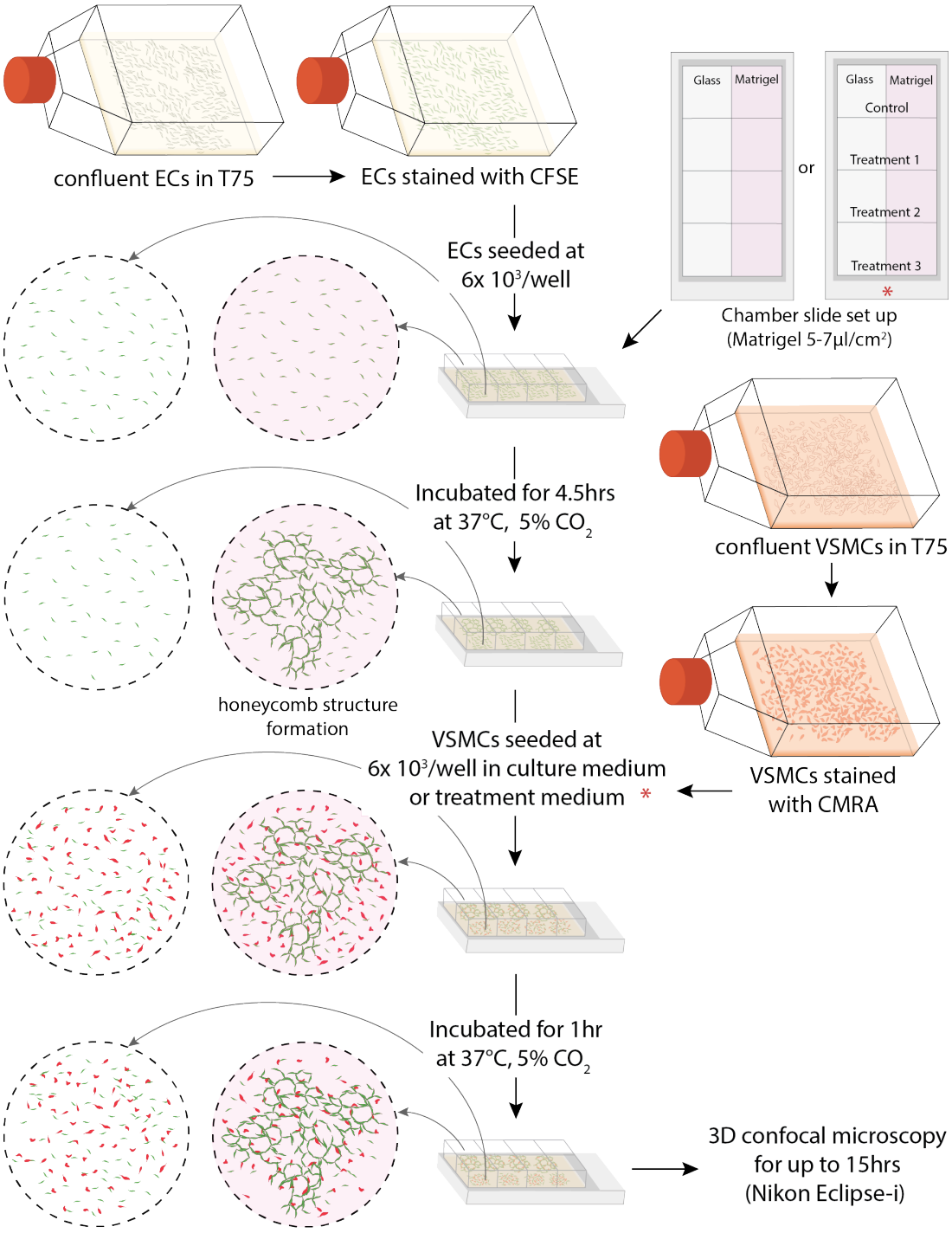


Figure 5.2: Principal steps involved in the *in vitro* tubule formation and EC-VSMC association assay.

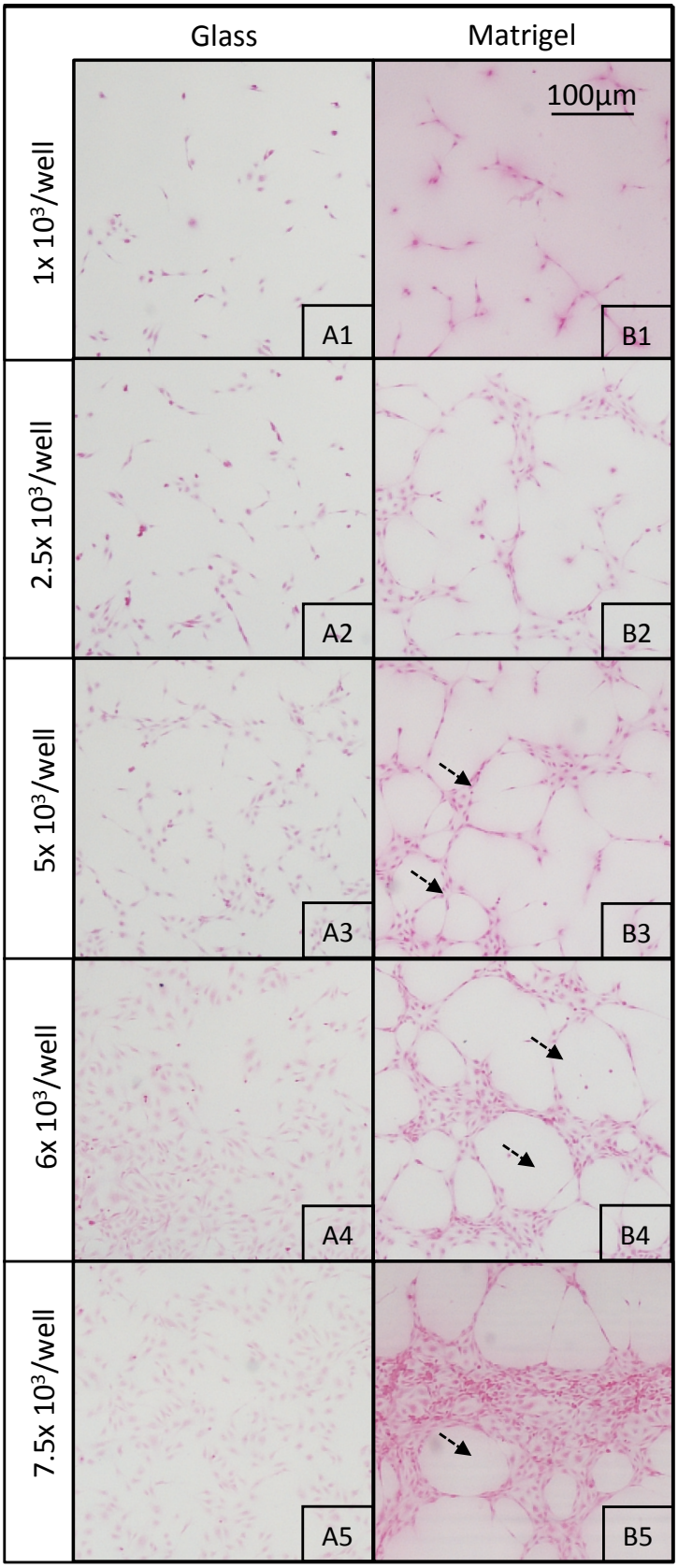


Figure 5.3: Seeding density of saphenous vein derived endothelial cells on glass (**A1-A4**) and matrigel (**B1-B4**). Images were captured at 100x magnification. Arrows indicate tubule or honeycomb structure formation. Note that 6x10^3/well (**B4**) was chosen as optimal. (**B5**) Higher than optimal number of ECs clustered to disrupt efficient tubule formation.

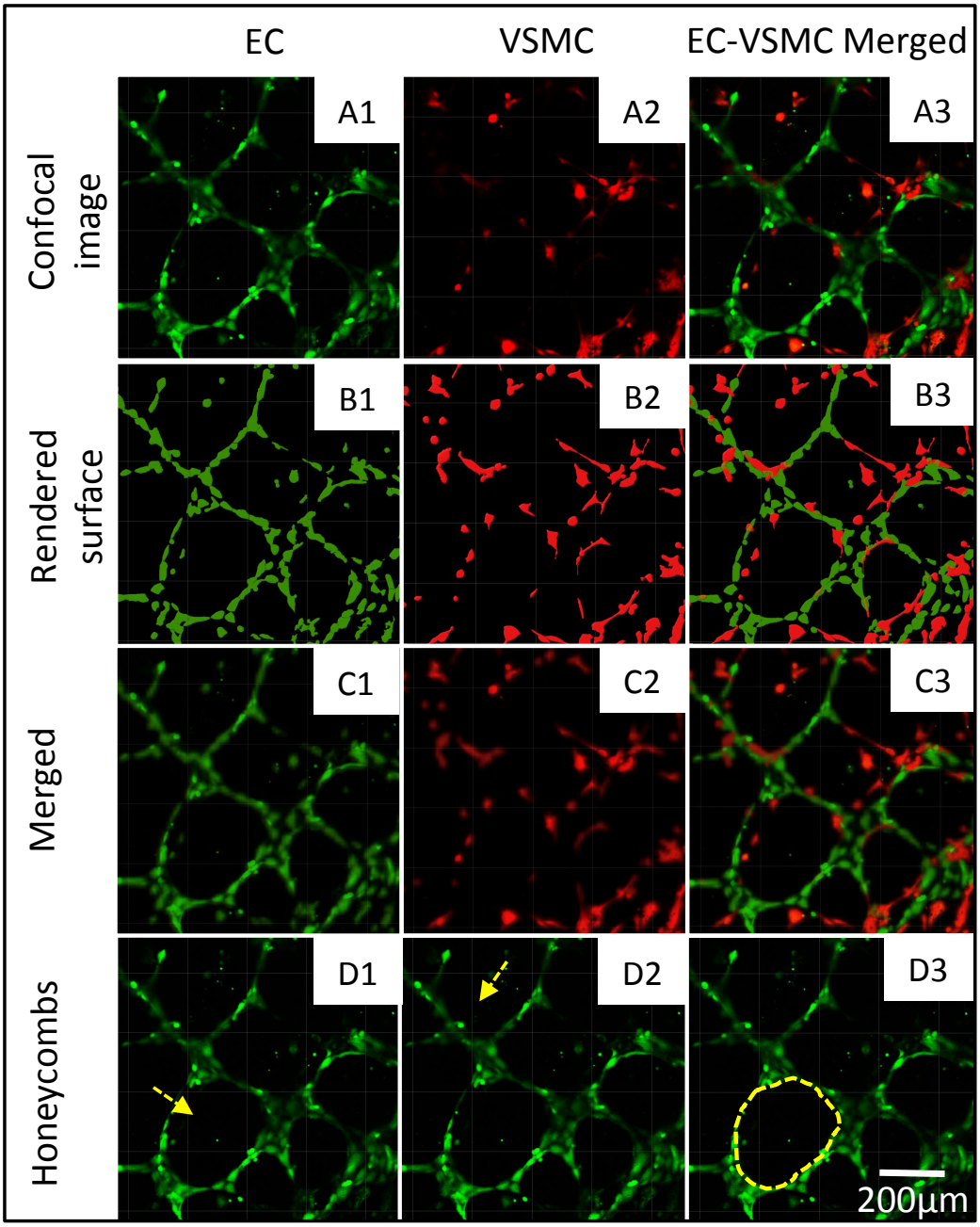


Figure 5.4: Quantitative image analysis utilised for the *in vitro* assay. (**A-C**) show surface rendering using IMARIS software package and (**D**) shows types of honeycombs (yellow arrows, dotted lines; **D1** shows complete honeycomb, **D2** shows incomplete honeycomb and **D3** shows perimeter of a complete honeycomb.

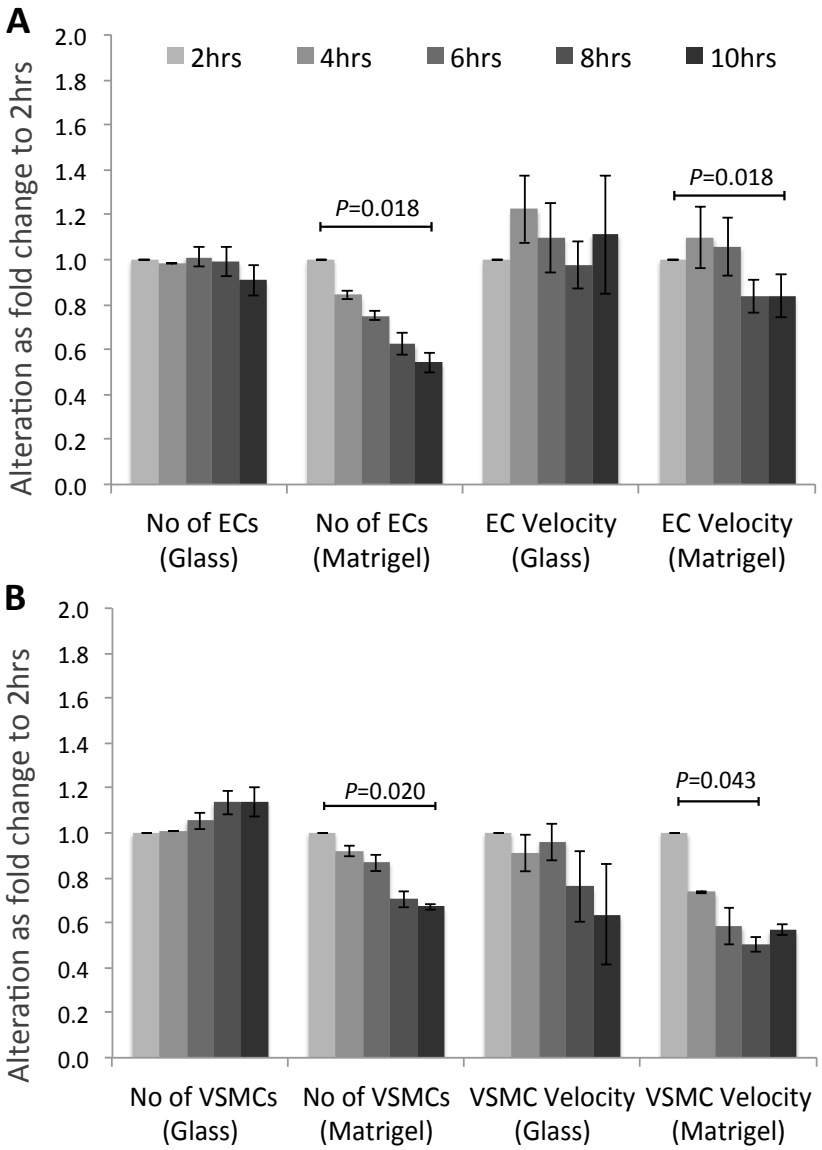


Figure 5.5: Graphical representation (mean ± SEM) of fold change in number and velocity of endothelial cells (ECs) and vascular smooth muscle cells (VSMCs). Saphenous vein derived (**A**) ECs and (**B**) VSMCs were cultured on glass and matrigel (N=3 each group) for up to 10 hr. Mann-Whitney U test determined significant difference between glass and matrigel while Pairwise Kruskal-Wallis one way ANOVA determined significant difference between different time points.

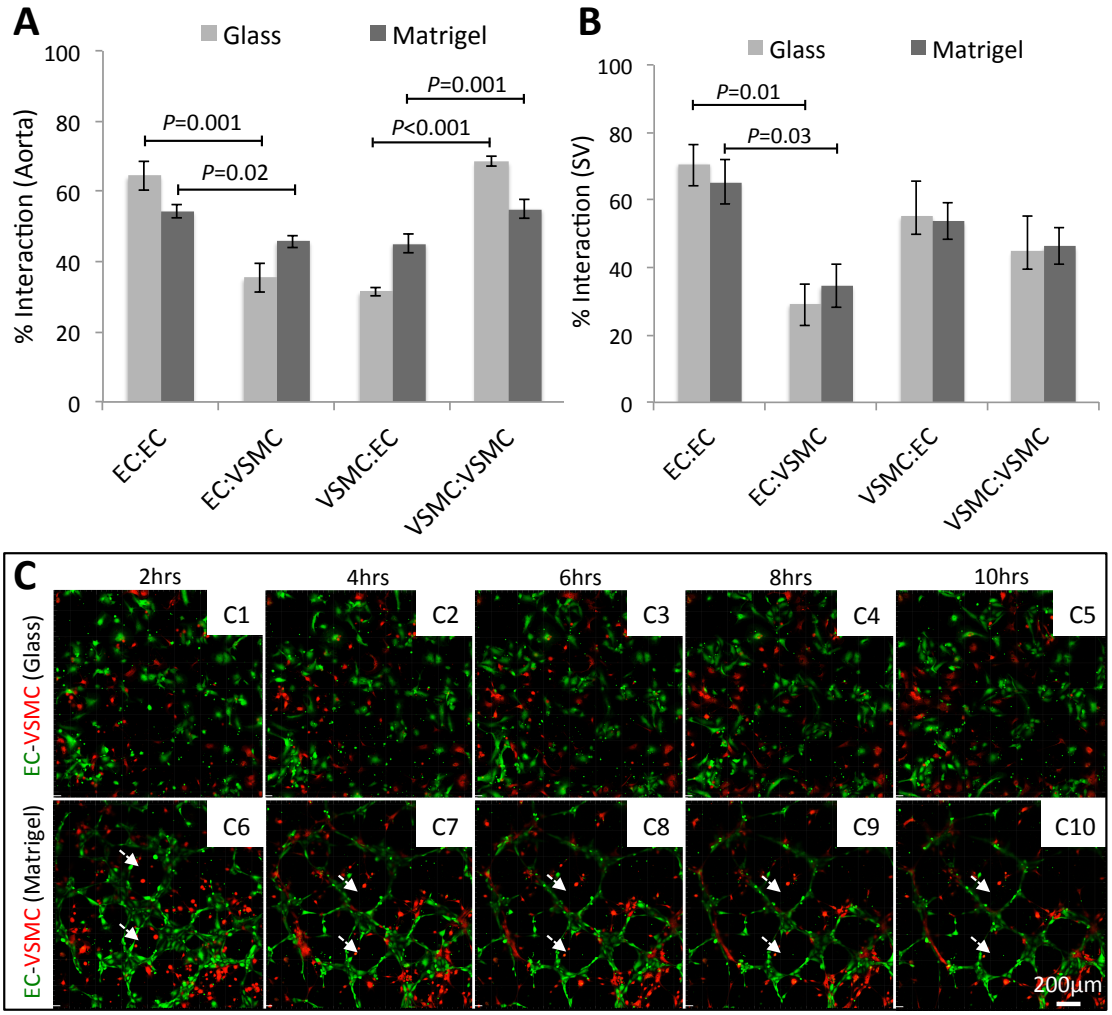


Figure 5.6: Graphical representation (mean ± SEM) of percentage of endothelial cells (ECs), which interacted with other ECs or with vascular smooth muscle cells (VSMCs). Cellular interaction during the course of a 10 hr assay (N=3 each group) using cells from human (**A**) aorta and (**B**) saphenous vein. Mann-Whitney U test determined significant difference in EC:EC, EC:VSMC, VSMC:EC and VSMC:VSMC interaction between glass and matrigel as well as between aorta and saphenous vein. (**C**) ECs (green) form honeycomb structures indicated by arrows, to which VSMCS (red) are recruited, only when they are cultured on matrigel (**C6-C10**), but not on glass (**C1-C5**).

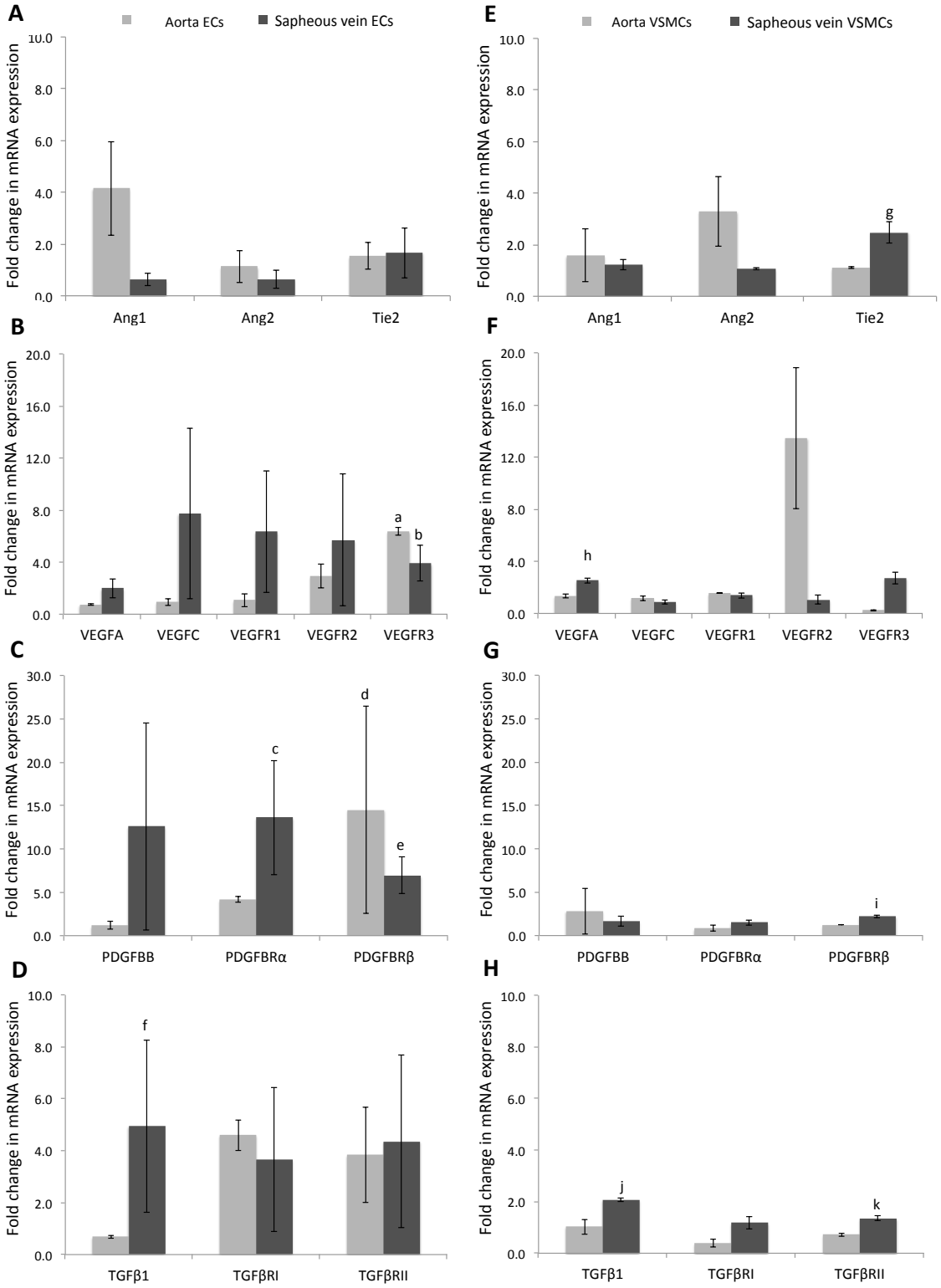


Figure 5.7: Graphical representation (mean ± SEM) of fold change in mRNA expression of angiogenic growth factors. **(A-D)** endothelial cells (ECs) and **(E-H)** vascular smooth muscle cells (VSMCs) from human aorta or saphenous vein cultured on matrigel compared with plastic (N=3 each group). Mann-Whitney U test determined significant difference in fold change mRNA expression on matrigel compared with plastic (indicated by a-k; ^{a}P=0.015, $^{b,f,k}P$=0.05, $^{c,j}P$=0.016, ^{d}P=0.03, ^{e}P=0.022, ^{g}P=0.006, $^{h,i}P$=0.004, ^{b}P=0.05).

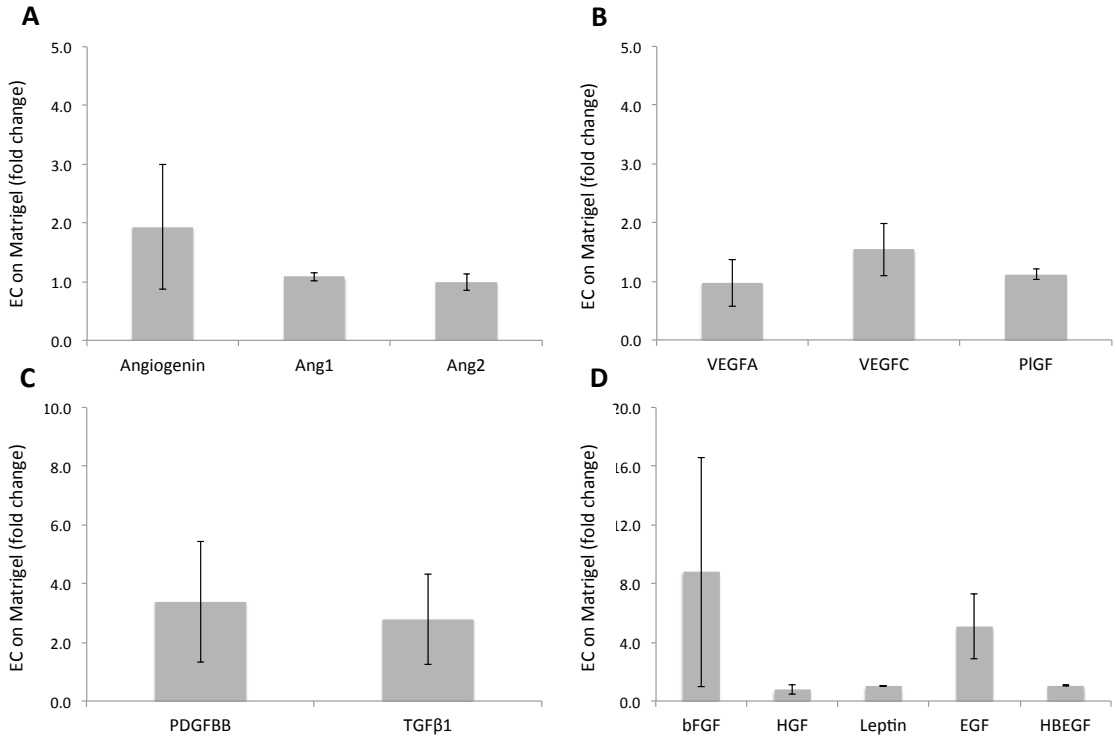


Figure 5.8: Graphical representation (mean ± SEM) of fold change in angiogenic growth factor secretion SV derived endothelial cells (ECs). (**A-D**) Saphenous vein derived ECs cultured on matrigel (N=3 each group). Mann-Whitney U test determined significant difference between fold changes in AGF secretion on matrigel compared with plastic. No significant differences were observed.

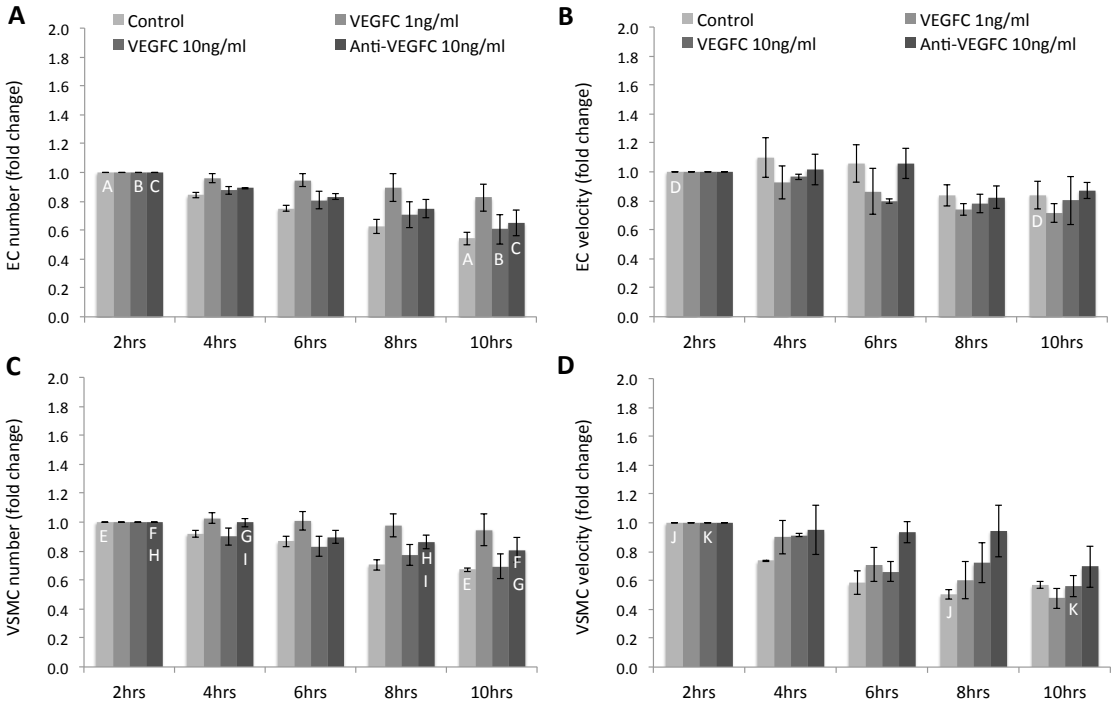


Figure 5.9: Graphical representation (mean ± SEM) of fold change in number and velocity of VEGF-C treated endothelial cells (EC) and vascular smooth muscle cells (VSMC) on matrigel. Fold change in saphenous vein derived EC (**A**) number and (**B**) velocity and VSMC (**C**) number and (**D**) velocity (N=3 each group) at different time points relative to 2 hr between untreated control or VEGF-C treatments, on matrigel. Pairwise Kruskal-Wallis one way ANOVA determined significant difference between different time points and between untreated control or VEGF-C treatments. Bars with same letters are significantly different from each other; $^{A,C}P$=0.018, ^{B}P=0.033, $^{D,F}P$=0.020, ^{E}P=0.035, ^{G}P=0.044, ^{H}P=0.028, ^{I}P=0.043, ^{J}P=0.025.

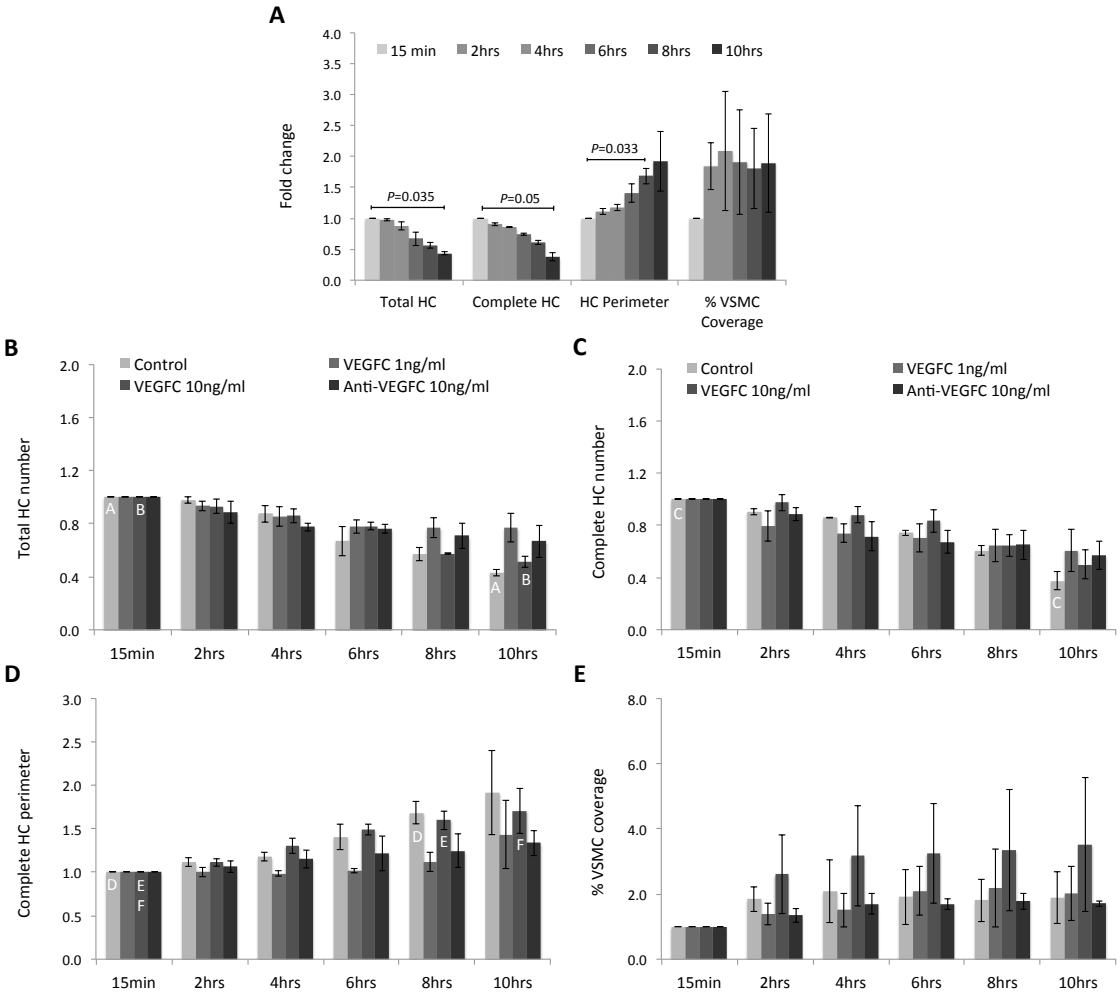


Figure 5.10: Graphical representation (mean ± SEM) of fold change in VEGF-C treated (EC) honeycombs (HC) and vascular smooth muscle cell (VSMC) coverage. Fold change at different time points relative to 15 min in number of (**A, B**) total HC with ≥3arms, (**A, C**) complete honeycomb, (**A, D**) perimeter of complete honeycomb and (**E**) percentage of VSMC coverage of complete honeycomb by saphenous vein derived ECs and VSMCs (N=3 each group). Pairwise Kruskal-Wallis one way ANOVA determined significant difference between different time points and between untreated control or VEGF-C treatments. Bars with same letters are significantly different from each other. 'P' values represent differences between different time points; ^{A}P=0.035, ^{B}P=0.024, ^{C}P=0.050, ^{D}P=0.033, $^{E,F}P$=0.047.

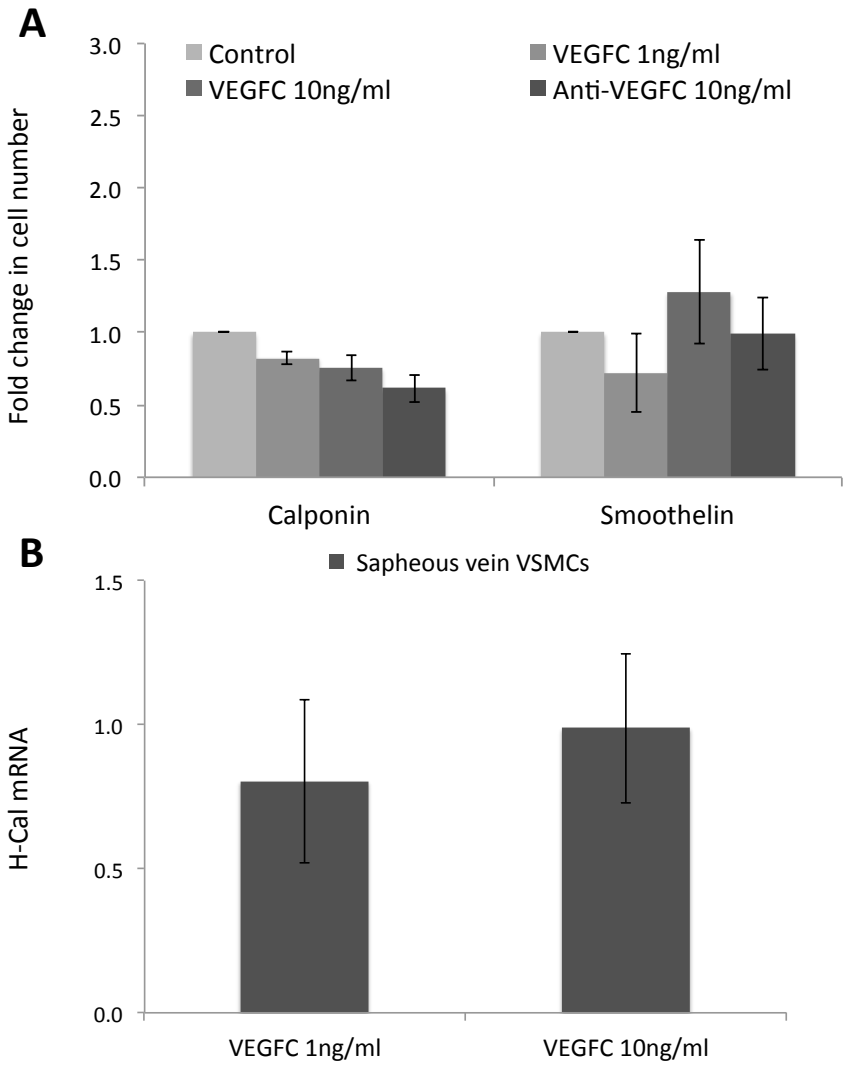


Figure 5.11: Graphical representation (mean ± SEM) of fold change in calponin$^+$ or smoothelin$^+$ saphenous vein derived vascular smooth muscle cells (VSMCs). Fold change compared with untreated control (**A**) in percentage calponin$^+$ or smoothelin$^+$ VSMCs and (**B**) in H-Cal mRNA in saphenous vein derived VSMCs cultured on matrigel (N=3 each group). Pairwise Kruskal-Wallis one way ANOVA. No significant differences were observed.

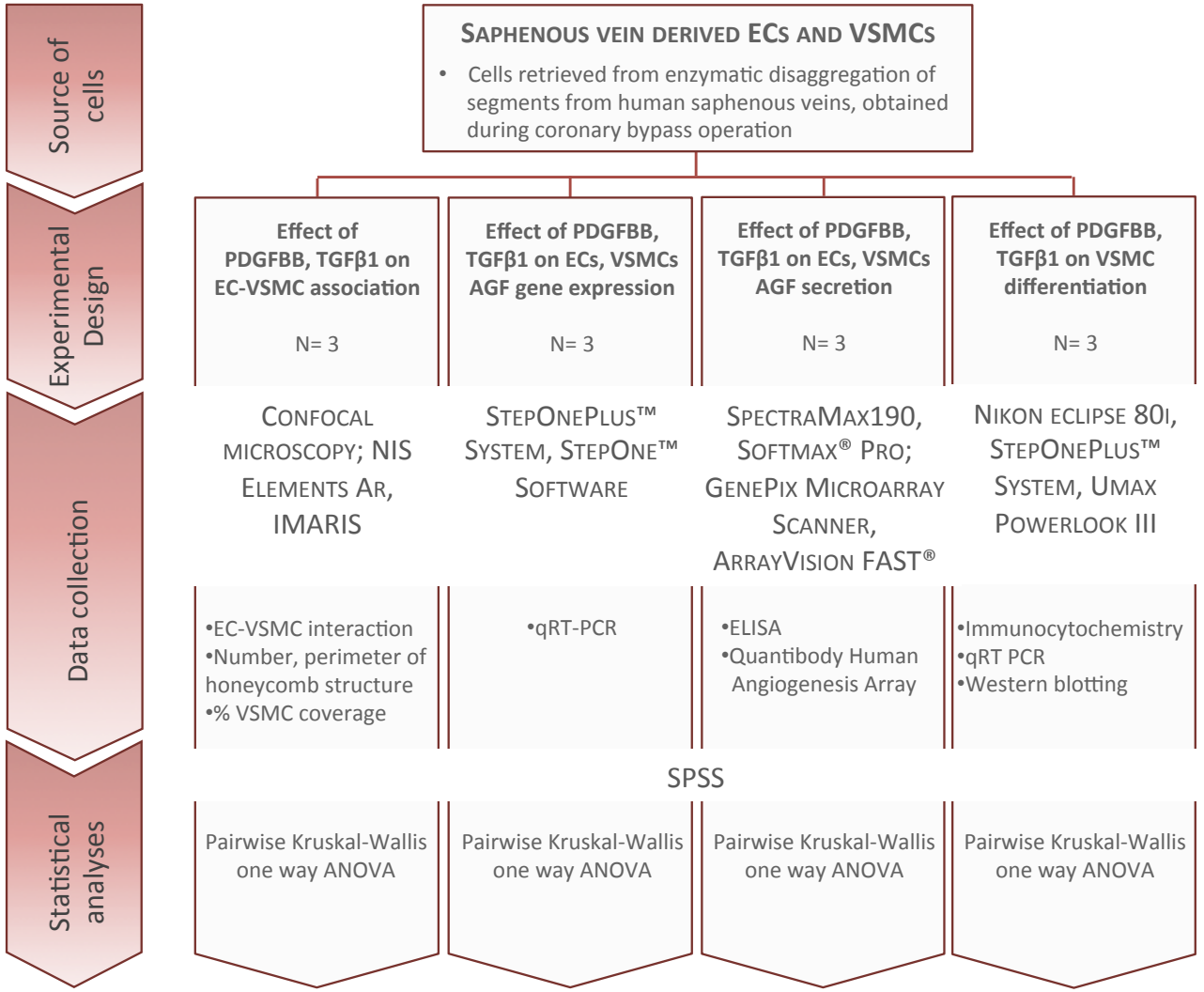


Figure 6.1: Experimental design to study the effect of PDGF-BB and TGFβ1 on EC-VSMC association and VSMC differentiation *in vitro*.

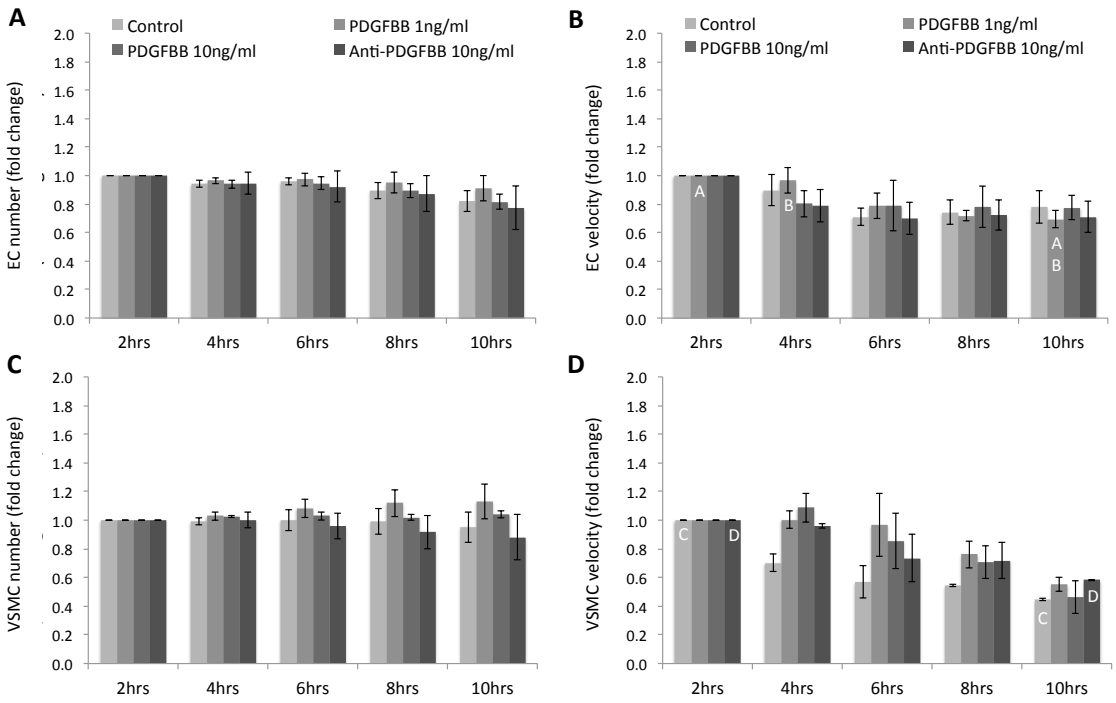


Figure 6.2: Graphical representation (mean ± SEM) of fold change in number and velocity of PDGF-BB treated endothelial cells (EC) and vascular smooth muscle cells (VSMC) on matrigel. Fold change in saphenous vein derived EC (**A**) number and (**B**) velocity and VSMC (**C**) number and (**D**) velocity (N=3 each group) at different time points relative to 2 hr between untreated control or PDGF-BB treatments, on matrigel. Pairwise Kruskal-Wallis one way ANOVA determined significant difference between different time points and between untreated control or PDGF-BB treatments. Bars with same letters are significantly different from each other; ^{A}P=0.035, ^{B}P=0.022, ^{C}P=0.009, ^{D}P=0.006.

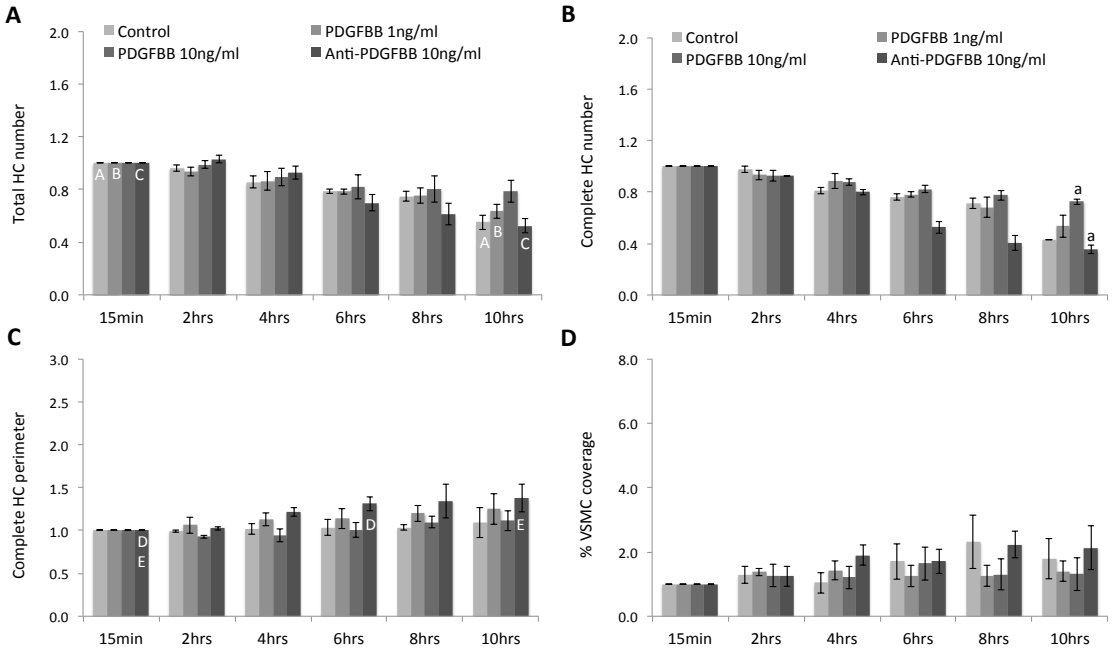


Figure 6.3: Graphical representation (mean ± SEM) of fold change in PDGF-BB treated (EC) honeycombs (HC) and vascular smooth muscle cell (VSMC) coverage. Fold change at different time points relative to 15 min in number of (**A**) total HC with ≥3arms, (**B**) complete HC, (**C**) perimeter of complete HC and (**D**) percentage of VSMC coverage of complete HC by saphenous vein derived ECs and VSMCs (N=3 each group). Pairwise Kruskal-Wallis one way ANOVA determined significant difference between different time points and between untreated control or PDGF-BB treatments. Bars with same letters are significantly different from each other. 'a' represents difference between treatments, 'A-E' represent difference between time points; ^{a}P=0.012, ^{A}P=0.012, ^{B}P=0.021, ^{C}P=0.046, ^{D}P=0.016, ^{E}P=0.017.

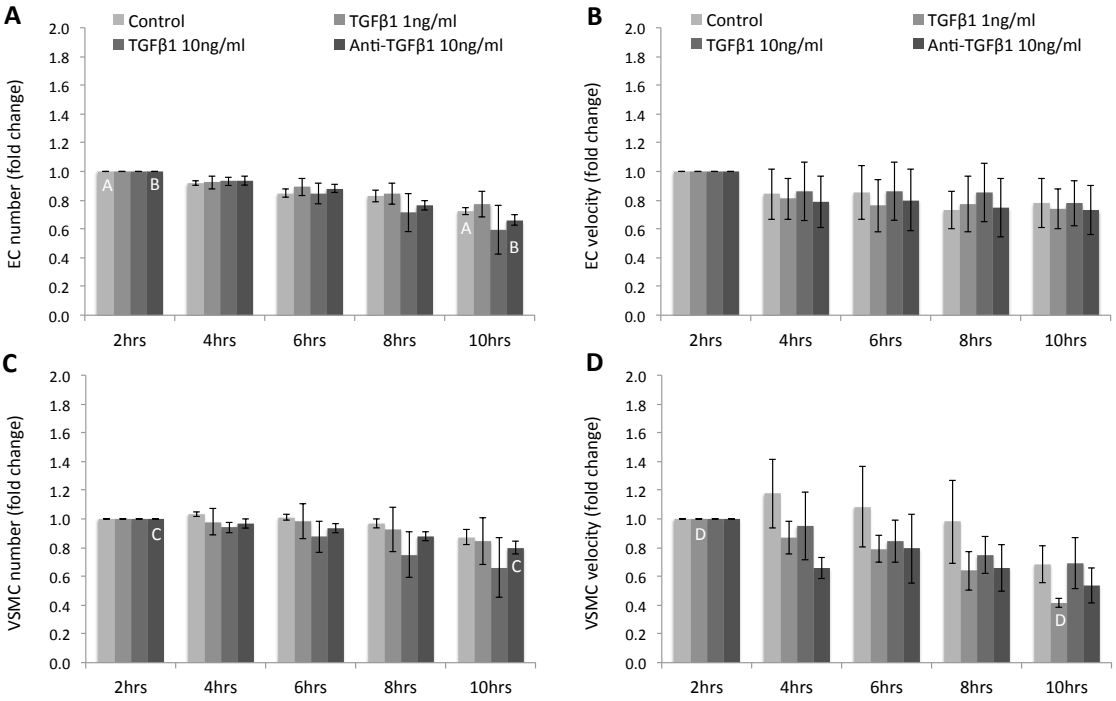


Figure 6.4: Graphical representation (mean ± SEM) of fold change in number and velocity of TGFβ1 treated endothelial cells (EC) and vascular smooth muscle cells (VSMC) on matrigel. Fold change in saphenous vein derived EC (**A**) number and (**B**) velocity and VSMC (**C**) number and (**D**) velocity (N=3 each group) at different time points relative to 2 hr between untreated control or PDGF-BB treatments, on matrigel. Pairwise Kruskal-Wallis one way ANOVA determined significant difference between different time points and between untreated control or TGFβ1 treatments. Bars with same letters are significantly different from each other; $^{A,B}P$=0.013, ^{C}P=0.006, ^{D}P=0.005.

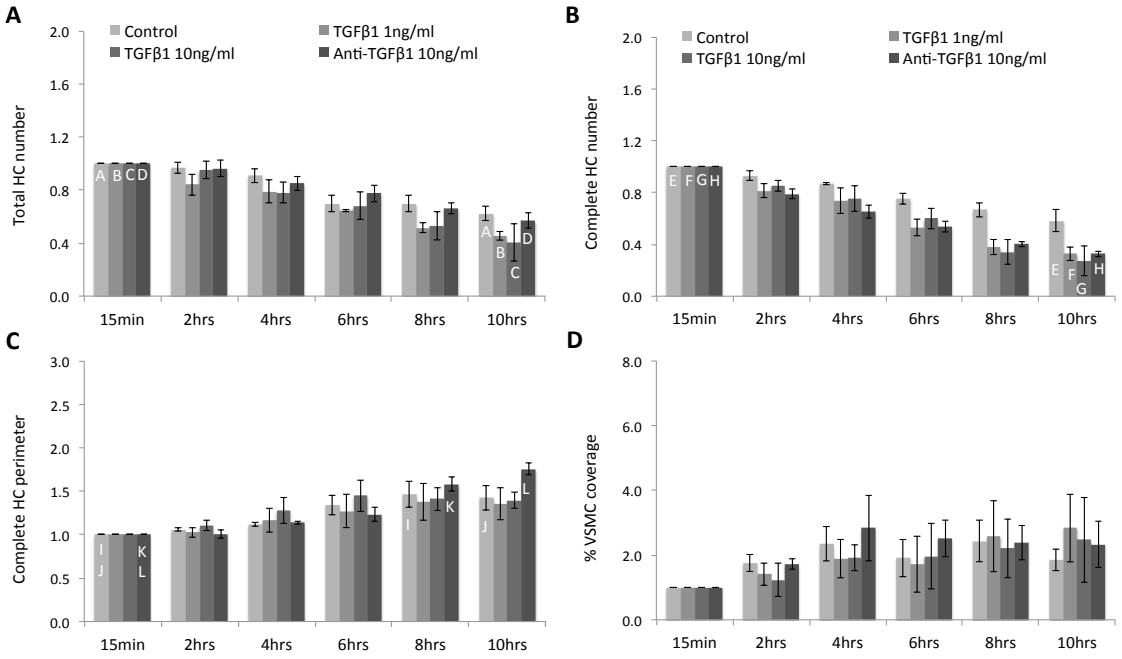


Figure 6.5: Graphical representation (mean ± SEM) of fold change in TGFβ1 treated (EC) honeycombs (HC) and vascular smooth muscle cell (VSMC) coverage. Fold change at different time points relative to 15 min in number of (**A**) total HC with ≥3arms, (**B**) complete HC, (**C**) perimeter of complete HC and (**D**) percentage of VSMC coverage of complete HC by saphenous vein derived ECs and VSMCs (N=3 each group). Pairwise Kruskal-Wallis one way ANOVA determined significant difference between different time points and between untreated control or TGFβ1 treatments. Bars with same letters are significantly different from each other. 'A-L' represent difference between time points; ^{A}P=0.005, ^{B}P=0.001, ^{C}P=0.006, $^{D,I}P$=0.003, ^{E}P=0.040, ^{F}P=0.022, ^{G}P=0.028, ^{H}P=0.010, ^{J}P=0.004, ^{K}P=0.007, ^{L}P=0.002.

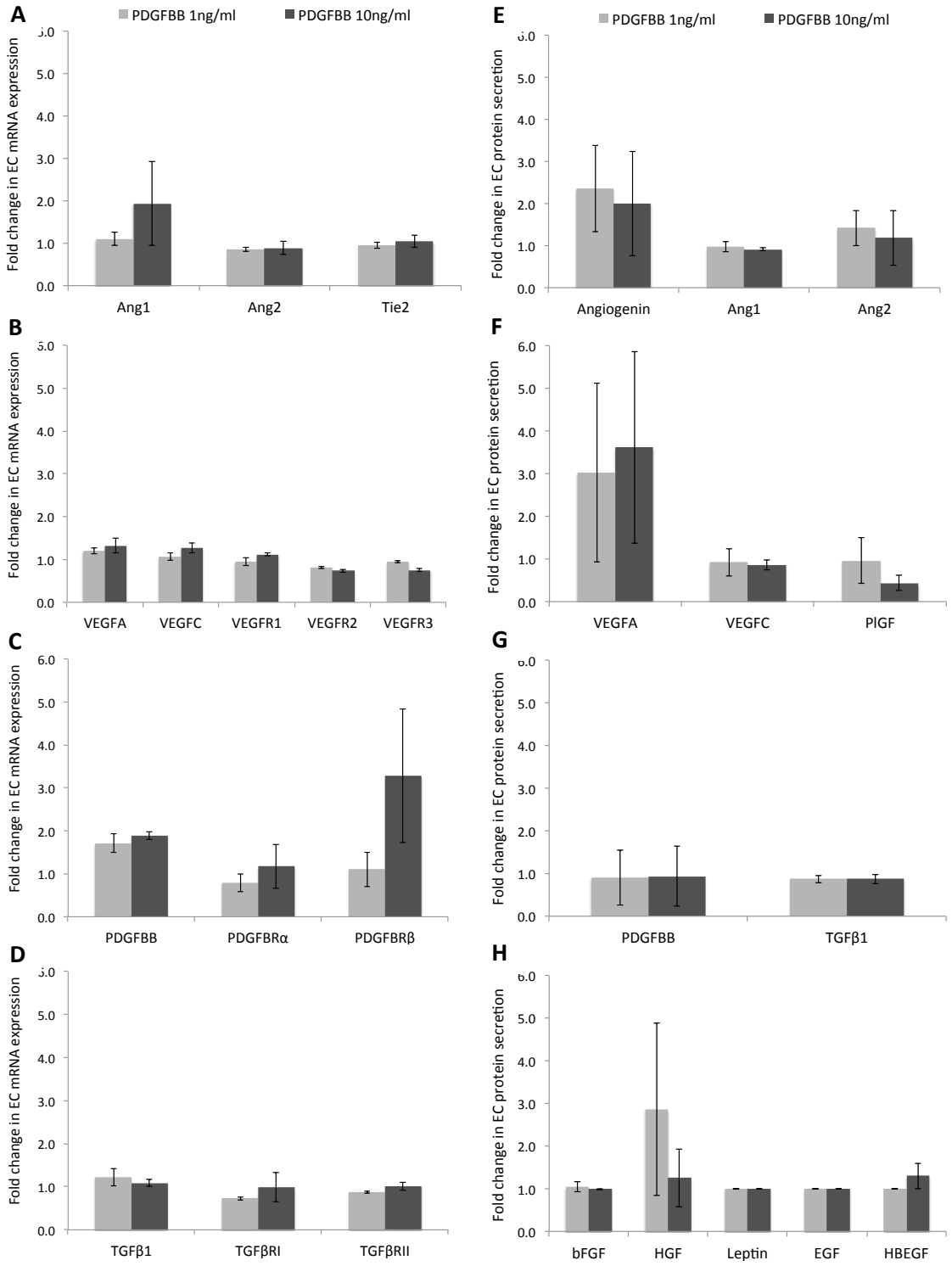


Figure 6.6: Graphical representation (mean ± SEM) of fold change in (**A-D**) mRNA and (**E-H**) secretion of angiogenic growth factors by PDGF-BB treated saphenous vein derived endothelial cells (N=3 each group) cultured on matrigel. Pairwise Kruskal-Wallis one way ANOVA determined significant difference in fold change between control or PDGF-BB treatments. No significant differences were observed.

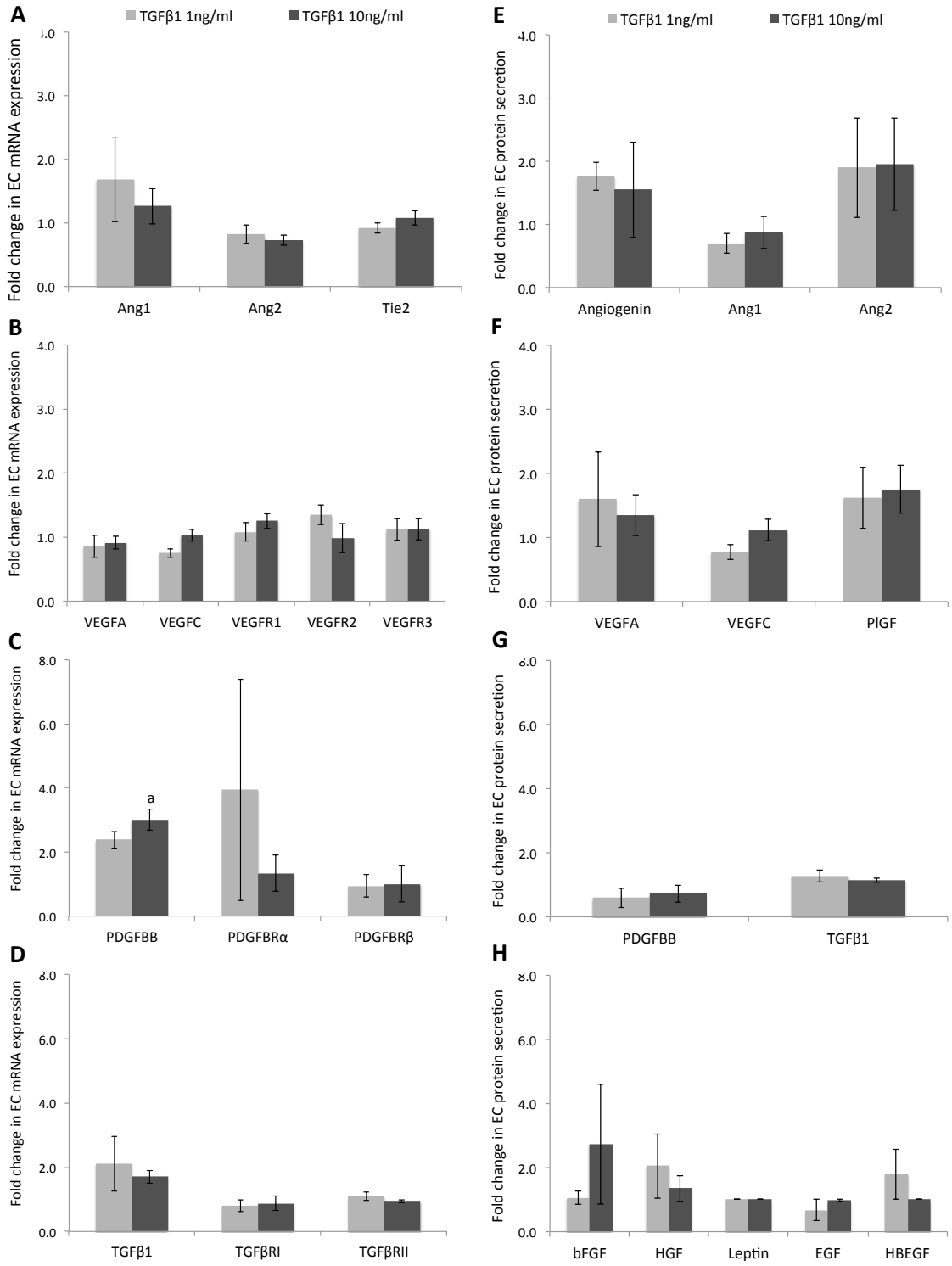


Figure 6.7: Graphical representation (mean ± SEM) of fold change in (**A-D**) mRNA and (**E-H**) secretion of angiogenic growth factors by TGFβ1 treated saphenous vein derived endothelial cells (N=3 each group) cultured on matrigel. Pairwise Kruskal-Wallis one way ANOVA determined significant difference in fold change between control or TGFβ1 treatments. 'a' represents difference between control and 10ng/ml TGFβ1 treatment; ^{a}P=0.03.

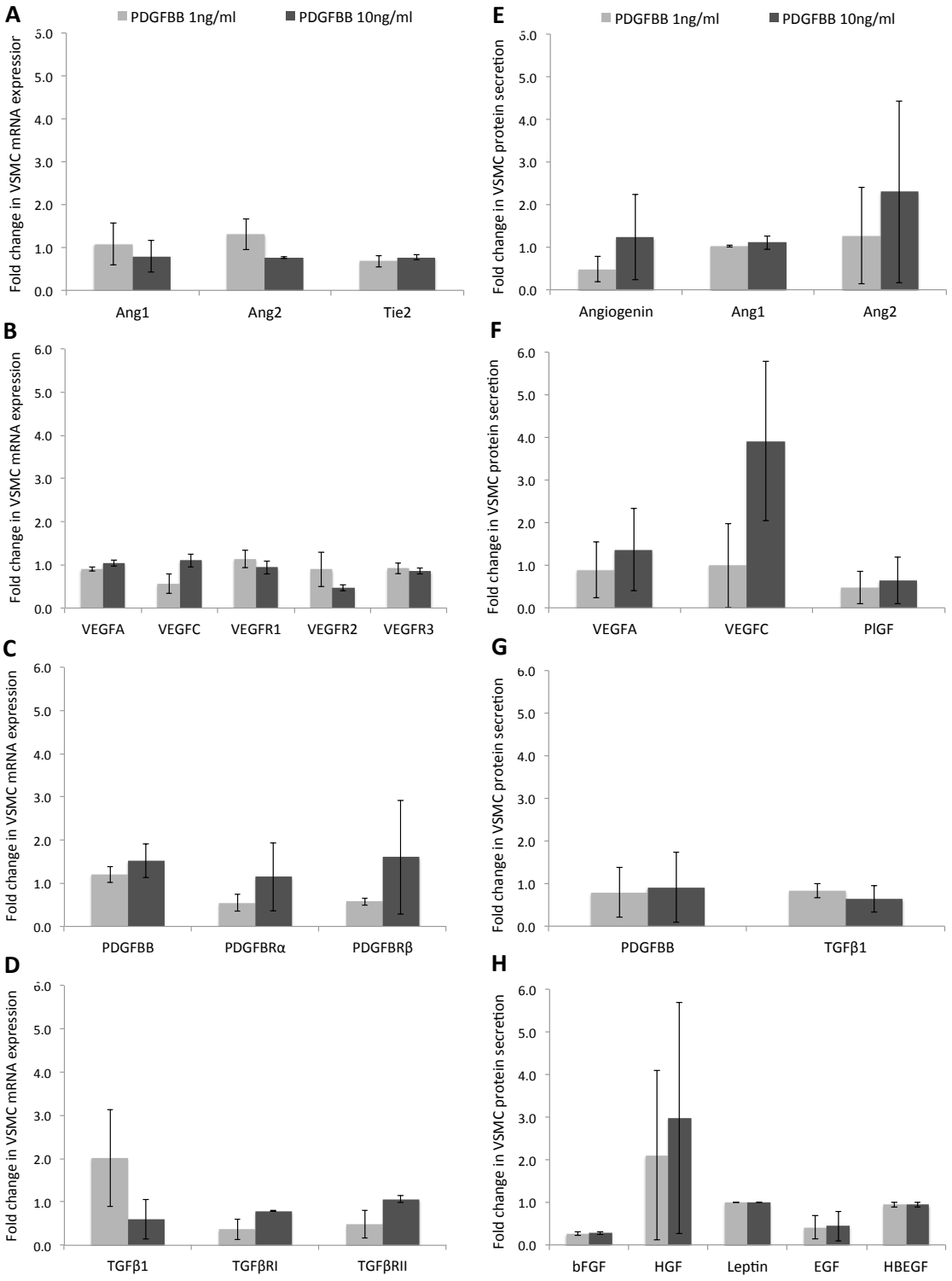


Figure 6.8: Graphical representation (mean ± SEM) of fold change in (**A-D**) mRNA and (**E-H**) secretion of angiogenic growth factors by PDGF-BB treated saphenous vein derived vascular smooth muscle cells (N=3 each group) cultured on matrigel. Pairwise Kruskal-Wallis one way ANOVA determined significant difference in fold change between control or PDGF-BB treatments. No significant differences were observed.

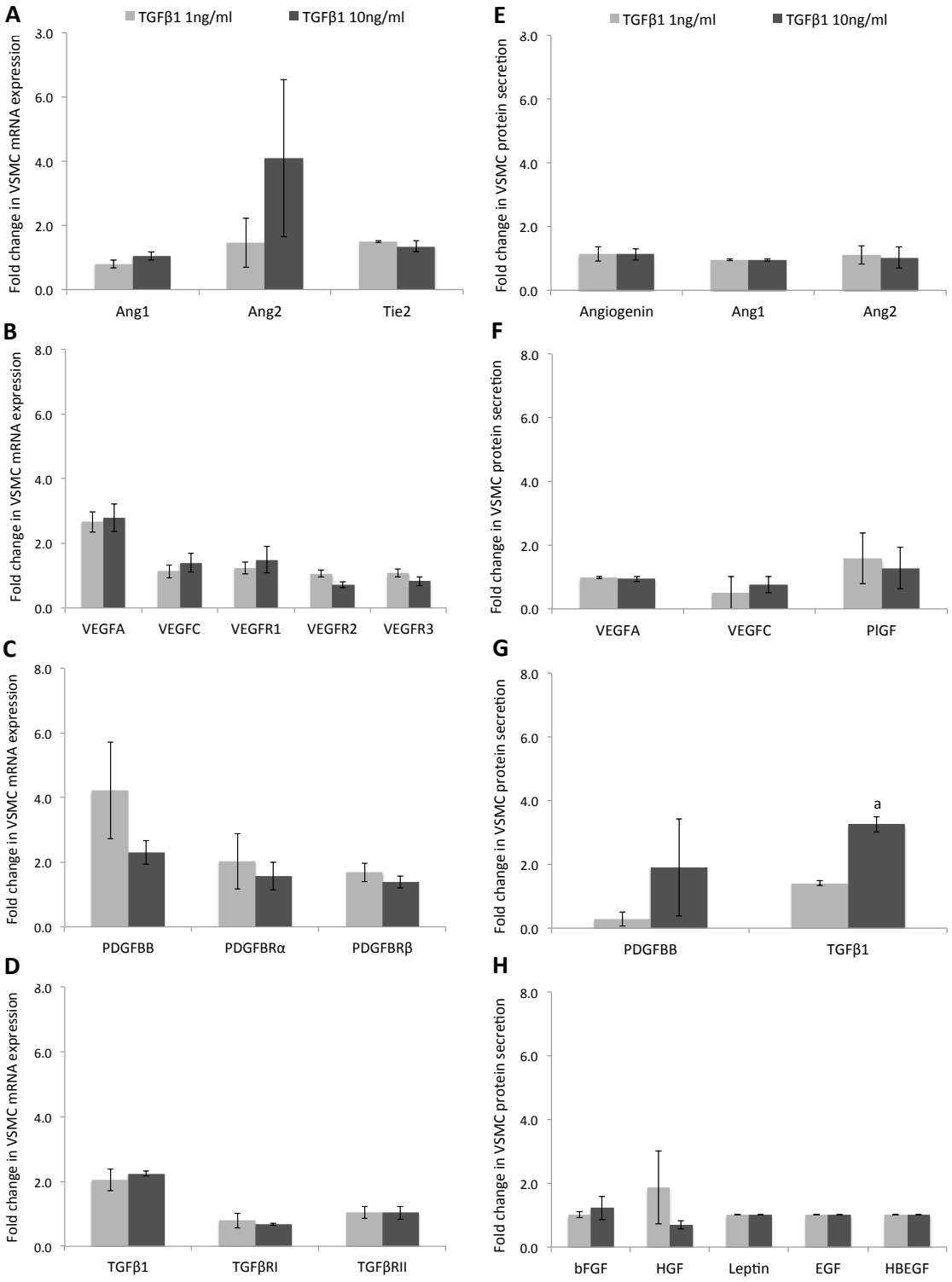


Figure 6.9: Graphical representation (mean ± SEM) of fold change in (**A-D**) mRNA and (**E-H**) secretion of angiogenic growth factors by TGFβ1 treated saphenous vein derived vascular smooth muscle cells (N=3 each group) cultured on matrigel. Pairwise Kruskal-Wallis one way ANOVA determined significant difference in fold change between control or TGFβ1 treatments. 'a' represents difference between control and 10ng/ml TGFβ1 treatment; ^{a}P=0.019.

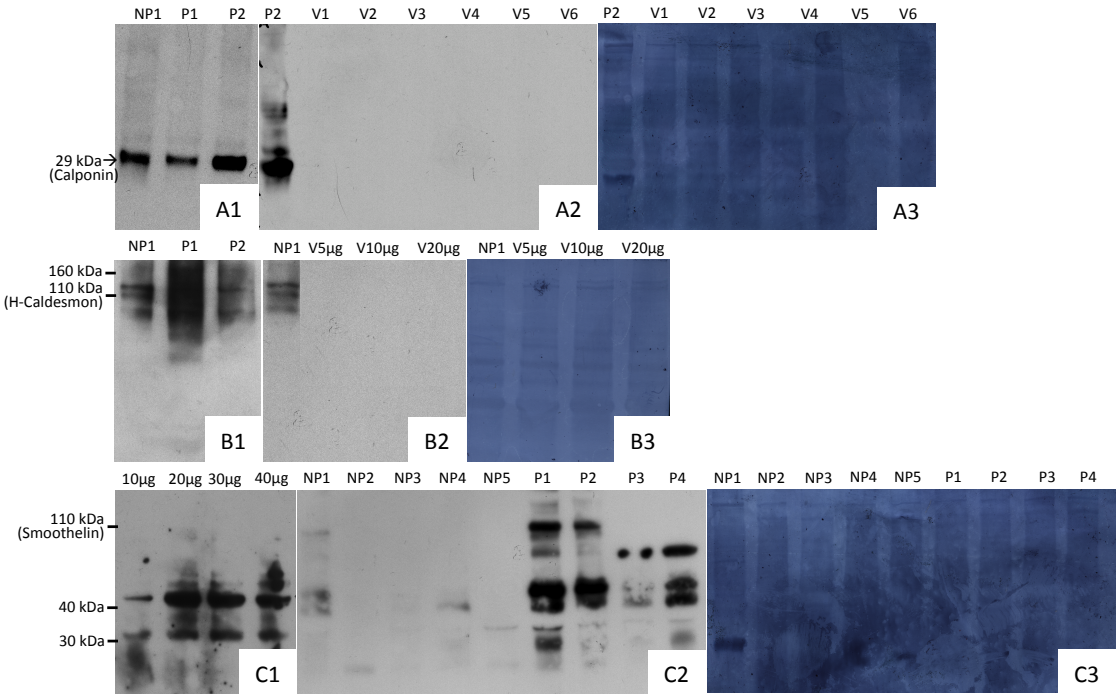


Figure 6.10: Western blot analysis for calponin, smoothelin and h-Caldesmon. (**A1, B1**) respectively shows calponin (~29kDa) and h-Caldesmon (~110kDa) in non-pregnant (NP1) and pregnant (P1-2) myometrial protein extract (10µg). (**C1**) shows non-specific bands for smoothelin (~110kDa) in pregnant myometrial protein extract (10-40µg). (**A2**) shows undetectable calponin in saphenous vein derived vascular smooth muscle cells (VSMCs) (V1-6; 14µg). (**B2**) shows undetectable h-Caldesmon in aortic VSMCs (10-40µg). (**C2**) shows smoothelin specific bands around 110kDa only in P1-2 (100µg protein). (**A3, B3, C3**) shows napthol blue black staining of PVDF membranes corresponding to **A2, B2** and **C2** respectively.

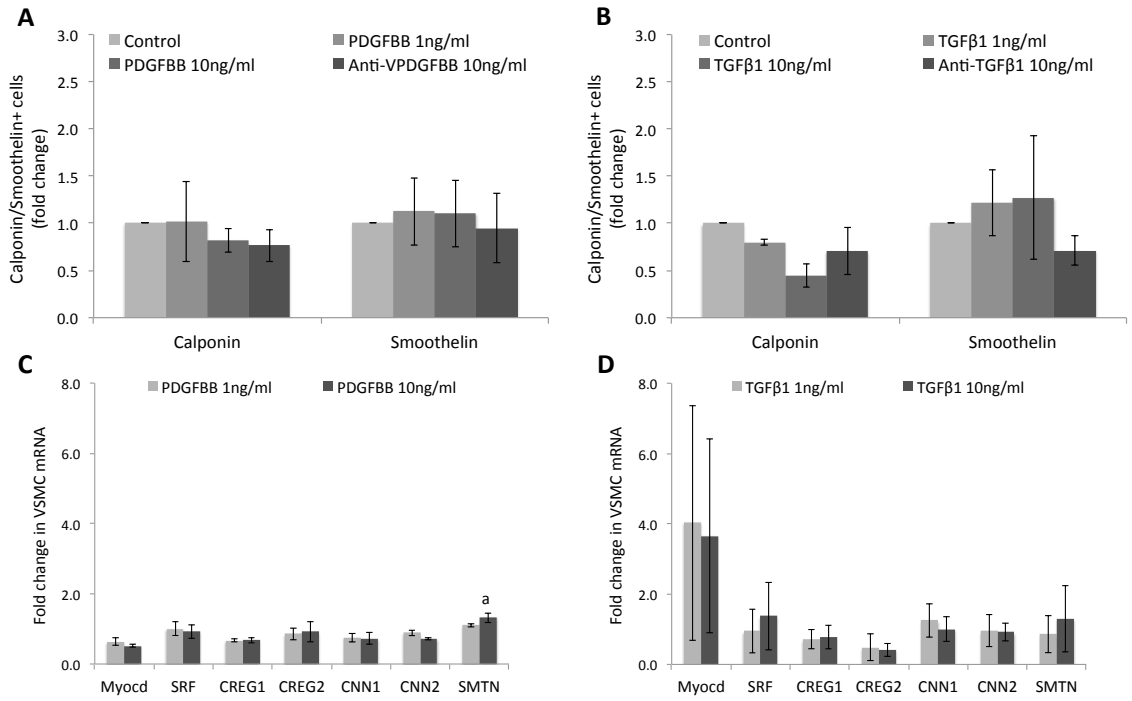


Figure 6.11: Graphical representation (mean ± SEM) of fold change in protein and mRNA of differentiation markers in saphenous vein derived vascular smooth muscle cells (VSMCs) treated with PDGFBB or TGFβ1. Fold change, compared with control in (**A-B**) percentage of calponin^{+} or smoothelin^{+} saphenous vein VSMCs and (**C-D**) mRNA of different genes involved in VSMC differentiation; myocardin (Myocd), cellular repressor of E1A-stimulated genes (CREG1, CREG2), SRF, calponin (basic-CNN1, CNN2), and smoothelin (SMTN) in VSMCs cultured on matrigel (N=3 each group). Pairwise Kruskal-Wallis one way ANOVA determined significant difference between control or (**A-C**) PDGFBB, and (**B-D**) TGFβ1 treatments. 'a' represents difference between control and 10ng/ml PDGFBB treatment; ^{a}P=0.023.

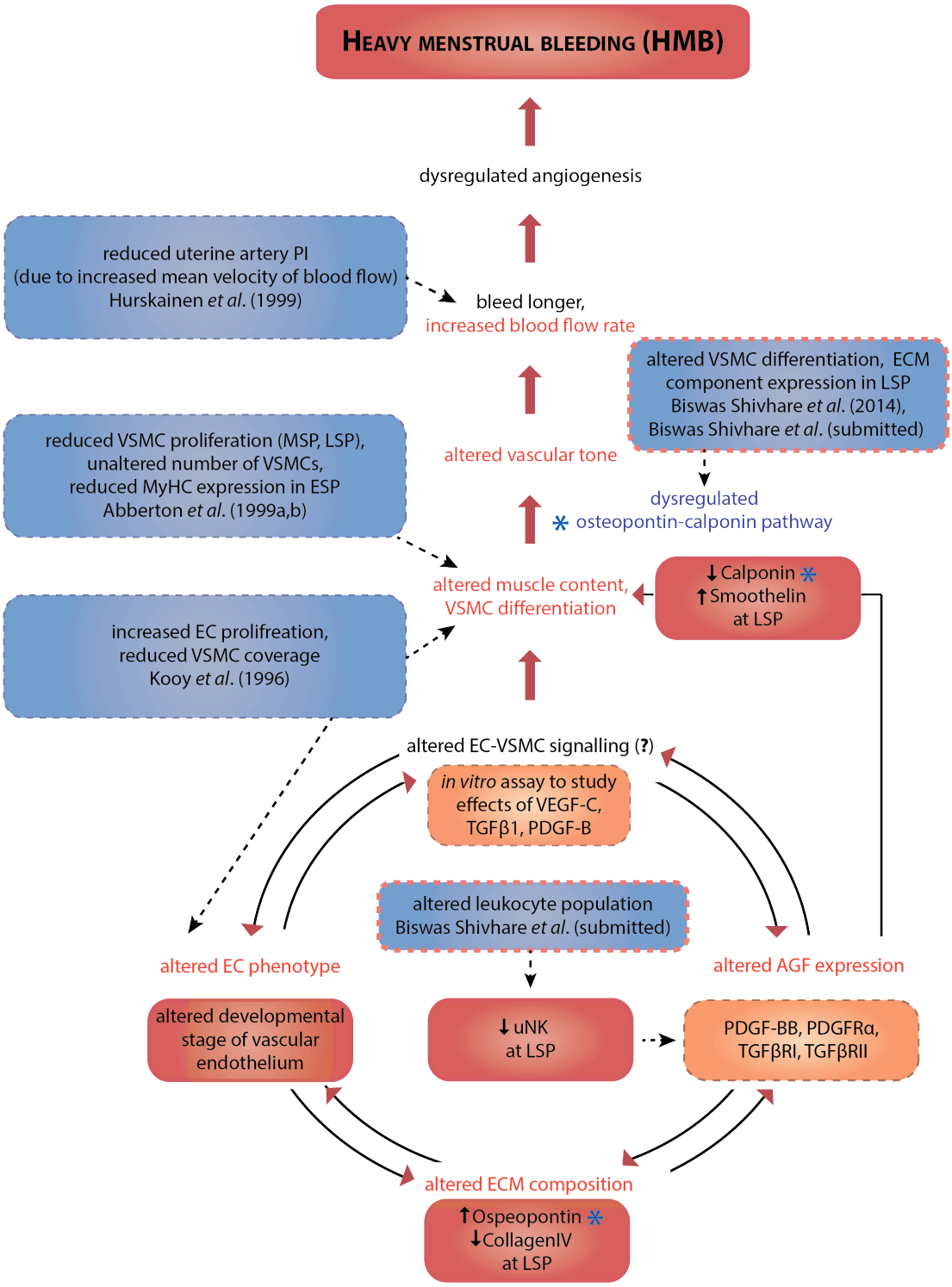


Figure 7.1: Key outcomes from the investigation of uterine blood vessel development in heavy menstrual bleeding.